RELATIONSHIP BETWEEN OBSERVATIONS IN MINI-RHIZOTRONS AND TRUE ROOT LENGTH DENSITY

by

DAN ROYCE UPCHURCH, B.S. In Ag., M.S.

A DISSERTATION

IN

AGRICULTURE

Submitted to the Graduate Faculty
of Texas Tech University in
Partial Fulfillment of
the Requirements for
the Degree of

DOCTOR OF PHILOSOPHY

Approved

August, 1985

CONTENTS

ABSTRACT iv

LIST OF TABLES vi

LIST OF FIGURES vii

I. INTRODUCTION 1

II. DEVELOPMENT OF THE MINI-RHIZOTRON TECHNIQUE 4

III. MINI-RHIZOTRON RATIO HYPOTHESIS 10

Introduction 10

Mathematical Development of Hypothesis 11

Hypothesis Testing 20

Conclusions 36

IV. RELATIONSHIP BETWEEN INTERSECTIONS AND ROOT LENGTH DENSITY 37

Introduction 37

Mathematical Development of the Model 39

Region 1. 68
Region 2. 73
Region 3. 80
Region 4. 80
Region 5. 82
Region 6. 82
Region 7. 87
Region 8. 90
Region 9. 91
Region 10. 91

Integration Routine 94

Model testing 97

V. STATISTICAL PROPERTIES OF THE MINI-RHIZOTRON TECHNIQUE 109

VI. SUMMARY AND CONCLUSIONS 118

LITERATURE CITED 122

APPENDIX 124

A. FORTRAN INTEGRATION ROUTINE 124
B. MODEL NOMOGRAPHS 146

ABSTRACT

This project has resulted in the development of two models which can be applied to the mini-rhizotron technique for root observations. The models are based on probabilistic assumptions concerning root growth directions in the soil. The models apply to the average number of roots which intersect the wall of several tubes buried in the soil, and not to individual observation tubes. The usefulness of the mini-rhizotron technique has been expanded to include indications of the orientation of the root system through the ratio hypothesis. The conversion of root counts to root length density (RLD) has been given a mathematical basis, with few assumptions. The primary disadvantage of the system is the number of samples required.

By determining the ratio of the number of roots which intersect the top to the number which intersect the bottom, the model predicts the direction of deviation from a random orientation. Observations made on the wall of a trench confirmed the horizontal orientation of a cotton root system and the existence of upward growth which had been predicted by the model from observations in mini-rhizotrons.

A model, relating the number of root intersections on a mini-rhizotron to the bulk soil RLD, predicted a linear relationship. The average length to associate with each intersection was determined assuming that root growth was affected only after an intersection occurred, that roots can be represented by straight line segments, and that root growth direction followed some probability density function. The assumption that roots can be represented by straight lines can be removed if the

tortuousity of the path of root growth is known. The length can be weighted by the probability of root growth in that direction, if it is known.

The correlation coefficient between RLD determined by applying the model to mini-rhizotron observations and that from soil cores was low but significant at the 99% level, when all treatments and angles were considered. The correlation was largest, 0.70, in the dryland treatment at the 30^{o} installation angle. The higher correlation in the dryland treatment may have resulted from of the reestablishment of the natural soil structure at the interface as the soil dried.

The statistical properties of the mini-rhizotron system emphasize the need for a large sample size. The number of samples required to detect specific differences in RLD is large for both soil cores and mini-rhizotrons when the difference is small. The decision about the number of tubes to install will be affected by the reported variance, the magnitude of the expected RLD, the difference in RLD which is important to the project, and the resources of the project. The variance of the mini-rhizotron was larger than soil cores in this project, but in another project reported in the literature this result was reversed.

LIST OF TABLES

Table 4.1: Definition of the 10 regions to be used in calculating the average ρ..... 68

Table 4.2: Comparison of model output for average and the minimum and maximum possible values for selected regions and cylinder parameters..... 96

Table 5.1: Variance and coefficient of variability for RLD determined by soil cores and mini-rhizotrons for the dryland and irrigated treatments..... 111

Table 5.2: Variance and coefficient of variability for RLD reported in several projects..... 114

LIST OF FIGURES

Figure 3.1: Definition of axis system, all root growth angles are within the first quadrant..... 13

Figure 3.2: Axis system with line representing the face of a mini-rhizotron at an angle g..... 16

Figure 3.3: Relationship between the ratio p_T/p_B to tube installation angle..... 19

Figure 3.4: Regions where the relationship between the ratio p_T/p_B to tube installation angle predicts a horizontally or vertically oriented root system..... 22

Figure 3.5: Photograph of the pit wall with grid in place, used to measure the frequency distribution for root growth angles..... 25

Figure 3.6: Root growth angle frequency distribution for all depths and both treatments, angles are the mid-points of each class in degrees..... 28

Figure 3.7: Predicted versus observed ratio for all installation angles, depths and treatments..... 30

Figure 3.8: Observed ratio versus soil depth for the 30^o installation angle. Day indicates observation date, as day of year..... 33

Figure 3.9: Predicted versus observed ratio for all installation angles, depths and treatments, using the adjusted frequency distribution..... 35

Figure 4.1: Generalized right circular cylinder centered on the origin..... 41

Figure 4.2: Right circular cylinder with radius, r, centered at (0,r,0)..... 44

Figure 4.3: a) Rotation of axis through and angle, g, b) the cylinder is then at an angle, g, with respect to a new axis system..... 46

Figure 4.4: a) Intersection of line, with direction (α,β,γ), with b) cylinder..... 50

Figure 4.5: Representation of a point (x,y,z) in cylindrical coordinates (ρ,θ,γ)..... 55

Figure 4.6: Termination of the cylinder by the planes z = L/2 and z = -L/2..... 60

Figure 4.7: Two conditions for the lower end of the cylinder a) case a, where the lower end does not intersect the xz plane, b) case b, where the lower end is divided by the xz plane, c) nomograph to predict the condition at the lower end of the cylinder..... 63

Figure 4.8: Limits of integration for region 1 for a) case a and b) case b..... 70

Figure 4.9: Limit of integration for region 2, applies to both case a and b..... 75

Figure 4.10: Limits of θ for region 2..... 77

Figure 4.11: Limits of integration for region 4, applies only to case b..... 84

Figure 4.12: Limits of integration for region 6, applies only to case a..... 86

Figure 4.13: Limits of integration for region 7, applies only to case a..... 89

Figure 4.14: Limits of integration for region 9, applies only to case b..... 93

Figure 4.15: Root length density measured by mini-rhizotrons versus that measured by soil cores, for all treatments and installation angles..... 99

Figure 4.16: Root length density measured by mini-rhizotrons versus that measured by soil cores, for the dryland treatment for all angles..... 103

Figure 4.17: Root length density measured by mini-rhizotrons versus that measured by soil cores, for the irrigated treatment for all angles..... 105

Figure 4.18: Root length density measured by mini-rhizotrons versus that measured by soil cores, for the dryland treatment and 30^{o} installation angle..... 107

Figure 5.1: Relationship between the number of samples required and the detectable difference, at the 95% level, for the present project..... 113

Figure 5.2: Relationship between the number of samples required and the detectable difference, at the 95% level, from published reports..... 116

Figure B.1: Nomograph for determining the average length to associate with each intersection, with an interval length of 10 cm..... 148

Figure B.2: Nomograph for determining the average length to associate with each intersection, with an interval length of 15 cm..... 150

Figure B.3: Nomograph for determining the average length to associate with each intersection, with an interval length of 20 cm..... 152

CHAPTER I

INTRODUCTION

The study of root growth in situ is a difficult task because of the physical environment in which roots exist. When a plant is grown in the field, the root system is shielded from visual observation by the soil matrix. In order to study the root system, you must remove the soil matrix, encourage roots to grow in a location which can be observed, or observe some other factor which can be used to infer the condition of the root system.

Several techniques have been developed for each of these approaches. Bates (1937) proposed a technique to observe roots growing against a clear surface buried in the soil. Several researchers have applied this technique since 1937, with each individual introducing new technology to the procedure.

The technique was named, 'mini-rhizotron,' by Bohm (1974) and has become a promising technique with the introduction of video technology by Dyer and Brown (1980) and Upchurch and Ritchie (1983, 1984). The advantages and limitations of the mini-rhizotron over other techniques have been described by Upchurch and Ritchie (1983). A problem has arisen in comparing results obtained by various researchers using mini-rhizotrons because there has not been a uniform procedure used in making the observations. The results of the observations have been empirically related to the true root length density by some scientists, while others have made relative comparisons of the experimental treatments without

relating them to any physical parameter describing the root system. These approaches have provided valuable information concerning root systems but have not provided a general mechanism for comparing research results. The full potential of this technique has therefore not been explored. A theoretical relationship between the probability of a root growing _in situ_ intersecting an observable surface should provide a key to expanded use of this technique. This expansion could open the door to improved approaches for studying root systems.

This project defines a relationship between the number of root intersections observed on the face of a clear tube buried in the soil, and the root length density in the soil surrounding the tube. No attempt is made to describe the root length density around a single tube but rather the density that exists in a layer of soil of finite thickness extending over the entire plot or field being studied. The relationship will be probabilistic in the sense that it will apply only when the number of tubes and number of root intersections are sufficient to represent the entire population. Assumptions will be made concerning the probability density function for root growth angles in developing the model. Therefore the sample to which the model is applied must be of sufficient size to account for these assumptions. For example, an average length will be assigned to each root intersection, assuming some density function for root growth direction. This length should not be considered the exact length for each intersection but rather the average length of a large number of intersections. Similarly, the total length derived from observations of a single tube should not be expected to represent the

true root length density in that entire layer. Experimental evidence suggests that as many as eight tubes may be required before a significant relationship is found. Roots are not uniformly distributed in the soil so it is possible that, at a particular depth, there may be no intersections for a particular tube while another tube may have several intersections. However, the average of observations of several tubes should be related to root length density in a soil layer. An analogy can be made between this technique for estimating root length density and a blind man attempting to estimate leaf area index in a canopy using only his sense of touch. If the blind man reaches between the rows of a crop he will find no leaves, but if he reaches into a crop row he will touch several leaves. Neither of these observations independently will give him a mental picture of the crop canopy but together they begin to describe the architecture of the crop canopy. If the blind man reaches his arm into the crop at various points and determines the number of leaves which touch his arm at different heights he can began to estimate the density of the canopy. By counting the number of roots intersecting a tube in certain intervals along the tube and repeating this process in several tubes we can begin to estimate the density of the root system at each depth in the soil.

CHAPTER II

DEVELOPMENT OF THE MINI-RHIZOTRON TECHNIQUE

Bates (1937) used glass tubing buried in the soil for observing sugar beet root systems and the growth of grass root systems as affected by cutting. A cavity larger than the tubing was excavated, the tubing was placed in the cavity, and the void space was filled with dry soil taken from the appropriate depth. Bates suggested the use of lamp glasses cemented end to end as an alternative to specially constructed glass tubing. He also described using half sections of drain pipe faced with glass as an observation tube. A mirror, attached to a rod, was inserted into the tube in such a way that an individual could observe the roots which grew against the wall of the tube. The wall of the tube was lighted by a battery operated lamp attached to the rod. Bates did not indicate how the results were related to rooting patterns other than to indicate that a grid marked on the tube would "facilitate observation and sketching." After being proposed by Bates in 1937 there was no mention of the technique in the literature until the early 1970's.

Waddington (1971) used the observation tube technique to study the development of wheat roots in pots in a greenhouse. He replaced the mirror and rod with a coherent fiberoptics scope with a right angle viewing attachment at the objective end. Square plexiglas tubes were placed in a pot and soil filled around the tube. The tube was angled to limit the number of roots which followed the tube and two faces of the

tube were oriented upward. Later in the project Waddington replaced the square tube with a round tube and the void space filled with soil allowing new root growth to be observed. Drawings were made of the roots which fell in the field of view of the scope and used to infer rooting density. The development of the wheat root system was followed for a period of 6 weeks, and showed a continual increase in the density over time. Waddington gave no explanation of how the observations were converted to root density other than visual observation of the drawings.

Bohm (1974) used the system proposed by Waddington but eliminated the fiberoptics scope because of the cost of the equipment. Using the mirror system suggested by Bates, Bohm observed root systems in the field. A magnifying glass was used on the top of the tube to allow roots to be seen at greater depths. He was the first to apply the name, mini-rhizotron, to this technique. Bohm also provided the first field calibration of the system by comparing the results obtained from the mini-rhizotron to roots observed at the wall of a pit. No details of the comparison were given in the paper, only a statement that the number of roots seen on the wall of the tube was similar to the number seen on the trench wall. Bohm also demonstrated the sensitivity of the technique to detect the differences in rooting in a tilled versus a non-tilled soil, and to follow the decomposition of roots when the shoot was removed. Bohm, Maduakor, and Taylor (1977) compared five methods for characterizing root systems, including mini-rhizotrons. Their conclusions included an indication of a problem of root concentration near vertically oriented plastic tubes. They recommended that plastic not be

used for root observations. The results of their observations in the mini-rhizotrons did not agree well with the other techniques they used, which included trench-profile, framed-monolith, core-sampling, and water extraction patterns. They indicated that the technique would be useful for phenological observations but not for complete characterization of the rooting profile.

Sanders and Brown (1978) described a system for observing roots in square, plexiglass tubes installed in field soil in the manner described by Waddington (1971). A fiber optic duodenoscope was attached to a 35mm camera and used to photograph the two upper faces of the tubes. An electronic flash unit provided light for the photographs. The photographs provided extremely high quality observations for quantifying the root system and reduced the time required for field observations. The results from mini-rhizotrons and from soil cores showed good agreement. The total root lengths for the 0 to 72 cm depth were not significantly different for the two techniques. The mini-rhizotron data had a coefficient of variation of less than 15% while that of the soil cores was 39%, indicating an advantage for the mini-rhizotron. They presented a methodology for converting the observations in the mini-rhizotron to root length density which was based on Newman's line intersect technique (Newman, 1966). The negatives of the photographs made with the scope and camera were projected onto a screen with an inscribed Newman-type grid. The number of roots intersecting the grid lines were counted and the total length of root in contact with the plexiglass tube calculated using the equation proposed by Newman. They assumed that all roots

within 3 mm of the tube could be seen, and converted root length to root length density by dividing by the volume represented by this depth of view. Sanders and Brown list several of the advantages of this technique including portability, non-destructive nature of the technique, and reduced time requirements. They also noted the possibility of incorporating an 8mm movie camera into the system for sequence or time lapse photography. Although they recognized the problems with plexiglas pointed out by Bohm, they felt the effect in their work was not sufficient to significantly affect the root length measurements. Gregory (1979) described a system similar to Sanders and Brown's, in which a rigid periscope was used in place of the fiber scope. He used glass tubes installed vertically to observe the root system of wheat and millet. When compared with root densities determined by soil coring, the mini-rhizotron system underestimated the density near the soil surface and overestimated at depth. The overestimation at depth was attributed to roots following the vertical tubes. Since the root length at the interface was estimated from intersections with a grid the preferential root growth along the tube would increase the density at depth. Maertens and Clauzel (1982) and Vos and Groenwold (1983) described systems similar to that proposed by Sanders and Brown and found similar results. Vos and Groenwold obtained an empirical relationship between root length at the tube interface and bulk soil root length density by regression for wheat and potatoes. The regression line for the wheat had an r value of 0.76 and for potatoes it was 0.51. The regression line differed between crops indicating that there was was no unique relation-

ship for all experimental conditions.

Dyer and Brown (1980) added a black and white video camera to the fiber scope used previously by Sanders and Brown (1978). This modification allowed more rapid observations in the mini-rhizotrons, decreased film cost and compared well with the results from the previous system. Upchurch and Ritchie (1983) used a rigid borescope and a black and white video camera in plexiglass tubes for root observations. The system was calibrated against root densities determined from soil cores. Several installation orientations were evaluated with no orientation having a significantly better correlation than another. Three particular problems were identified in the use of this technique: 1) The system requires averaging the results from several tubes before a relationship is found between mini-rhizotron observations and the bulk soil root density; 2) The number of root intersections near the soil surface does not correlate well with the rooting density in this zone; 3) The results obtained are dependent upon the observation procedure and therefore a general relationship will not exist unless standardized procedures are used. A method for converting the number of roots observed intersecting the mini-rhizotron to root length density was proposed which involved assumptions concerning the in situ root growth angles and morphology of the root system. The proposed procedure involved counting root intersections within a zone on the tube rather than intersections between roots and a line. This minimized the effect of the interface on the results.

Upchurch and Ritchie (1984) described a battery operated system

including a color video camera for use in mini-rhizotrons. This system improved the picture quality such that relative root age could be determined. The battery operated system decreased the time required and minimized the damage to the crop during observations caused by the power cords and bulky equipment. Brown (1984) described the use of a color video camera for root observations, which was similar to that described by Upchurch and Ritchie (1984). In these systems the camera was small enough to fit inside the tube thereby eliminating the need for other optics. A set of lenses and a prism was attached to the camera and the camera lowered into the tube. The equipment was miniaturized such that all of the recording and monitoring equipment was mounted on a single back pack for use in the field.

A portable system is now available with extremely high resolution. A large number of tubes can be observed with relative ease and at frequent time intervals. There is little difficulty in identifying and quantifying the number of roots which intersect the tube at all depths. However, with the exception of the relationship proposed by Upchurch and Ritchie (1983) the interpretation of the results has been entirely empirical. No single procedure has been developed for quantifying the number of intersections or relating this number to RLD. This has led to limited use and usefulness of the technique. The systems must be calibrated with each crop, soil, and observation procedure which is applied, and therefore have offered no real advantage over other techniques available.

CHAPTER III

MINI-RHIZOTRON RATIO HYPOTHESIS

Introduction

The use of mini-rhizotrons for quantifying the development of root systems has been limited primarily to estimates of root length density and rooting depth. The relationship between root intersections on the face of the tubes and the bulk soil RLD has been developed empirically and no general relationship has been found. This chapter presents a hypothesis that may provide a mechanism for using the mini-rhizotron technique to describe the *in situ* root morphology. The hypothesis should also aid in the development of a general relationship between root intersections and RLD.

We will first develop the hypothesis for a specific case in which all root growth is considered random and upward root growth is eliminated and then will expand the mathematics to the general case. We will reduce root growth angles to the two dimensional plane. Root growth angles are then the projection of the three dimensional space onto a two dimensional plane. For mini-rhizotrons placed in the row and sloping parallel to the row direction this restriction is probably a fair approximation.

It is important to remember in the development of this model that we must deal in probabilistic terms. The model developed will not apply to single observation tubes, but rather the average of some large number of tubes. The model is based on the probability density function for

root growth angles, therefore a sufficient number of tubes must be sampled to represent the entire population of root growth angles. Also, the model is intended to represent a layer of soil that covers the entire area of the plot or field being studied, not the zone immediately surrounding a particular tube. For a particular tube there is a possibility that no root intersections will occur if the roots are non-uniformly distributed in the soil. It is the entire plot that is of interest, not the small volume of soil that is adjacent to a particular tube.

Mathematical Development of Hypothesis

Assume that all root growth angles have equal probability with the restriction that there is no upward root growth. Defining a set of axis (figure 3.1) such that the x-axis is normal to the soil surface and is positive downward and the y-axis is parallel to the soil surface, we can define all root growth angles to be in the first quadrant. Since there will be root growth angles in both the first and fourth quadrants, calculations done in the first quadrant will be twice the appropriate value. When the angles in the fourth quadrant are significant to the calculation a correction must be made.

In this system,the probability for a root growth angle, p(t), with t between 0 and $\pi/2$, is a constant which is equal for all values of t in this range. That is;

$$p(t)=k \qquad 0 < t < \pi/2 \qquad (3.1)$$

and since upward root growth is excluded,

$$p(t)=0 \qquad \pi/2 < t < \pi. \qquad (3.2)$$

Figure 3.1: Definition of axis system, all root growth angles are within the first quadrant.

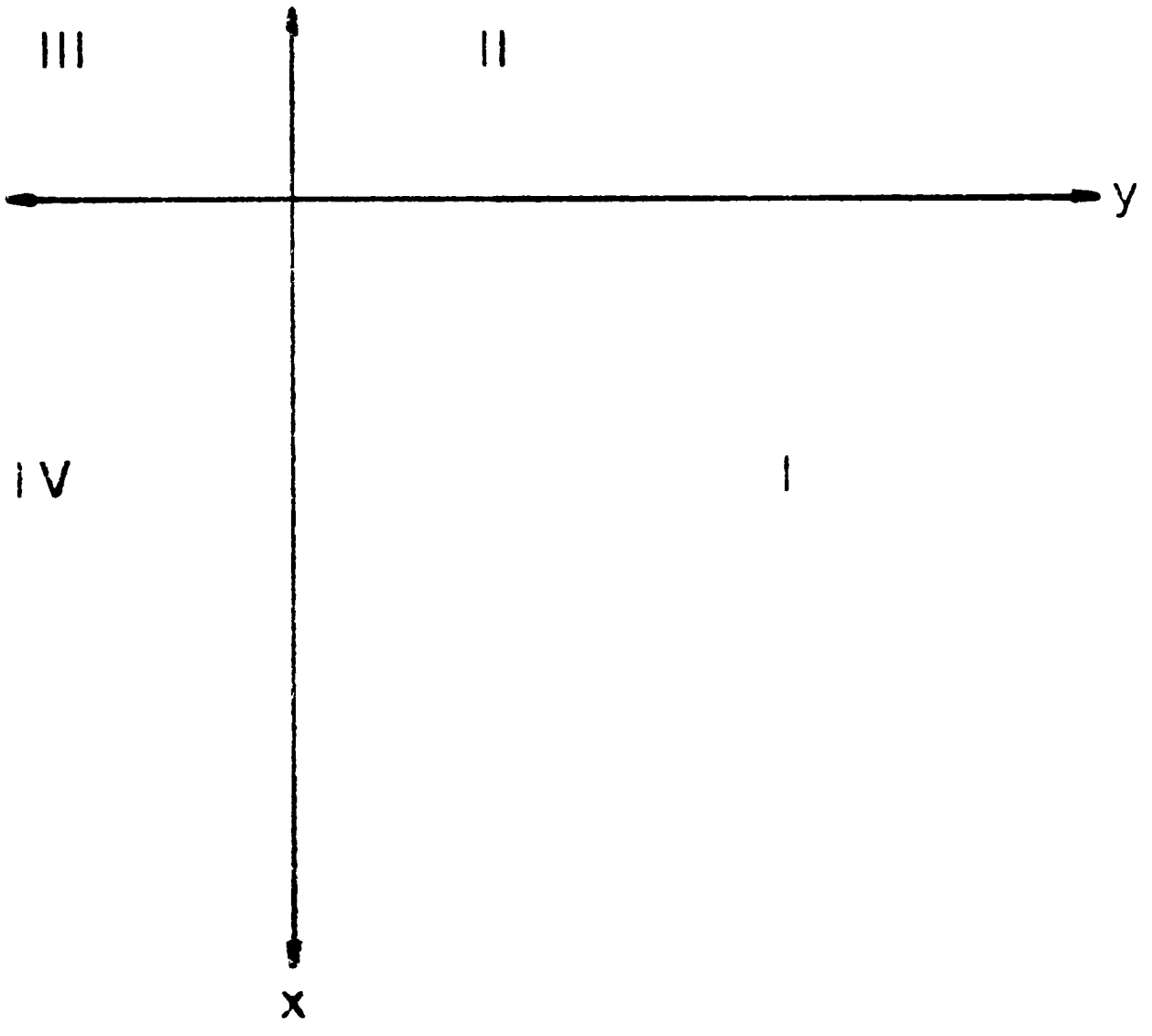
III
II
y
IV
I
x

All root growth can be included in the first quadrant by a translation of axis. Angles in the fourth quadrant are symmetric to those in the first quadrant and those in the third are symmetric to the second quadrant.

Since the total probability must equal 1, we can solve for the value of k by integrating between the limits of root growth angles.

$$\int_0^{\pi/2} p(t)dt = k \int_0^{\pi/2} dt = k\ \pi/2 = 1 \quad . \tag{3.3}$$

therefore;

$$k = 2/\pi. \tag{3.4}$$

Now, imagine a line placed arbitrarily in the xy plane, defined in figure 3.2, which makes an angle, g, with respect to the x-axis. Let g be between 0 and $\pi/2$, then the probability of a root intersecting the line from the top, p_T, is equal to the integral of the probabilities in this interval minus 1/2 the integral from g to $\pi/2$. One half the integral from g to $\pi/2$ represents the angles in the first quadrant which would not intersect the top because they are too steep.

$$p_t = \int_0^{\pi/2} k\ dt - 1/2 \int_g^{\pi/2} k\ dt$$

$$= K[\pi/2 - 1/2(\pi/2-g)]$$

$$= K(\pi/4 + g/2) \tag{3.5}$$

Figure 3.2: Axis system with line representing the face of a mini-rhizotron at an angle g.

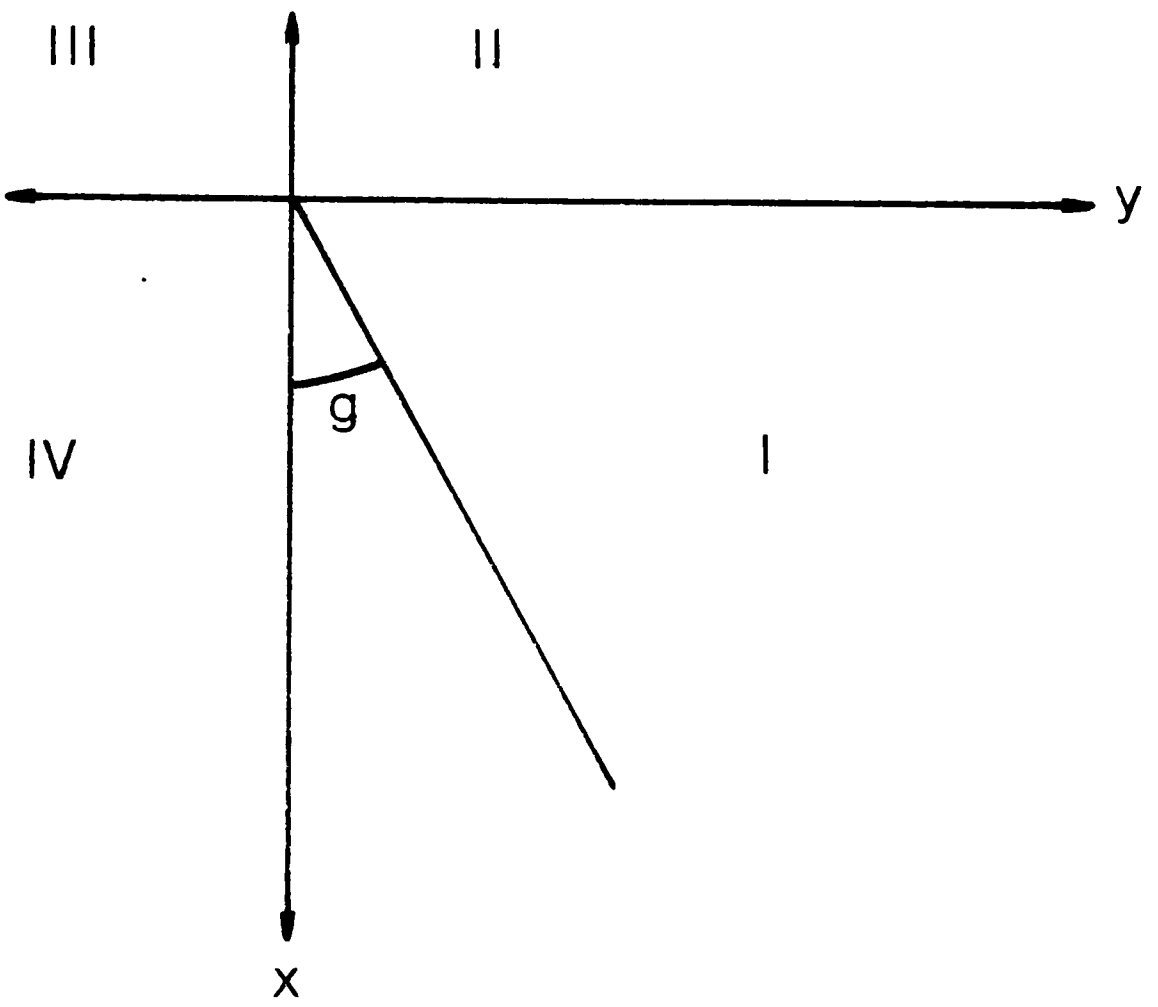
III
II
y
g
IV
I
x

The probability of a root intersecting the line from the bottom, p_B, is equal to the probability of all root growth angles greater than g, and in the first quadrant. This is 1/2 the integral between g and $\pi/2$.

$$P_b = 1/2 \int_g^{\pi/2} K\, dt = K(\pi/4 - g/2) \tag{3.6}$$

Now with the assumptions previously stated, we can calculate the probable ratio of the number of top intersections to bottom intersections. This will be the same as the ratio of the probabilities for intersections on the top over the bottom.

$$p_T/p_B = (\pi/4 + g/2)/(\pi/4 - g/2) \tag{3.7}$$

This ratio varies from 1, when g = 0, to infinity, when g = $\pi/2$, as shown in figure 3.3. It approaches infinity as g approaches $\pi/2$ and is fairly stable when g is between 0 and $\pi/4$, rising from 1 to 3.

To generalize this relation we will let f'(t) represent the probability distribution of root growth angles. Then

$$P_t = \int_0^{\pi/2} f'(t)\, dt - 1/2 \int_g^{\pi/2} f'(t)\, dt$$

$$= [f(\pi/2)-f(0)] - 1/2[f(\pi/2)-f(g)]$$

$$= 1/2[f(\pi/2)+f(g)] - f(0) \tag{3.8}$$

Figure 3.3: Relationship between the ratio P_T/P_B to tube installation angle.

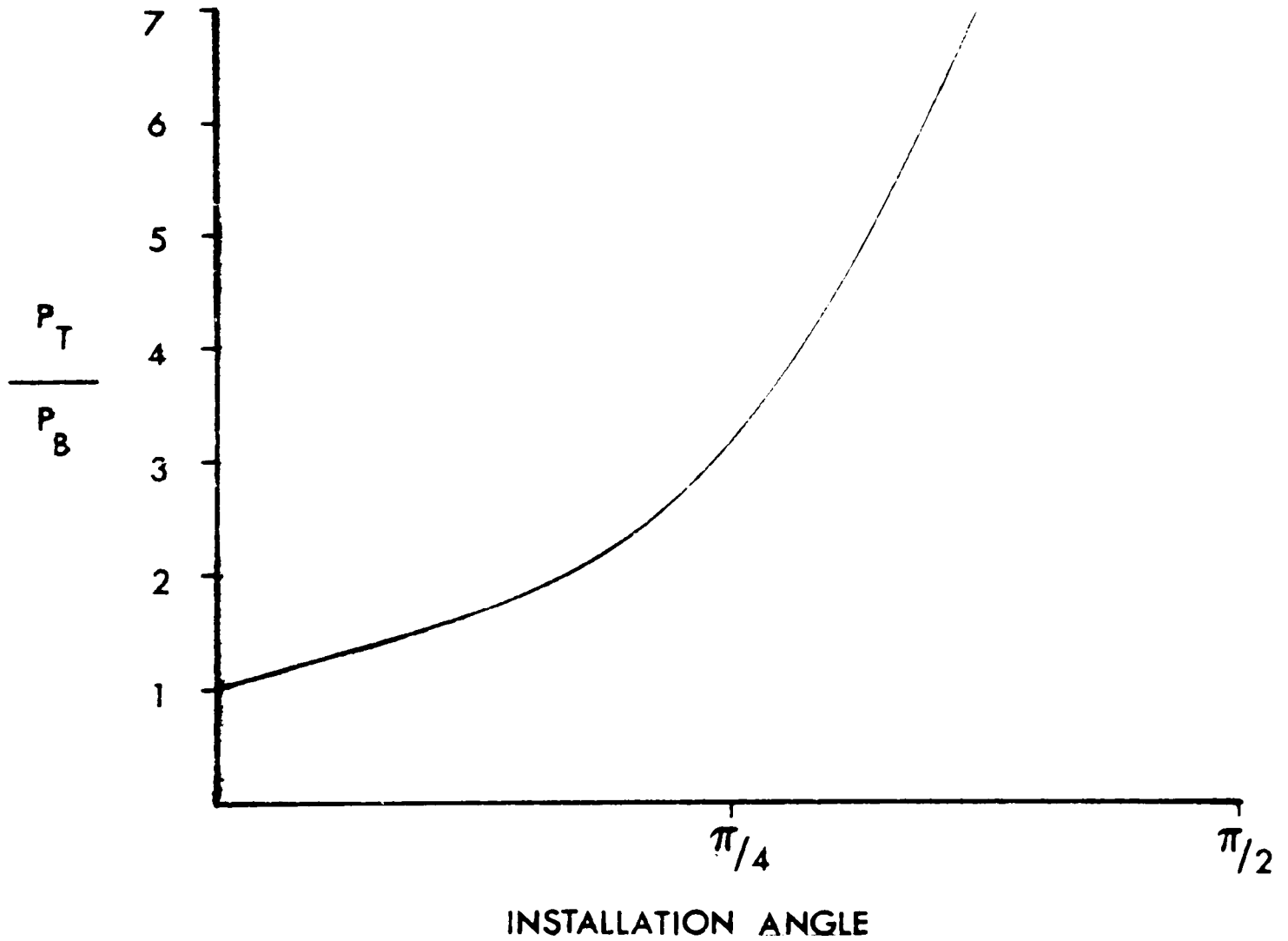
7
6
5
4
3
2
1
$\frac{P_T}{P_B}$
$\pi/4$
$\pi/2$
INSTALLATION ANGLE

and,

$$P_b = 1/2 \int_g^{\pi/2} f'(t)dt = 1/2[f(\pi/2) - f(g)] \tag{3.9}$$

therefore,

$$\frac{P_T}{P_B} = \frac{1/2\ [f(\ \pi/2 + f(g)] - f(0)}{1/2\ [f(\ \pi/2) - f(g)]}\ . \tag{3.10}$$

This ratio again varies from 1 to infinity as g goes from 0 to $\pi/2$, but the exact form is dependent upon f'(t).

It should be possible to approximate the probability function, f'(t), by installing tubes at several angles and measuring the ratio p_T/p_B. Using multivariate analysis to fit the data, values for f(t) can be approximated from which f'(t) can be calculated.

It can be seen from equations 3.7 and 3.10 that if the ratio at a particular installation angle is greater than that predicted by equation 3.7 you have a more vertically oriented root system. Conversely, if the ratio is below the value predicted by equation 3.7, the root system is more horizontally oriented. This relationship is depicted in figure 3.4, where the region above the line represents a root system which is more vertically oriented than random and the region below the line represent a root system which is more horizontal than random.

Hypothesis Testing

During the 1984 growing season an experiment was conducted to test

Figure 3.4: Regions where the relationship between the ratio P_T/P_B to tube installation angle predicts a horizontally or vertically oriented root system.

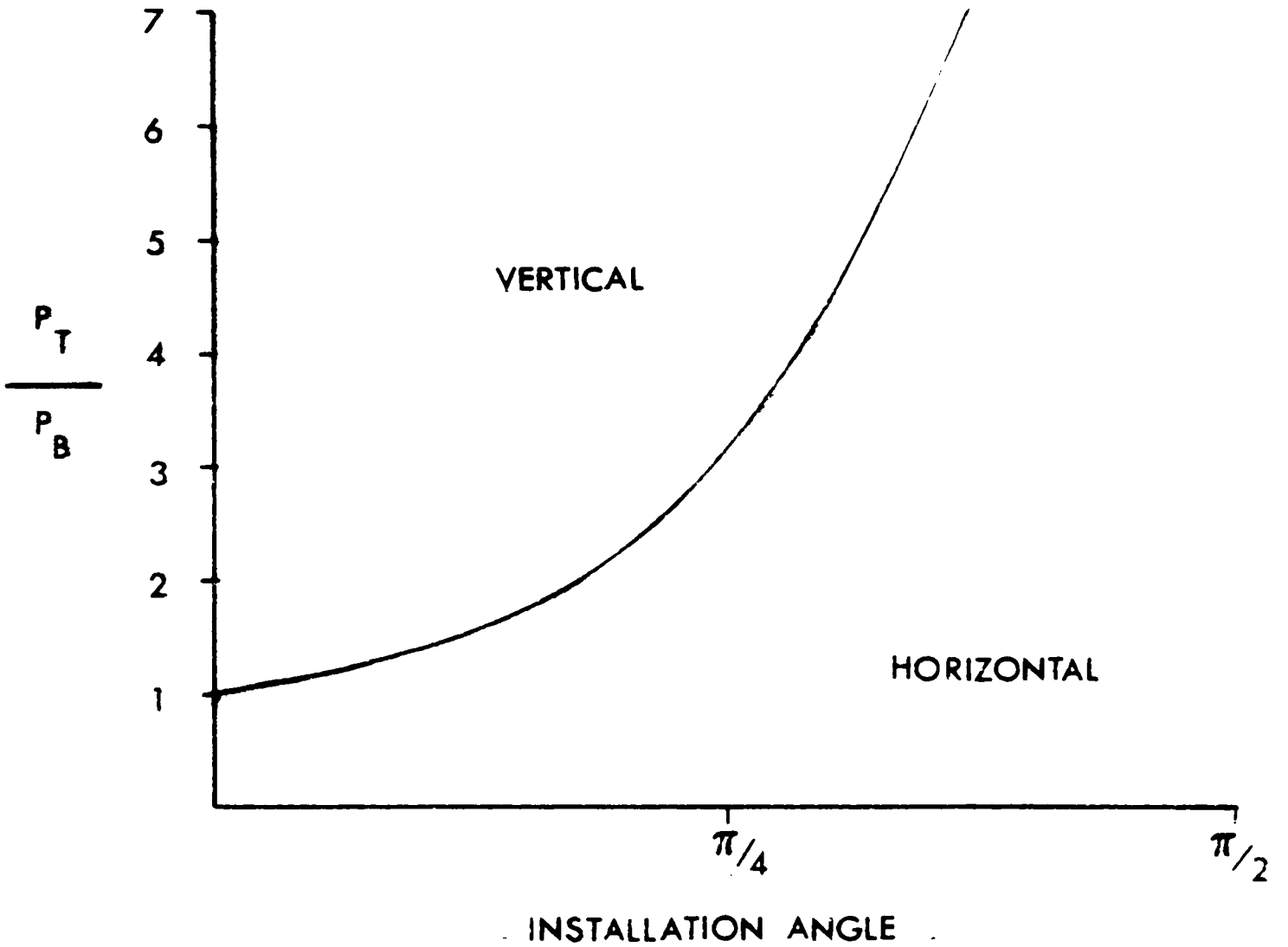
7
6
5
4
3
2
1
$\frac{P_T}{P_B}$
VERTICAL
HORIZONTAL
$\pi/4$
$\pi/2$
INSTALLATION ANGLE

this model. Cotton, Gossypium hirsutum L. c.v. Paymaster 404, was planted in two large field plots which were equipped with 54 mini-rhizotrons installed at three angles. Nine mini-rhizotrons were installed in each plot at each of the angles, vertical, 15^{o} from vertical and 30^{o} from vertical. The two plots were differentially irrigated with one plot receiving only a preplant irrigation and the other irrigated as needed. The roots intersecting each of the mini-rhizotrons was observed on a weekly basis following the procedure described in Upchurch and Ritchie (1983), with the addition of observing the lower face of the mini-rhizotron. From these observations the ratio of top to bottom intersections was calculated.

On August 17, 1984, a pit was excavated in each of the plots, soil cores were collected and observations of all mini-rhizotrons were made, in order to obtain all the information required to test the model. The wall of each pit was smoothed, and a 1-m. square grid system with 5 cm square grid size was attached to the wall (Bohm, 1979) (figure 3.5). Soil was removed in thin layers from the wall of the pit within each of the squares and the angle of each root encountered recorded. The angles were measured as the projection of the root onto the plane of the pit wall, with an angle of 0^{o} representing vertical downward and 90^{o} being horizontal. If it could be determined, by the branching of the root, that the direction of growth was upward an angle greater than 90^{o} was recored, with 180^{o} representing vertically upward root growth.

From this information the relative frequency distribution was determined for root growth angles. The frequency distribution for each

Figure 3.5: Photograph of the pit wall with grid in place, used to measure the frequency distribution for root growth angles.

depth and treatment was calculated and a Chi-square test established that there were no differences in distribution across treatments or depths. Figure 3.6 is the frequency distribution across all depth and treatments. Two angles predominate the distribution with approximately 40% of all observed roots between 80 and 90 degrees, 24% between 0 and 10 degrees, and no other angle with a fraction larger than 8%. Approximately 3% of the roots observed were growing upward. The fraction of roots which were considered to be growing upward is probably an underestimate of the true value, since only roots which branched in the layer of soil observed could be established to be growing upward. It is possible that roots which were counted in one of the classes below 90^{o} were in fact oriented upward, but in the absence of direct evidence they were assumed to be growing downward. This error in the measurements is impossible to remove and can significantly affect the testing of the model.

Since the distribution shown in figure 3.6 does not fall into any of the family of known distributions the testing of the model was accomplished by numerically applying the observed distribution to the model to calculate the predicted ratio. Figure 3.7 is a plot of the ratio predicted by the model based on the observed distribution versus the ratio observed in the mini-rhizotrons. The plot does not show a tight coupling of the model with the observed ratio, however the magnitude of the predicted and observed ratios are the same, both being between 0.0 and 3.5. The predicted ratio has a range of about 2.0 and the observed ratio has a range of about 1.3. The predicted ratio is in

Figure 3.6: Root growth angle frequency distribution for all depths and both treatments, angles are the mid-points of each class in degrees.

ROOT GROWTH ANGLE DISTRIBUTION

ALL TREATMENTS

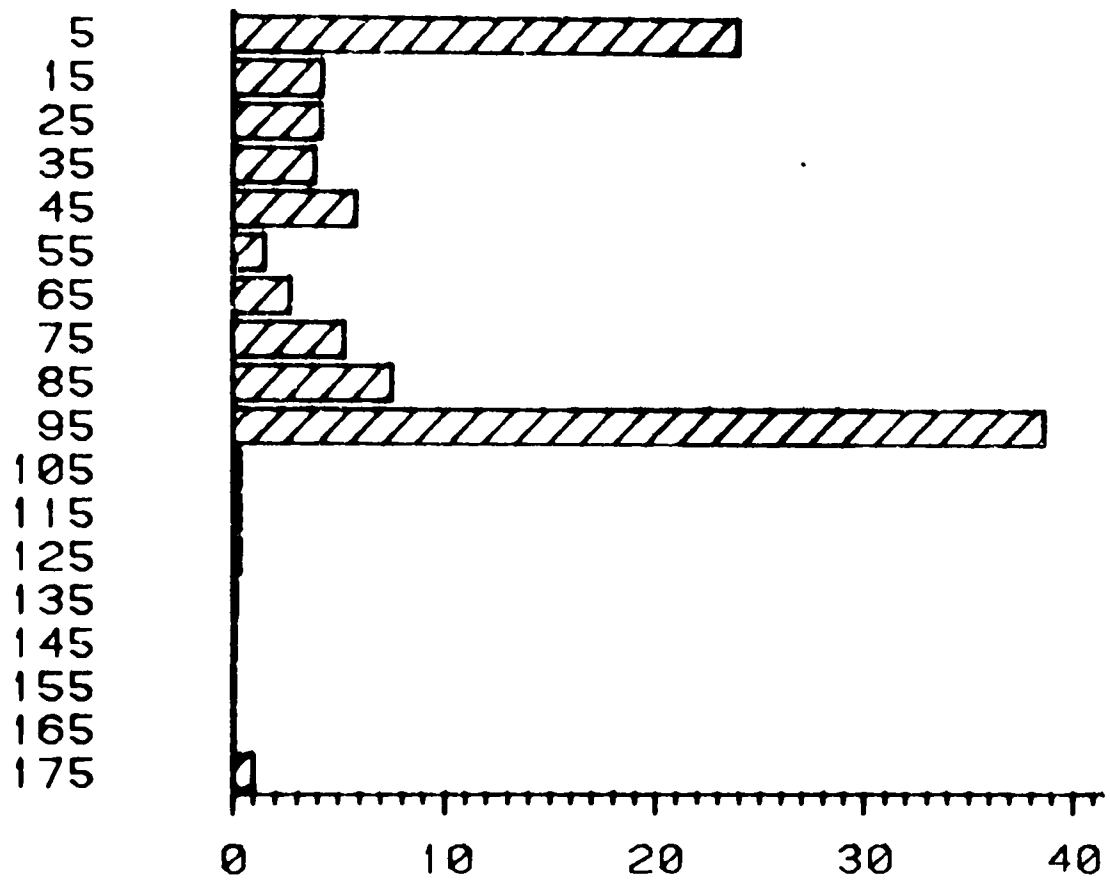

ANGLE	FREQ	CUM. FREQ	PERCENT	CUM. PERCENT
5	922	922	23.90	23.90
15	163	1085	4.22	28.12
25	160	1245	4.15	32.27
35	151	1396	3.91	36.18
45	224	1620	5.81	41.99
55	59	1679	1.53	43.52
65	105	1784	2.72	46.24
75	205	1989	5.31	51.56
85	290	2279	7.52	59.07
95	1486	3765	38.52	97.59
105	13	3778	0.34	97.93
115	15	3793	0.39	98.32
125	14	3807	0.36	98.68
135	6	3813	0.16	98.83
145	4	3817	0.10	98.94
155	1	3818	0.03	98.96
165	2	3820	0.05	99.02
175	38	3858	0.98	100.00

Figure 3.7: Predicted versus observed ratio for all installation angles, depths and treatments.

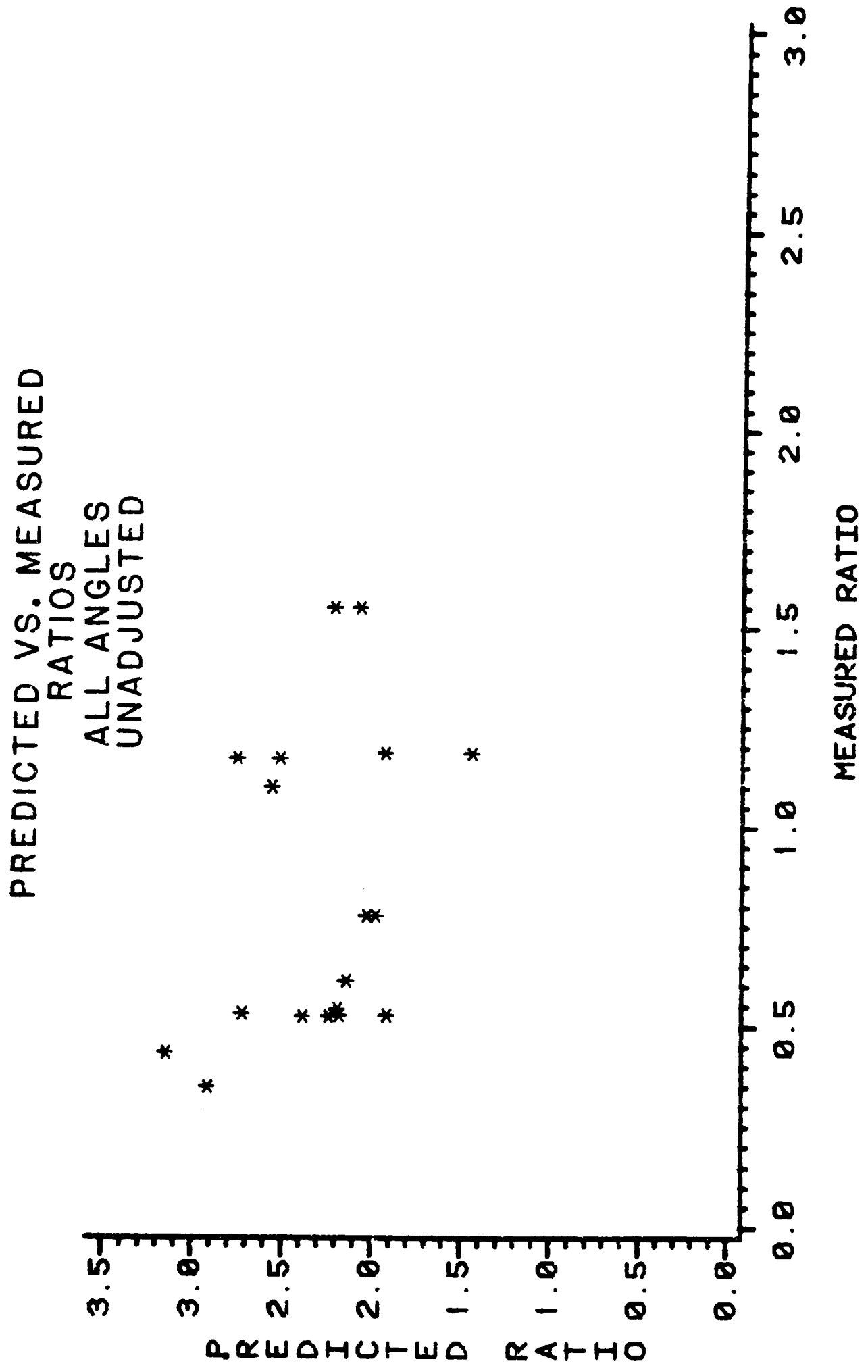
PREDICTED VS. MEASURED
RATIOS
ALL ANGLES
UNADJUSTED
PREDICTED RATIO
MEASURED RATIO
0.0
0.5
1.0
1.5
2.0
2.5
3.0
3.5

general larger than the observed ratio and does not go below 1.0 while the observed ratio had values as low as 0.3. From the model, a ratio less than one is an indication of upward root growth. Although the observed distribution included upward root growth the magnitude was small. The observed ratio was less than 1.0 over the majority of the profile and the season as can be seen in figure 3.8. In figure 3.8 each line and symbol represents a different observation date during the season. The ratio was fairly stable at most depths through the season, and was below 1.0, indicating the existence of upward root growth. The vertical line in figure 3.8 at a ratio of 2.0 indicates the value the model predicts for random root growth angles. Since the observed ratio is below this value, the root system is apparently more horizontal than random.

Because of the difficulty in determining the amount of upward root growth there may be error in the predicted ratio. To evaluate the impact of the upward root growth on the ratio an adjustment was made to the data and the a new predicted ratio calculated. The frequencies of the classes of angles above and below 90 degrees were averaged to yield a distribution symmetric around 90^{o}. That is, the average of the complementary classes in the first and second quadrant was determined and used to calculated the predicted ratio. The relationship between the predicted and observed ratio is shown in figure 3.9, for the adjusted distribution. Again there is not a tight coupling of the ratios but the predicted ratio is now within the same range as the observed. Approximately half of the predicted values are larger than the observed ratio.

Figure 3.8: Observed ratio versus soil depth for the 30^{o} installation angle. Day indicates observation date, as day of year.

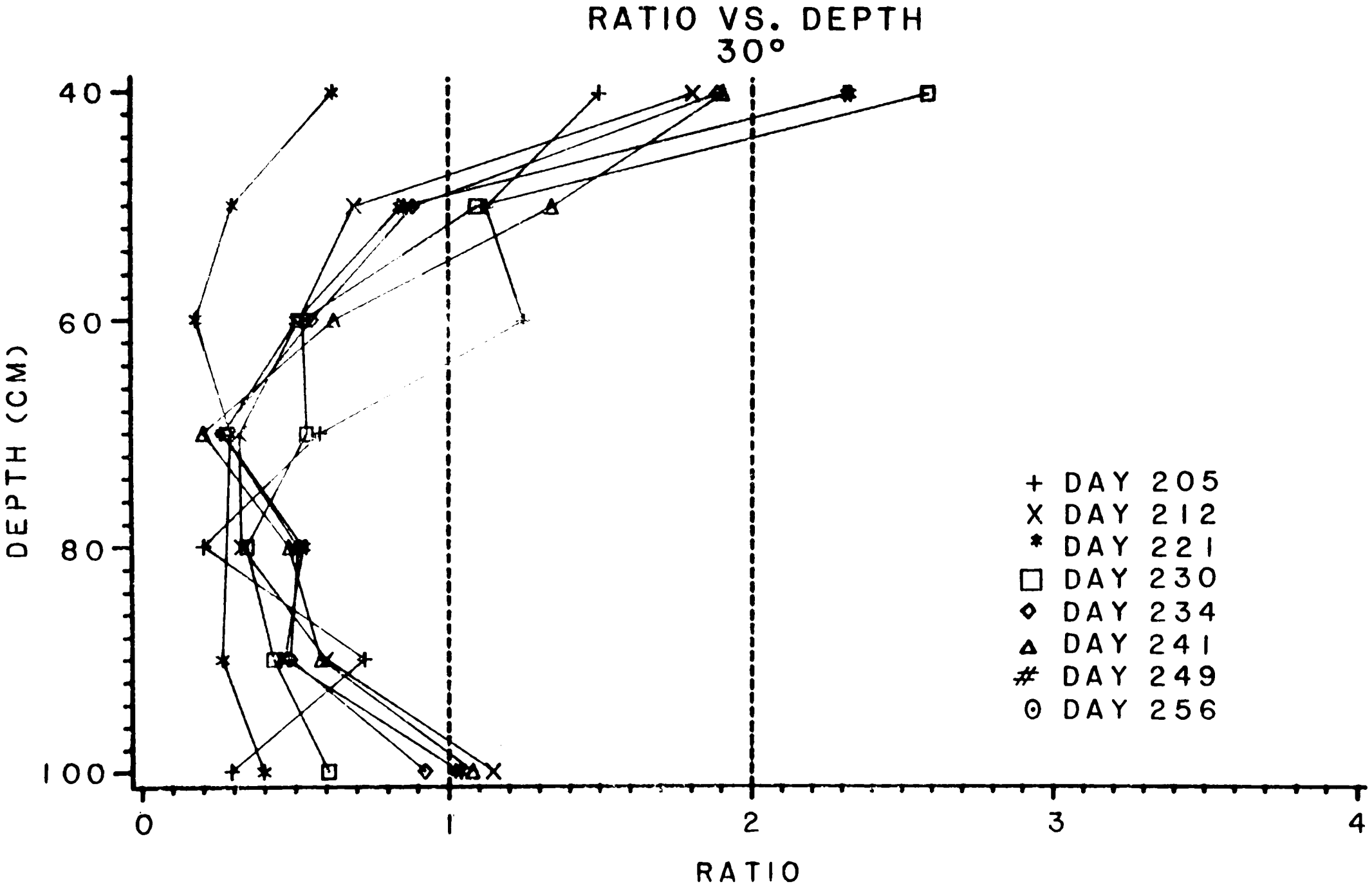
RATIO VS. DEPTH
30°
DEPTH (CM)
40
60
80
100
0
1
2
3
4
RATIO
+ DAY 205
X DAY 212
* DAY 221
□ DAY 230
◇ DAY 234
△ DAY 241
DAY 249
⊙ DAY 256

Figure 3.9: Predicted versus observed ratio for all installation angles, depths and treatments, using the adjusted frequency distribution.

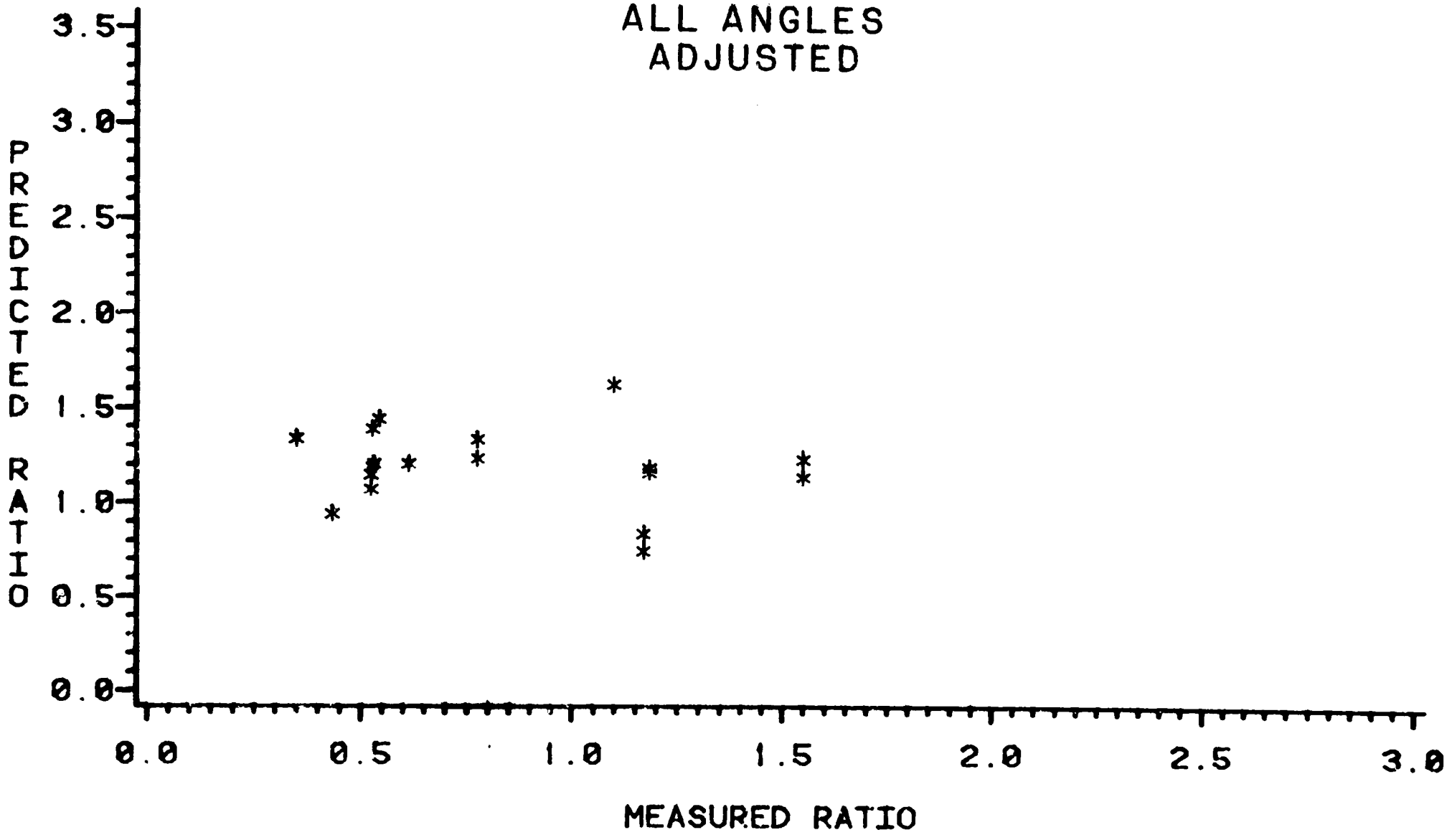
PREDICTED VS. MEASURED
RATIOS
ALL ANGLES
ADJUSTED
PREDICTED RATIO
3.5
3.0
2.5
2.0
1.5
1.0
0.5
0.0
0.0
0.5
1.0
1.5
2.0
2.5
3.0
MEASURED RATIO

Conclusions

Although the observed and predicted ratios did not show a tight coupling in the data collected, they were within the same range, and when the distribution was adjusted for upward root growth, the ratios tended toward the same absolute value. The range of values for the ratio was very narrow which would be expected from the observed frequency distributions. The distribution was similar for all depths and both treatments. The observed and predicted ratios can potentially vary from 0.0 to infinity, therefore the range between 0.0 and 3.5 is only a very small fraction of the potential values.

The observed ratio indicated the existence of upward root growth and a root system which was more horizontal than random. The observed frequency distribution provided evidence to support both of these observations. The largest fraction of the roots were horizontally oriented and upward root growth was apparent, but the magnitude was in question.

The testing has indicated the potential for the use of the minirhizotron to predict *in situ* root morphology, but has not totally validated the model. Another root system which has a substantially different root growth angle frequency distribution should provide the larger spread in the ratio values required to adequately assess the model.

CHAPTER IV

RELATIONSHIP BETWEEN INTERSECTIONS AND ROOT LENGTH DENSITY

Introduction

The relationship between the number of root intersections observed on the wall of a mini-rhizotron, and the root length density in the soil surrounding the tube has previously been established empirically. The relationships reported in the literature have been soil and crop specific, and also dependent upon the procedure used in making the counts. The intent of this project is to suggest a standardized procedure for making root counts and to establish a general relationship between counts of root intersections and root length density.

We suggested that the most appropriate parameter is the number of times that individual roots intersect the tube. Other parameters have been used to quantify the extent of root contact with the tube, such as the total length of root at the interface. Parameters such as the length of root are directly influenced by properties of the interface, independent of the soil surrounding the tube. If the soil adjacent to the tube has been compacted during installation, roots at the interface will have reduced extension rates. Conversely, if there are voids or loosened soil at the interface the root extension rate may be increased. The density of roots in the soil surrounding the tube should be the controlling factor in the number of intersections between roots and the soil-tube interface, not the properties of the interface. It is possi-

ble for a compacted zone to prevent a root from intersecting a tube if the compacted zone extends a significant distance from the tube. Also, a zone of soil around the tube which is of lower strength than the natural soil may encourage root branching thereby increasing the number of intersections. It is therefore imperative that care be taken when installing mini-rhizotrons. In developing this model it is assumed that the effect of the interface has been minimized. That is, a root which is growing in a direction that will intersect the tube will continue in that direction until the intersection occurs. The interface will affect the growth of the root only after it has intersected the tube.

A problem develops in the proposed procedure for measuring the extent of root contact when root branching occurs at the interface. The question is, Did the interface affect the extent of root branching? Measurements were reported in Upchurch and Ritchie (1983) on the branching intensity of roots at the interface of a mini-rhizotron and in the bulk soil surrounding the tube, with no significant difference being detected. Based on these measurements, we suggested that when a root branches at the soil-tube interface a count be recorded for the main root and for each branch observed.

In developing the model, we begin by considering a cylinder of soil equivalent to the volume occupied by a mini-rhizotron installed in the field. If counts are made of of roots at the exterior of the soil cylinder the number of root which penetrated the cylinder can be determined. This number should be directly related to the density of roots in the soil surrounding the cylinder. Based on the previous discussion,

the number of roots which intersect the mini-rhizotron is equivalent to the number of roots which would have penetrated that volume of soil had the tube not been there. The length of root inside a soil core can be estimated by the number of roots observed at the surface of the core, by assuming some average length for each root observed. The volume to associate with this length is then the volume of the soil core, thereby yielding an estimate of the root length density in the soil surrounding the core. With few modifications the root length density can be estimated from the number of root intersections observed on the wall of a mini-rhizotron. The problem is to determine the average length to associate with each intersection. A modification must be made in the volume associated with this length unless the entire circumference of the tube is observed and root intersections counted.

Mathematical Development of the Model

Consider a cylinder in space (figure 4.1), the general equation for this cylinder is;

$$\frac{x^2}{a^2} + \frac{y^2}{b^2} = 1 . \qquad (4.1)$$

Let this be a right circular cylinder of radius r and equation 4.1 becomes,

$$\frac{x^2}{r^2} + \frac{y^2}{r^2} = 1 . \qquad (4.2)$$

Now, translating this cylinder along the y axis such that the z

Figure 4.1: Generalized right circular cylinder centered on the origin.

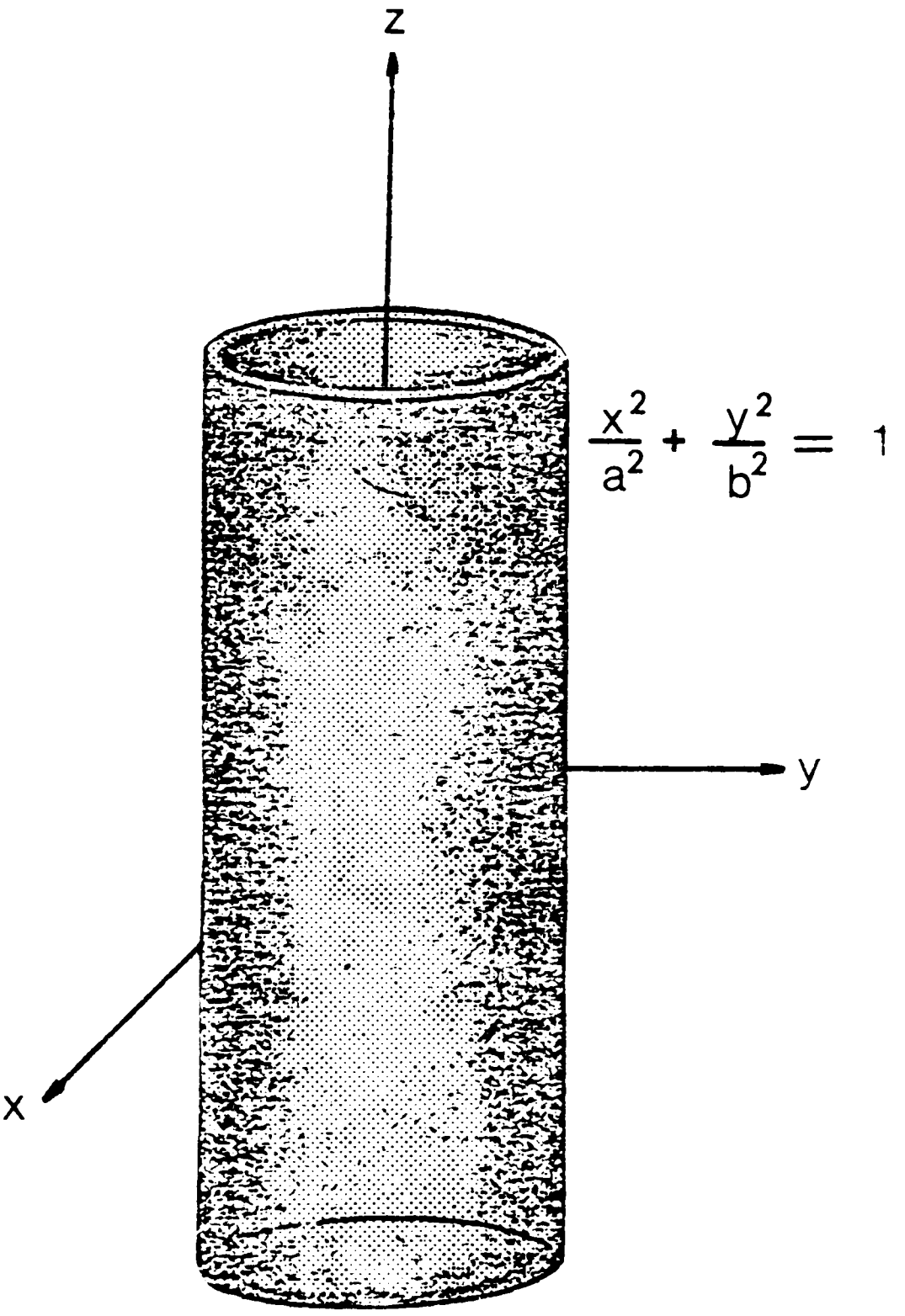
z
$\frac{x^2}{a^2} + \frac{y^2}{b^2} = 1$
y
x

axis forms a line on the cylinder and the cylinder intersects the x axis only at the origin we obtain, (figure 4.2)

$$\frac{x^2}{r^2} + \frac{(y-r)^2}{r^2} = 1 \quad . \tag{4.3}$$

We now rotate the axis through an angle g measured from the y axis in the yz plane, such that the cylinder is now at an angle g from the new axis (figure 4.3a). Let x, y' and z' represent the new axis system, then

$$y = y'\cos(g) - z'\sin(g). \tag{4.4}$$

Substituting for y in equation 4.3 yields,

$$\frac{x^2}{r^2} + \frac{(y'\cos(g) - z'\sin(g) - r)^2}{r^2} = 1 \quad . \tag{4.5}$$

We can now drop the primes from the y and z, and equation 4.5 will then represent a right circular cylinder in space which intersects the origin and makes an angle g with respect to the z axis (figure 4.3b). We will let this represent a mini-rhizotron installed at an angle g from vertical, with a diameter 2r. The origin will be assumed to be the point of intersection of the cylinder with a root. We will represent the root by a straight line segment intersecting the cylinder at the origin and forming angles α, β, γ and with the positive x, y, and z axis, respectively (figure 4.4a). We want to calculate the length of this line which would be internal to the cylinder if the line continued with

Figure 4.2: Right circular cylinder with radius, r, centered at (0,r,0).

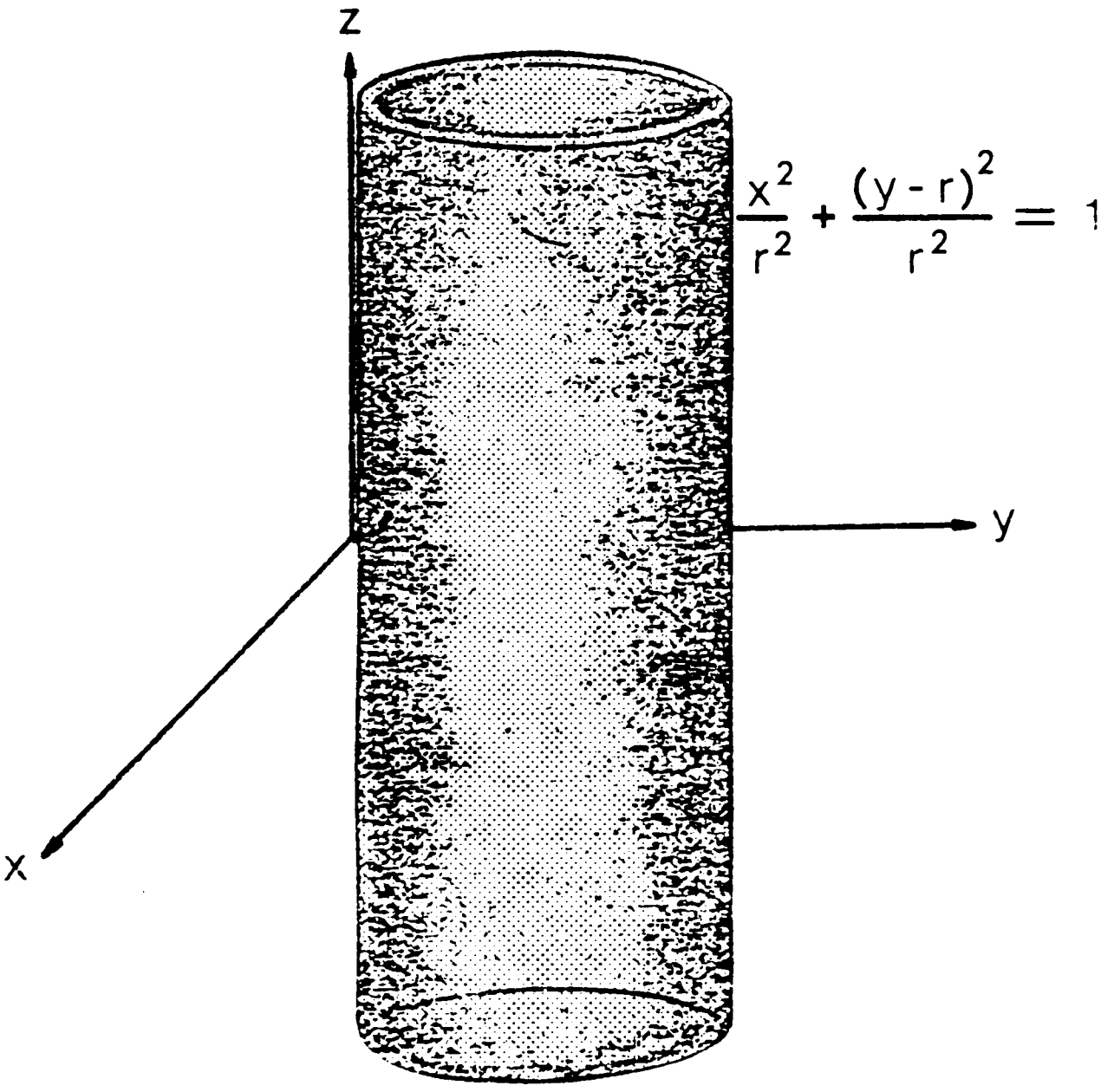
z
$\frac{x^2}{r^2} + \frac{(y-r)^2}{r^2} = 1$
y
x

Figure 4.3: a) Rotation of axis through and angle, g. b) the cylinder is then at an angle, g, with respect to a new axis system.

A

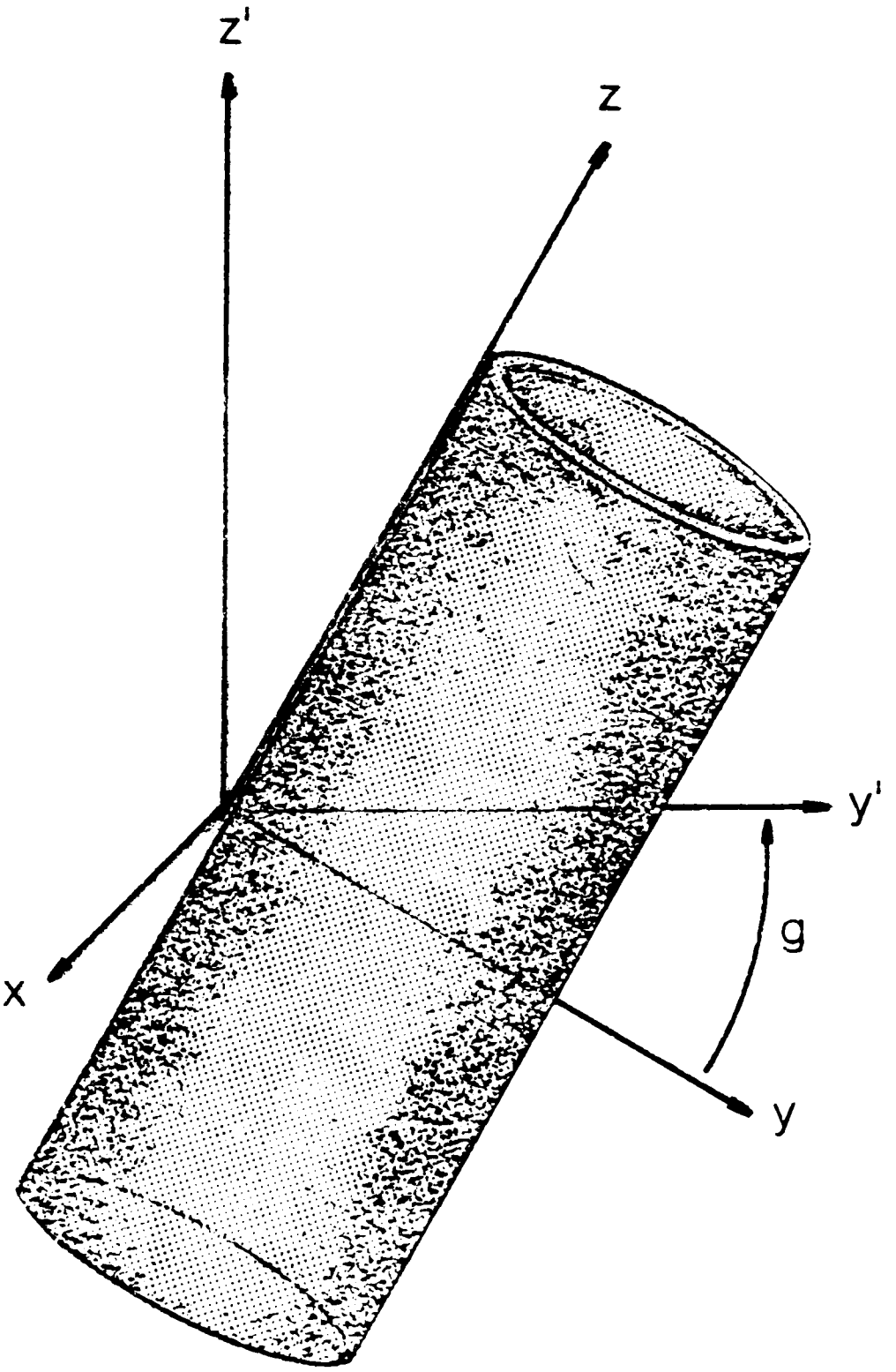

Figure 4.3: Continued

B

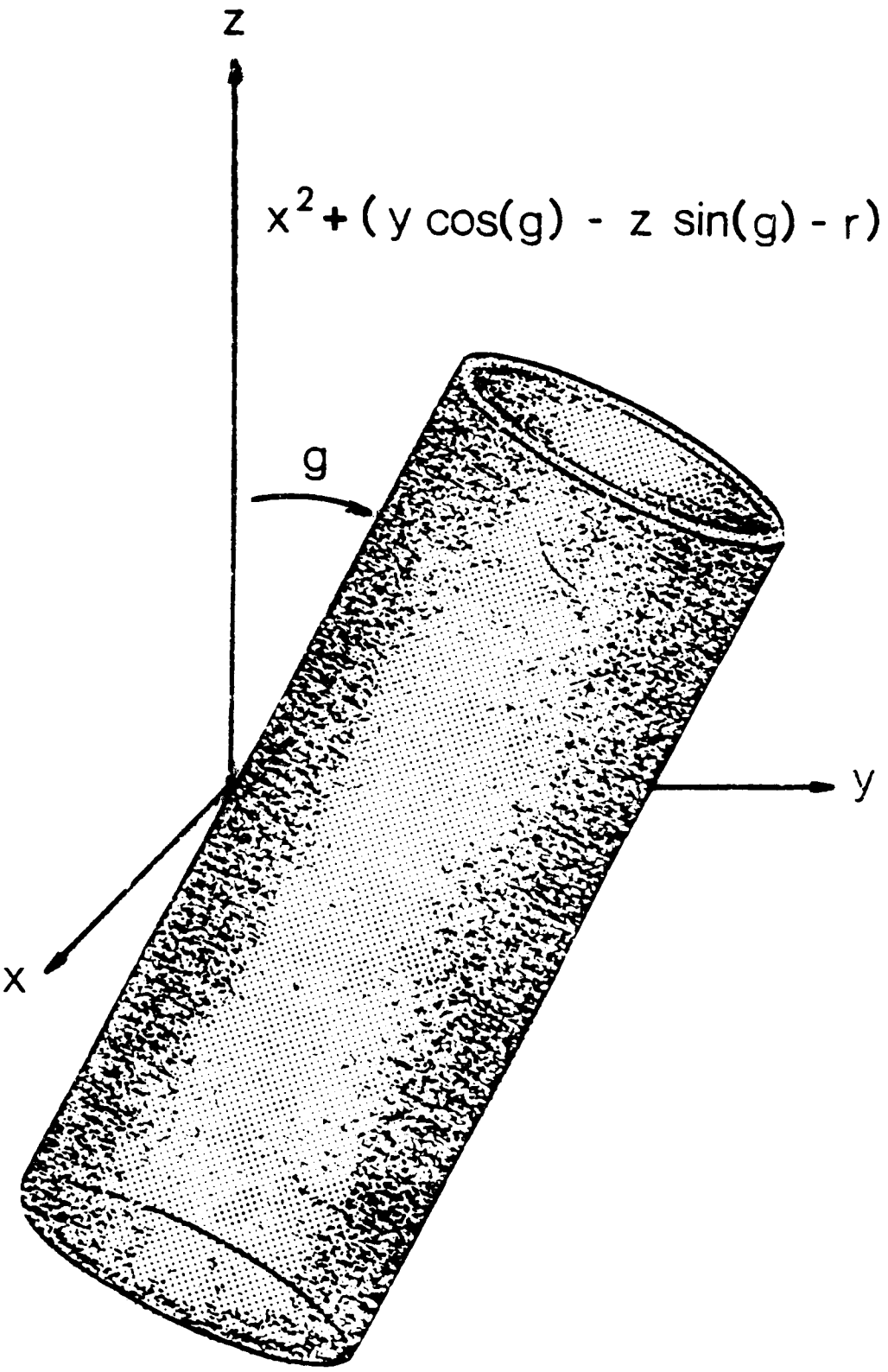

Figure 4.4: a) Intersection of line, with direction (α,β,γ), with b) cylinder. The points of intersection are the origin and (x,y,z).

A

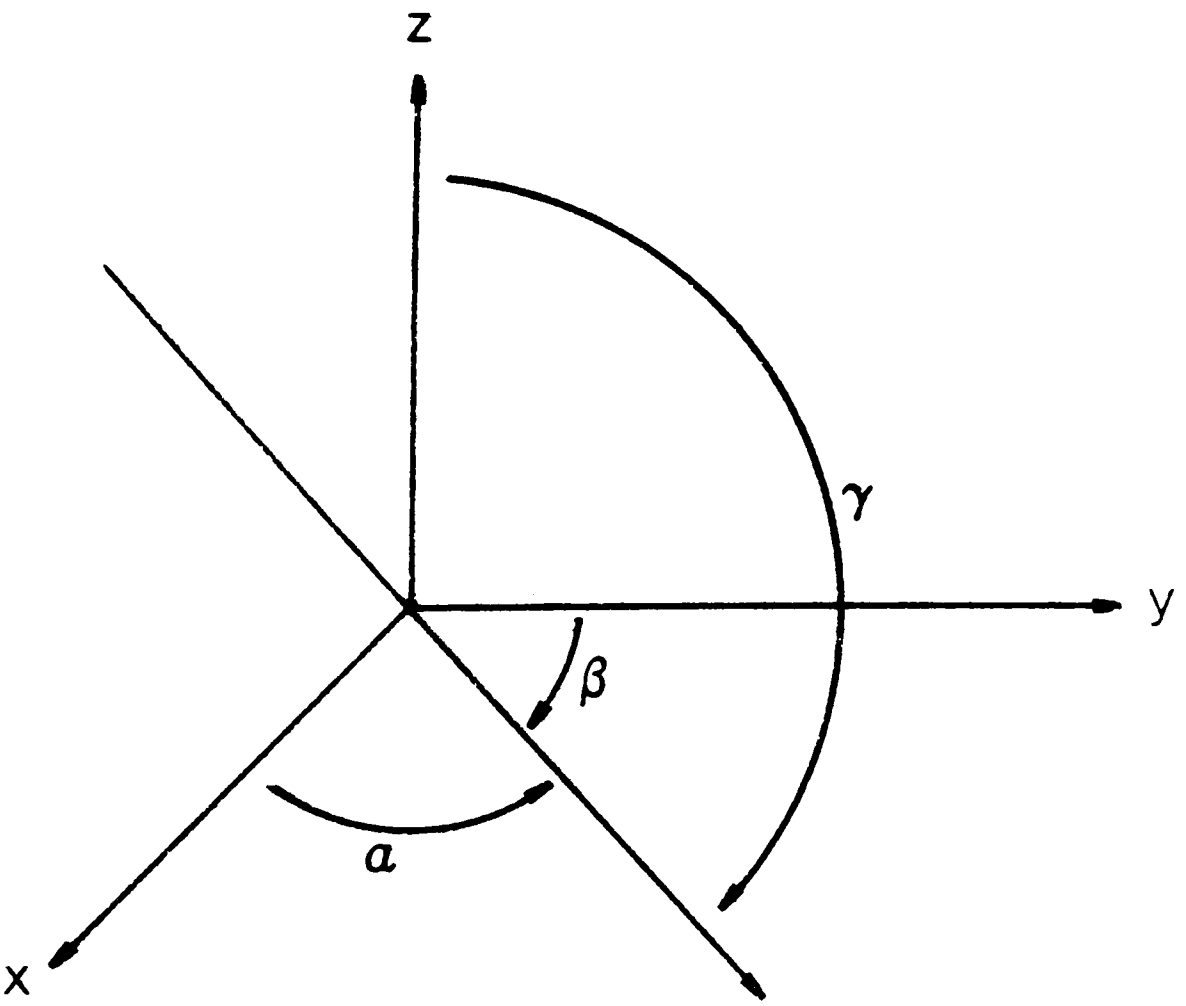

Figure 4.4: Continued

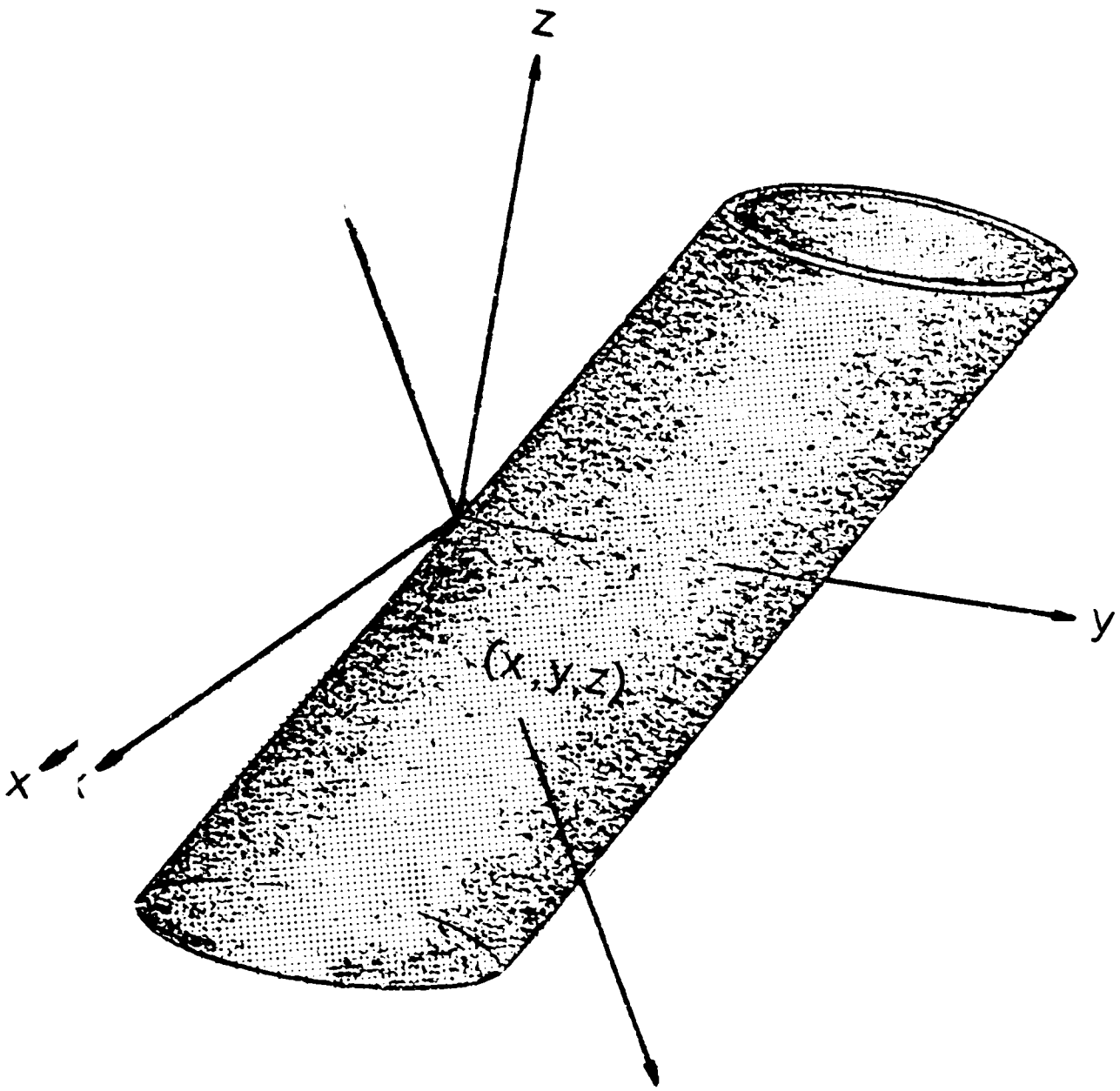
z
y
x
(x, y, z)

deviation. The line can be represented by,

$$\frac{x}{\cos(\alpha)} = \frac{y}{\cos(\beta)} = \frac{z}{\cos(\gamma)}. \tag{4.6}$$

where x, y, and z are the coordinates of the point at which the line exits the cylinder (figure 4.4b). Solving equation 4.6 for x and z in terms of y yields,

$$x = \frac{y\cos(\alpha)}{\cos(\beta)}$$

$$z = \frac{y\cos(\gamma)}{\cos(\beta)} \tag{4.7}$$

these expressions are then substituted into equation 4.5,

$$\left(\frac{y\cos(\alpha)}{\cos(\beta)}\right)^2 + \left(y\cos(g) - \frac{y\cos(\gamma)}{\cos(\beta)}\sin(g) - r\right)^2 = r^2$$

$$y^2\left[\left(\frac{\cos(\alpha)}{\cos(\beta)}\right)^2 + \left(\cos(g) - \frac{\sin(g)\cos(\gamma)}{\cos(\beta)}\right)\right]^2$$

$$- 2yr\left(\cos(g) - \frac{\sin(g)\cos(\gamma)}{\cos(\beta)}\right) = 0 \tag{4.8}$$

which can be solved for y using the quadratic formula.

We now convert to the cylindrical coordinate system for the further development of the system. A point will be represented by an ordered triplet (ρ, θ, γ) where ρ is the distance from the origin to the point, γ is the angle between the z axis and the line connecting the point with the origin, and θ is the angle that the projection of this line into the xy plane makes with the positive x axis (figure 4.5). In the cylindri-

Figure 4.5: Representation of a point (x,y,z) in cylindrical coordinates (ρ,θ,γ).

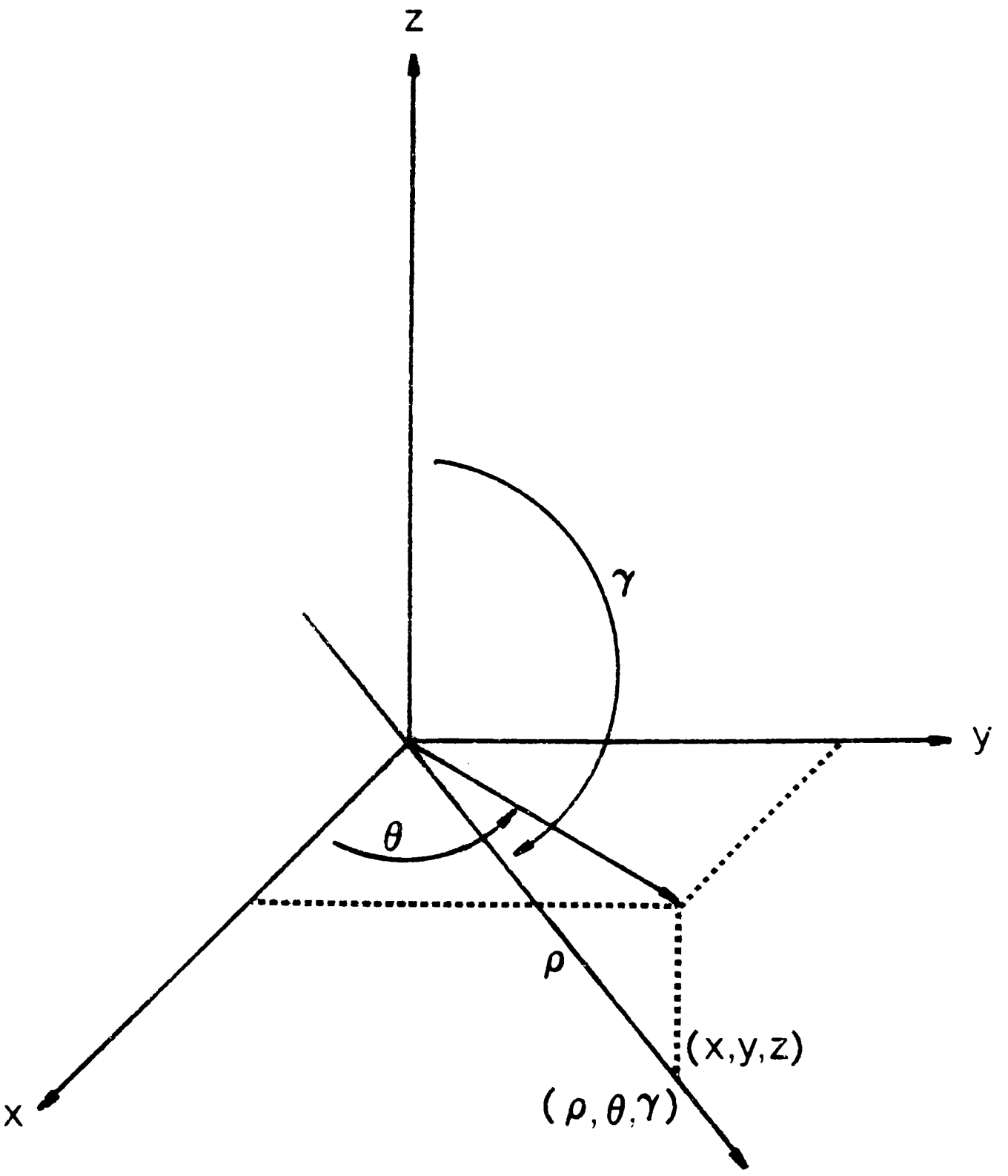
z
γ
y
θ
ρ
(x,y,z)
x
(ρ,θ,γ)

cal coordinate system,

$$Y = \rho \sin(\theta) \sin(\gamma)$$

$$\cos^2(\alpha) = 1 - \cos^2(\gamma) - \sin^2(\gamma) \sin^2(\theta)$$

$$\cos^2(\beta) = 1 - \cos^2(\gamma) - \sin^2(\gamma) \cos^2(\theta) \qquad (4.9)$$

which when substituted into equation 4.8 yields,

$$\rho^2 A + \rho B = 0 \qquad (4.10)$$

where,

$$A = \sin^2(\theta) \sin^2(\gamma) \left[\frac{1 - \cos^2(\gamma) - \sin^2(\gamma) \sin^2(\theta)}{1 - \cos^2(\gamma) - \sin^2(\gamma) \cos^2(\theta)} \right.$$

$$\left. + \left(\cos(g) - \frac{\sin(g) \cos(\gamma)}{\sqrt{1 - \cos^2(\gamma) - \sin^2(\gamma) \cos^2(\theta)}} \right)^2 \right] \qquad (4.10a)$$

and,

$$B = 2r \sin(\theta) \sin(\gamma) \left(\cos(g) - \frac{\sin(g) \cos(\gamma)}{\sqrt{1 - \cos^2(\gamma) - \sin^2(\gamma) \cos^2(\theta)}} \right). \qquad (4.10b)$$

Solving equation 4.10 for ,

$$\rho = \frac{-B}{A} \qquad (4.11)$$

since the negative root is always zero. ρ represents the length of the line which is internal to the cylinder, or the length of root displaced by the tube. The length, ρ, is then a function of the two angles, θ, γ and γ.

In order to estimate the total length of line which would be in-

ternal to the cylinder we should determine the average length for ρ over all possible values of θ and γ for a given r, L, and g. If all values of θ and γ have the same probability of occurrence then the average ρ is the double integral,

$$\text{Aver. } \rho = \frac{\int_a^b \int_c^d \rho(\theta,\gamma)\, d\theta\, d\gamma}{\int_a^b \int_c^d d\theta\, d\gamma} \quad . \tag{4.12}$$

If the values of θ and γ are not random, but follow some probability distribution then the average ρ is,

$$\text{Aver. } \rho = \frac{\int_a^b \int_c^d \rho(\theta,\gamma)\, f(\theta,\gamma) d\theta\, d\gamma}{\int_a^b \int_c^d d\theta \quad d\gamma} \tag{4.13}$$

where $f(\theta,\gamma)$ is the probability density function for the direction of root growth. If the assumption that roots can be represented by straight lines is invalid, a correction can be made to equation 4.13 by introducing a tortuousity term. This factor increases the length because of the tortuous path of the root and may or may not be a function of the root growth angle. If it is a function of the growth angle the term will be introduced inside the integral sign, if not it will be a constant multiple of the integral. The existence of an analytical solution to equation 4.13 is dependent upon the form of $f(\theta,\gamma)$, and

possibly the tortuousity, $t(\theta,\gamma)$. However, a numerical solution can be found for the integral if no analytical solution is available.

The average length determined by equation 4.13 can be multiplied by the number of roots observed at the interface to estimate the length factor in the root length density. The problem is to associate a volume with this length. If the entire circumference is observed the appropriate volume is the volume of the tube. However if only a fraction of the tube is observed this volume will be somewhat less than the volume of the tube.

The limits a, b, c, and d should be chosen such that every possible angle of intersection is considered. Since we have forced all intersections to occur at the origin which is on the top of the tube, we only need to consider those angles which will result in a top intersection. From Chapter III we know that a top intersection will only occur when,

$$0 \leq \theta \leq \pi \quad \text{and} \quad g \leq \gamma \leq \pi \tag{4.14a}$$

or,

$$\pi \leq \theta \leq \pi \quad \text{and} \quad (\pi - g) \leq \gamma \leq \ . \ \pi \tag{4.14b}$$

This integral implicitly considers the tube to be infinite in length. We will be dealing with segments of the tube of equal length, which will represent horizontal layers in the soil. Let the length of each interval be L, and let the intersection occur at the midpoint of the interval. The tube will be terminated at each end by planes which are normal to the z axis, and can be described by the equations, (figure 4.6),

$$\rho \cos(\gamma) = L/2 \tag{4.15a}$$

Figure 4.6: Termination of the cylinder by the planes $z = L/2$ and $z = -L/2$.

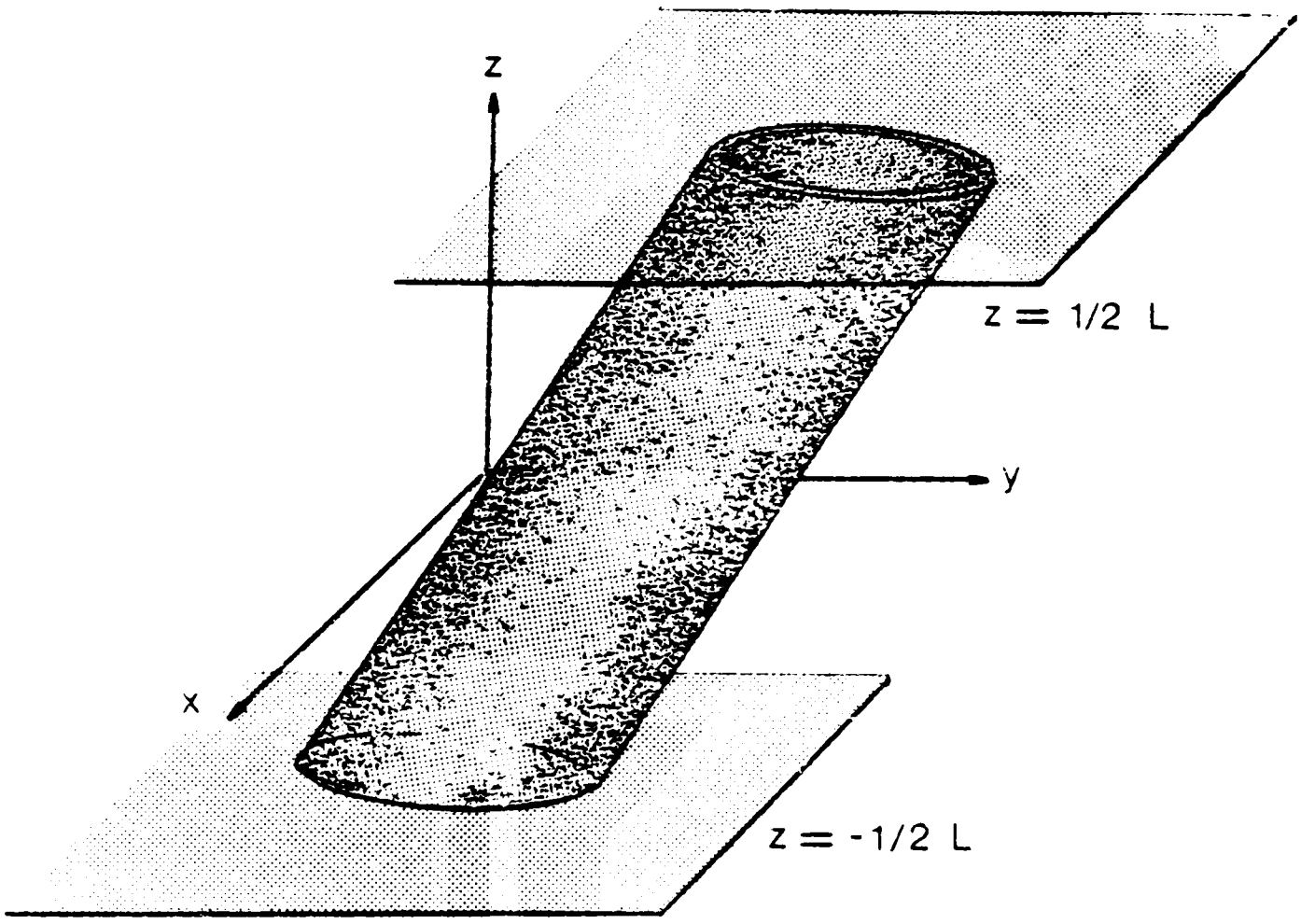
z
z = 1/2 L
y
x
z = -1/2 L

and,

$$\rho \cos(\gamma) = -L/2. \tag{4.15b}$$

Now we must consider those angles that will cause an intersection with the tube before the plane and those that will cause an intersection with the plane before the tube. Two possible conditions exists in the lower half space. The lower end of the tube may be totally in the left half space or it may be split between the left and right half space (figure 4.7). In the first case, figure 4.7a, we have the condition,

$$\frac{4r}{L \sin(g)} \leq 1 \tag{4.16a}$$

while in the second case, figure 4.7b, we have,

$$\frac{4r}{L \sin(g)} > 1 \quad . \tag{4.16b}$$

Figure 4.7c displays this relationship for three values of L. If the intersection point for a particular combination of r and sin(g) is above the line for L, then equation 4.16b is satisfied, and if it is below the line, equation 4.16a is satisfied.

The intersections between the line and the tube or plane can be divided into 10 regions. An average value for ρ will be found for each region and then the value for the appropriate regions will be averaged to obtain the desired average length. Table 4.1 gives the definition of the 10 regions in terms of three values for γ which will be defined in later sections.

Figure 4.7: Two conditions for the lower end of the cylinder a) case a, where the lower end does not intersect the xz plane, b) case b, where the lower end is divided by the xz plane, c) nomograph to predict the condition of the lower end of the cylinder. Each line represents the indicated observation interval. For points above the appropriate line case a applies and below the line case b applies.

A

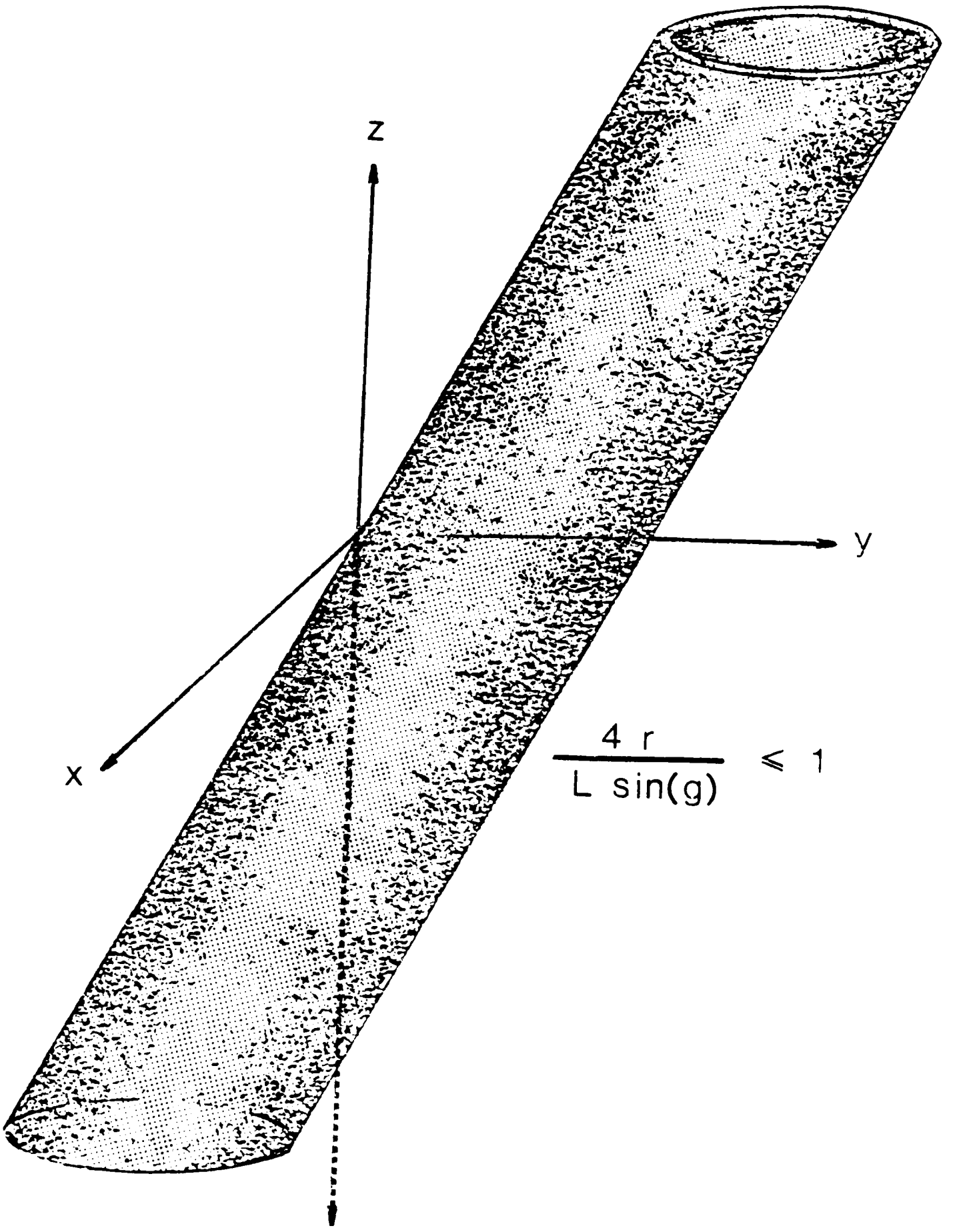

$$\frac{4\,r}{L\,\sin(g)} \leqslant 1$$

Figure 4.7: Continued

B

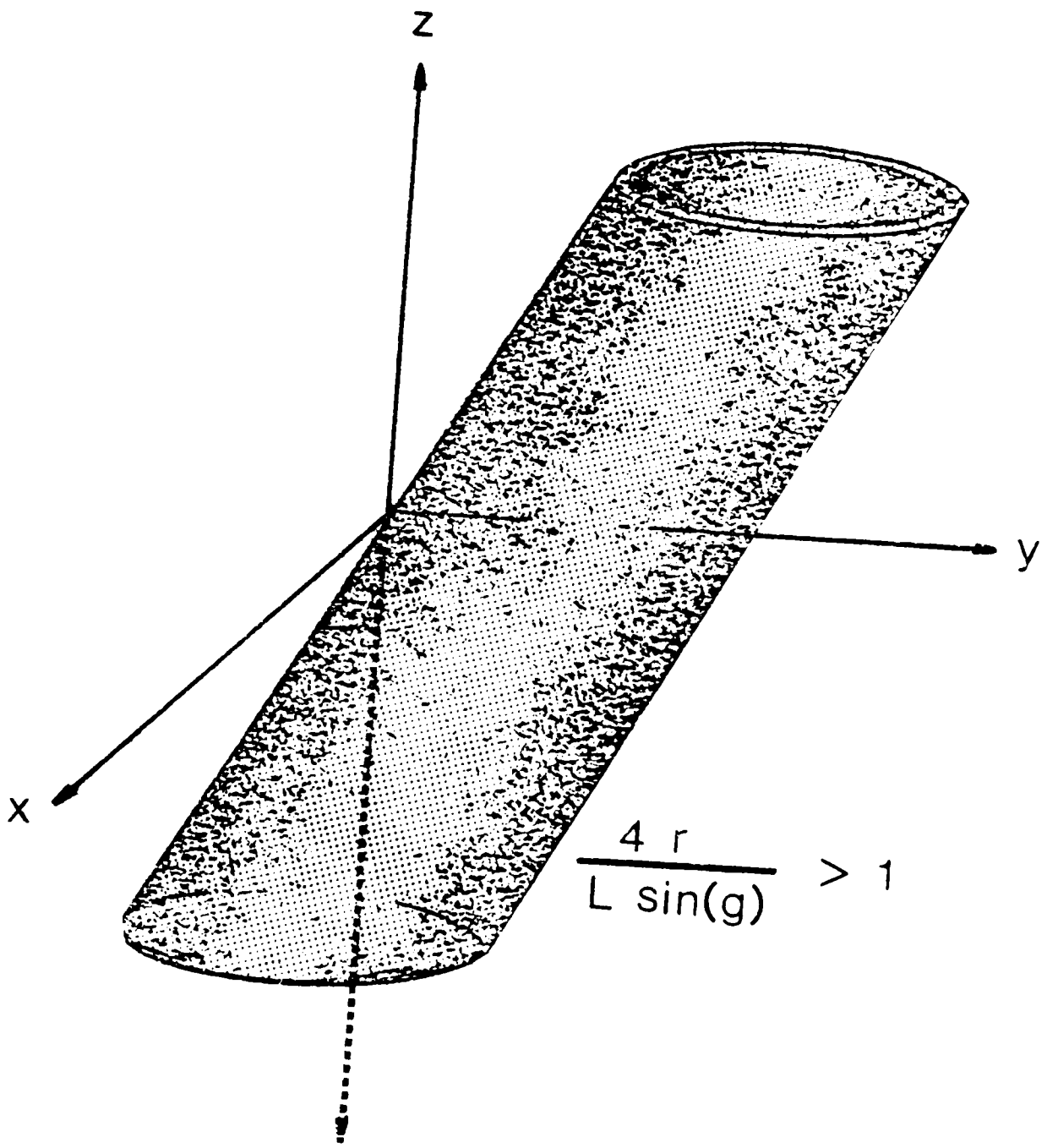

Figure 4.7: Continued

CASE NOMOGRAPH

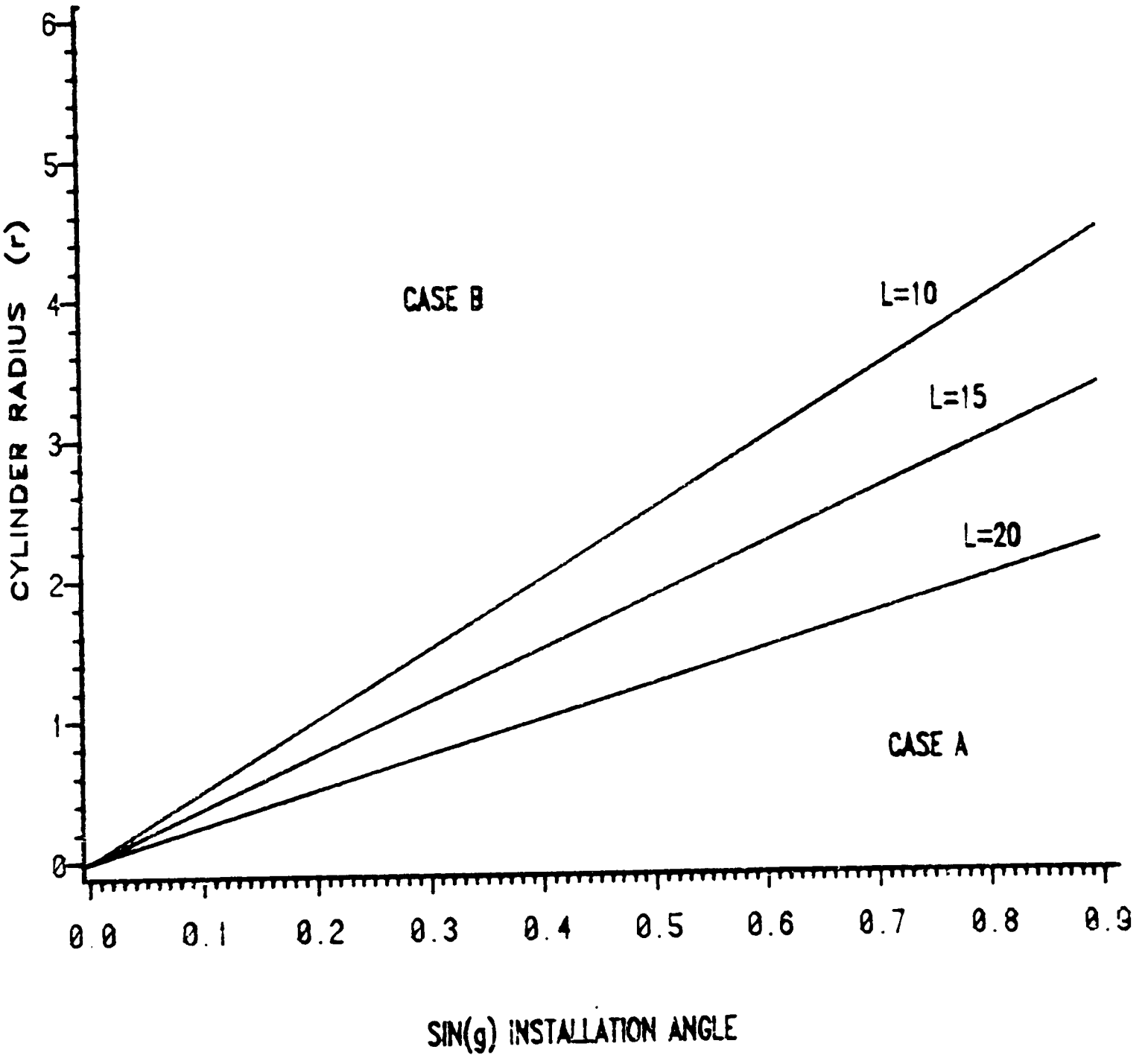

Table 4.1: Definition of the 10 regions to be used in calculating the average ρ.

Region				case involved
1	$0 \leq \theta \leq \pi$	$\gamma_2 \leq \gamma \leq \gamma_1$		a + b
2	$0 \leq \theta \leq \pi$	$\gamma < \gamma_2$	intersects tube	a + b
3	$0 \leq \theta \leq \pi$	$\gamma < \gamma_2$	intersects plane	a + b
4	$0 \leq \theta \leq \pi$	$\gamma_1 \leq \gamma \leq \pi$	intersects tube	b
5	$0 \leq \theta \leq \pi$	$\gamma_1 \leq \gamma \leq \pi$	intersects plane	b
6	$\pi \leq \theta \leq 2\pi$	$\gamma_3 \leq \gamma \leq \pi$		a
7	$\pi \leq \theta \leq 2\pi$	$\pi - g \leq \gamma \leq \gamma_3$	intersects tube	a
8	$\pi \leq \theta \leq 2\pi$	$\pi - g \leq \gamma \leq \gamma_3$	intersects plane	a
9	$\pi \leq \theta \leq 2\pi$	$\pi - g \leq \gamma \leq \pi$	intersects tube	b
10	$\pi \leq \theta \leq 2\pi$	$\pi - g \leq \gamma \leq \pi$	intersects plane	b

Region 1. In this region only the cylinder must be considered. The average ρ will be determined by considering only those values for γ which result in an intersection with the cylinder independent of the value of θ. This region is depicted in figure 4.8 for the two cases described in equation 4.16. In both cases γ_2 is,

$$\gamma_2 = \tan^{-1}\left[\tan(g) + \frac{4r}{L\cos(g)}\right] \tag{4.17a}$$

for case a (equation 4.16a is satisfied) γ_1 is π. However for case b (equation 4.16b is satisfied) γ_1 is,

$$\gamma_1 = \tan^{-1}\left[\tan(g) - \frac{4r}{L\cos(g)}\right]. \tag{4.17b}$$

Figure 4.8: Limits of integration for region 1 for a) case a and b) case b.

A

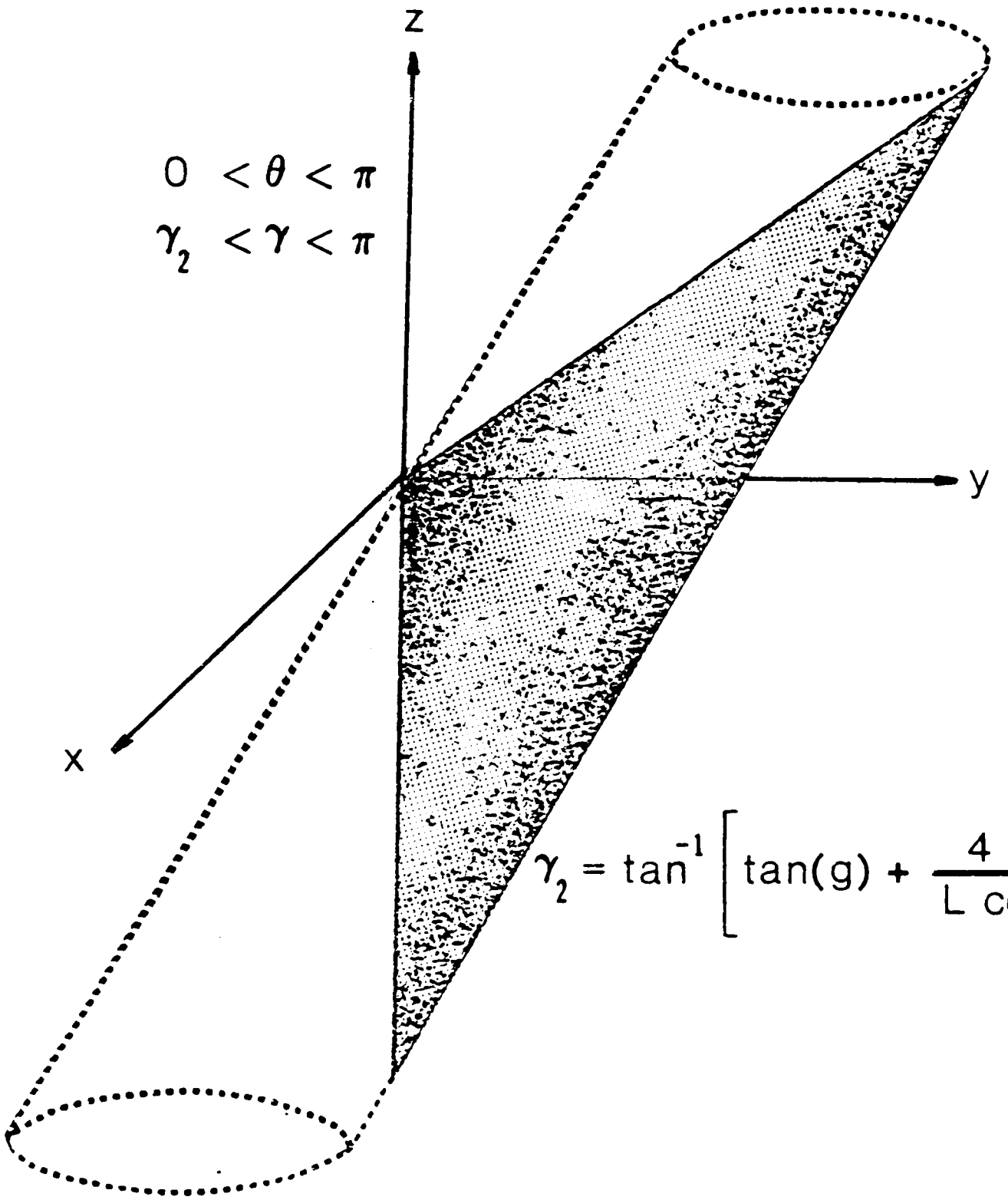

$$\gamma_2 = \tan^{-1}\left[\tan(g) + \frac{4\ r}{L\ \cos(g)}\right]$$

Figure 4.8: Continued

B

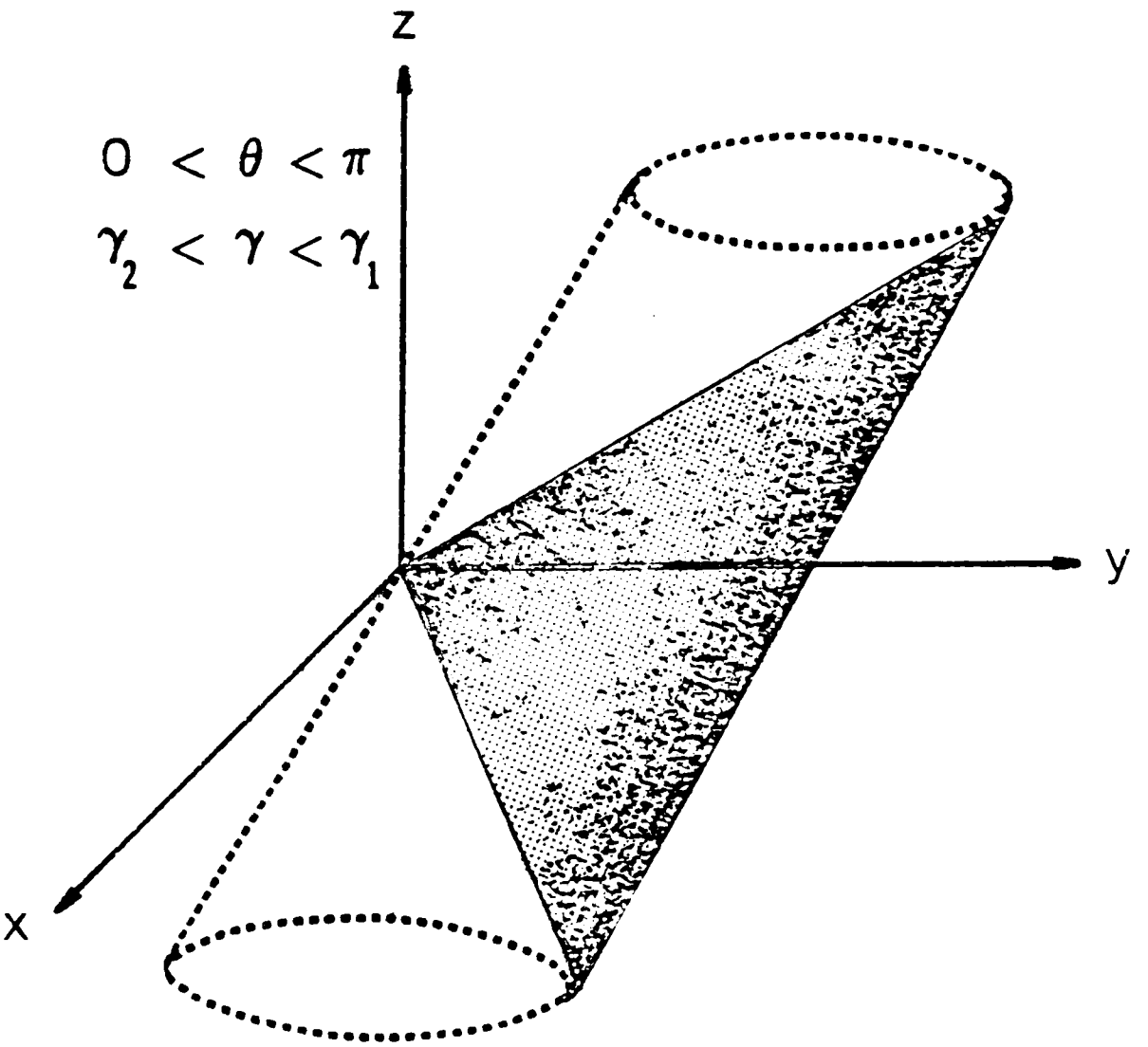

$$\gamma_1 = \tan^{-1}\left[\tan(g) - \frac{4\ r}{L\ \cos(g)}\right]$$

Applying these limits the average ρ for region 1 is

$$\rho_1 = \frac{\int_{\gamma_2}^{\gamma_1} \int_{0}^{\pi} \rho(\theta,\gamma)\, d\theta \; d\gamma}{\int_{\gamma_2}^{\gamma_1} \int_{0}^{\pi} d\theta \; d\gamma} \quad . \tag{4.18}$$

Region 2. Within this region intersections with both the cylinder and the plane must be considered. This region will consider the area above the area covered by region 1 (figure 4.9). There will be a narrow range for θ in that for certain values of θ no intersection with the plane can occur. Two values for θ will be determined to define this range. θ_1 is the angle in the xy plane between the x axis and a line formed by connecting the origin with the point of intersection between a line perpendicular to the positive x axis and tangent to the projection into the xy plane of the ellipse formed by the intersection of the cylinder and the plane z = L/2. θ_2 is the angle formed similar to θ_1 but the tangent line being perpendicular to the negative x axis. θ_1 and θ_2 are shown in figure 4.10 and are defined by,

$$\theta_1 = \tan^{-1}\left[\frac{1}{\cos(g)} + \frac{L\tan(g)}{2r}\right]$$

$$\theta_2 = \frac{\pi}{2} + \tan^{-1}\left[\frac{r}{\frac{r}{\cos(g)} + \frac{L\tan(g)}{2}}\right] . \tag{4.19}$$

Figure 4.9: Limit of integration for region 2, applies to both case a and b.

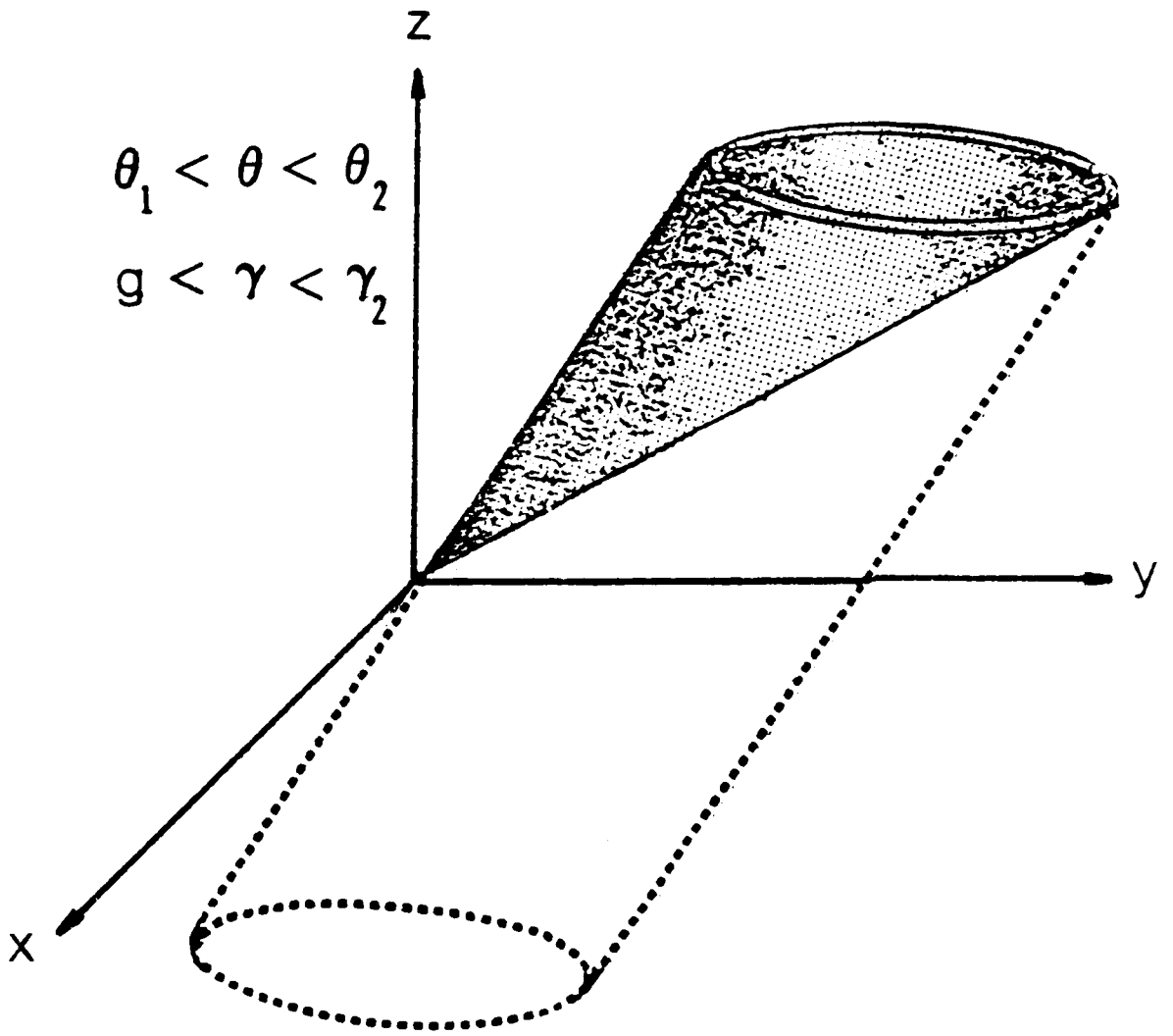
z
$\theta_1 < \theta < \theta_2$
$g < \gamma < \gamma_2$
y
x

Figure 4.10: Limits of θ for region 2.

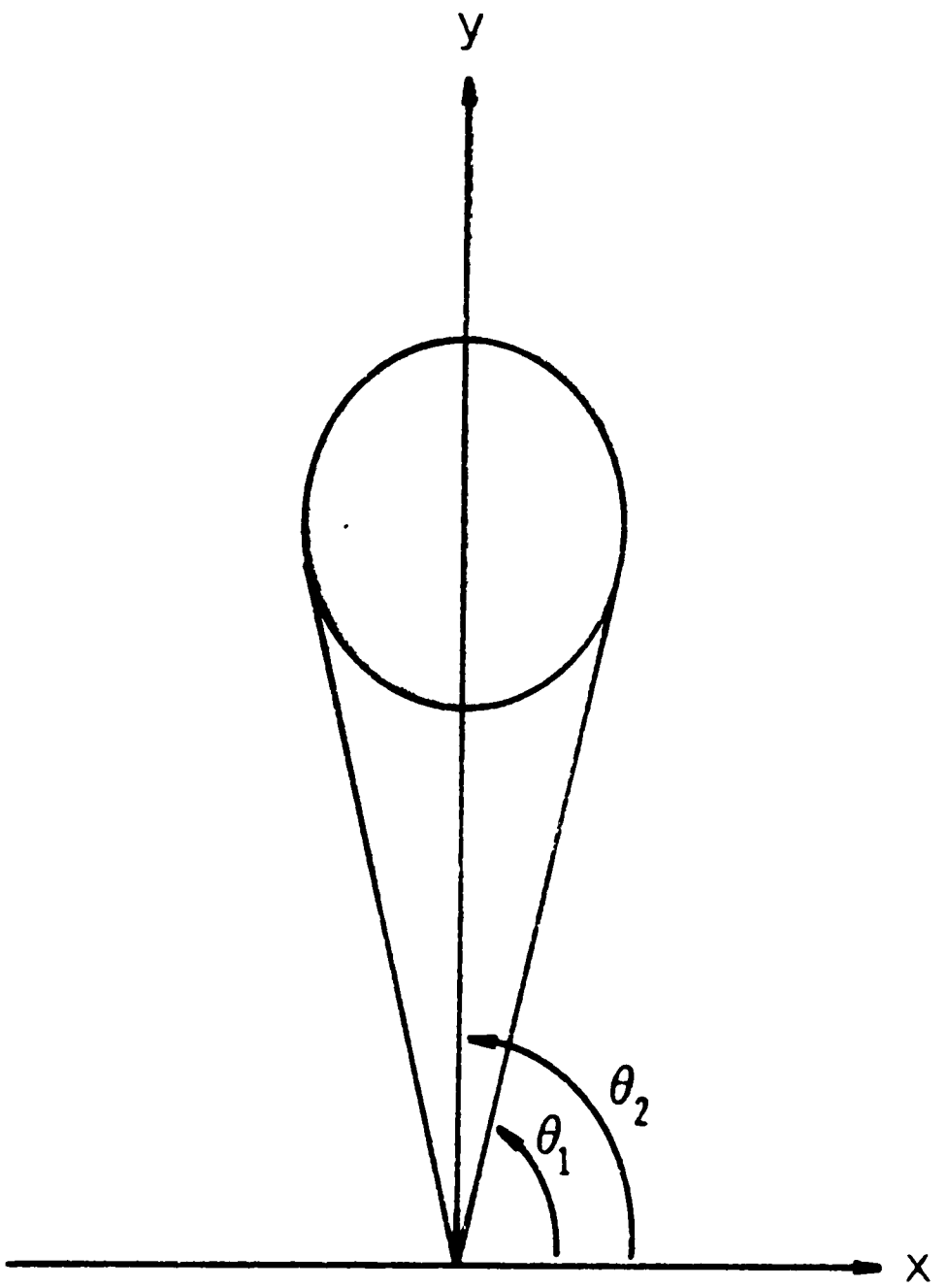

$$\theta_1 = \tan^{-1}\left[\frac{1}{\cos\{g\}} + \frac{L\ \tan\{g\}}{2\ r}\right]$$

$$\theta_2 = \pi/2 + \tan^{-1}\left[\frac{r}{r/\cos\{g\} + L\ \tan\{g\}/2}\right]$$

Within the range of θ defined above we must define the limits of the cylinder-plane intersection. We will define the limits of γ in terms of θ. The cylinder is described by equation 4.5, and its intersection with the plane will be described by replacing z with L/2. In cylindrical coordinates,

$$\begin{aligned} X &= \rho \sin(\gamma) \cos(\theta) \\ Y &= \rho \sin(\gamma) \sin(\theta) \\ Z &= \rho \cos(\gamma) \end{aligned} \tag{4.20}$$

but since z is fixed by the plane,

$$\rho = \frac{L}{2\cos(\gamma)} \tag{4.21}$$

therefore,

$$\begin{aligned} X &= \frac{L \tan(\gamma) \cos(\theta)}{2} \\ Y &= \frac{L \tan(\gamma) \sin(\theta)}{2} \\ Z &= L/2. \end{aligned} \tag{4.22}$$

Substituting into equation 4.5 and rearranging we have,

$$A \tan^2(\gamma) + B \tan(\gamma) + C = 0 \tag{4.23}$$

where,

$$\begin{aligned} A &= \frac{L^2 \cos^2(\theta)}{4} + \frac{L^2 \sin^2(\theta) \cos^2(g)}{4} \\ B &= -\left(\frac{L^2 \sin(\theta) \sin(g) \cos(g)}{2} + rL \sin(\theta) \cos(g) \right) \\ C &= \frac{L^2 \sin^2(g)}{4} + rL \sin(g) \end{aligned} . \tag{4.24}$$

Solving for γ we have,

$$\gamma(\theta) = \tan^{-1}\left[\frac{-B \pm \sqrt{B^2 - 4AC}}{2A}\right] . \tag{4.25}$$

We must know which of the two roots will yield the largest value for γ. Since γ is in the first quadrant its tangent will be positive, therefore the largest argument will yield the largest value of γ. Let the limits of γ be,

$$\gamma_1(\theta) = \tan^{-1}\left[\min\left(\frac{-B \pm \sqrt{B^2 - 4AC}}{2A}\right)\right]$$

$$\gamma_2(\theta) = \tan^{-1}\left[\max\left(\frac{-B \pm \sqrt{B^2 - 4AC}}{2A}\right)\right] . \tag{4.26}$$

The intersections with the cylinder will be split into two subregions.

The average ρ in these regions will be,

$$\rho_{2_1} = \frac{\int_{\theta_1}^{\theta_2}\int_{g}^{\gamma_1(\theta)} \rho(\theta,\gamma)\, d\gamma\, d\theta}{\int_{\theta_1}^{\theta_2}\int_{g}^{\gamma_1(\theta)} d\gamma\, d\theta} \tag{4.27a}$$

and,

$$\rho_{2_2} = \frac{\int_{\theta_1}^{\theta_2} \int_{\gamma_2(\theta)}^{\gamma_2} \rho(\theta,\gamma)\, d\gamma \quad d\theta}{\int_{\theta_1}^{\theta_2} \int_{\gamma_2(\theta)}^{\gamma_2} d\gamma \quad d\theta} \tag{4.27b}$$

where γ_2 is defined in region 1.

Region 3. In this region only intersections with the plane must be considered. This is the area of region 2 where the line intersects the plane, not the cylinder. The average ρ in this region is

$$\rho_3 = \frac{\int_{\theta_1}^{\theta_2} \int_{\gamma_1(\theta)}^{\gamma_2(\theta)} \frac{L}{2\cos(\gamma)}\, d\gamma \quad d\theta}{\int_{\theta_1}^{\theta_2} \int_{\gamma_1(\theta)}^{\gamma_2(\theta)} d\gamma \quad d\theta} \tag{4.28}$$

where the limits are defined in region 2.

Region 4. When equation 4.16b is satisfied, the lower end of the cylinder is divided by the xz plane such that we must consider the intersection of the plane, z= -L/2, and the cylinder on both sides of the xz plane. We have accounted for the area where γ is less than γ_1 in

region 1, now we will consider the area where γ is greater than γ_1. We will define the limits of the ellipse formed by the cylinder by considering γ to be a function of θ. Following the same procedure used in region 2, but letting $z = -L/2$, we can solve for γ. The result will be equation 4.25 with,

$$A = \frac{L^2 \cos^2(\theta)}{4} + \frac{L^2 \sin^2(\theta) \cos^2(g)}{4}$$

$$B = rL \sin(\theta) \cos(g) - \frac{L^2 \sin(\theta) \sin(g) \cos(g)}{2}$$

$$C = \frac{L^2 \sin^2(g)}{4} - rL \sin(g) \quad . \tag{4.29}$$

This will yield two solutions for γ, one will be in the first quadrant and the other in the second quadrant. In the second quadrant the tangent is negative therefore the argument must be negative. It can be seen that the negative root will result in the correct solution; therefore,

$$\gamma(\theta) = \tan^{-1}\left[\frac{-B - \sqrt{B^2 - 4AC}}{2A}\right] \tag{4.30}$$

will define the limits of the ellipse. The average ρ for this region is then,

$$\rho_4 = \frac{\int_0^{\pi} \int_{\gamma 1}^{\gamma(\theta)} \rho(\theta,\gamma)\, d\gamma \; d\theta}{\int_0^{\pi} \int_{\gamma_1}^{\gamma(\theta)} d\gamma \; d\theta} \tag{4.31}$$

where γ_1 has been defined previously. This describes the intersections with the cylinder. This region is shown in figure 4.11.

Region 5. In region 4 equation 4.31 described the average ρ for intersections with the cylinder. Region 5 considers the intersections with the plane in the same area. The average ρ is

$$\rho_5 = \frac{\int_0^{\pi} \int_{\gamma(\theta)}^{\pi} \frac{-L}{2\cos(\gamma)} \, d\gamma \, d\theta}{\int_0^{\pi} \int_{\gamma(\theta)}^{\pi} d\gamma \, d\theta} \tag{4.32}$$

with γ_1 and $\gamma(\theta)$ defined previously.

Region 6. This region involves the case when equation 4.16a is satisfied and is shown in figure 4.12. In this area all intersections will be with the cylinder for γ greater than γ_3 and θ between π and 2π. The angle γ_3 is defined as,

$$\gamma_3 = \tan^{-1}\left[\frac{4r}{L\cos(g)} - \tan(g)\right]. \tag{4.33}$$

The average ρ in this region is,

$$\rho_6 = \frac{\int_{\gamma_3}^{\pi} \int_{\pi}^{2\pi} \rho(\theta,\gamma) d\theta \quad d\gamma}{\int_{\gamma_3}^{\pi} \int_{\pi}^{2\pi} d\theta \quad d\gamma}. \tag{4.34}$$

Figure 4.11: Limits of integration for region 4, applies only to case b.

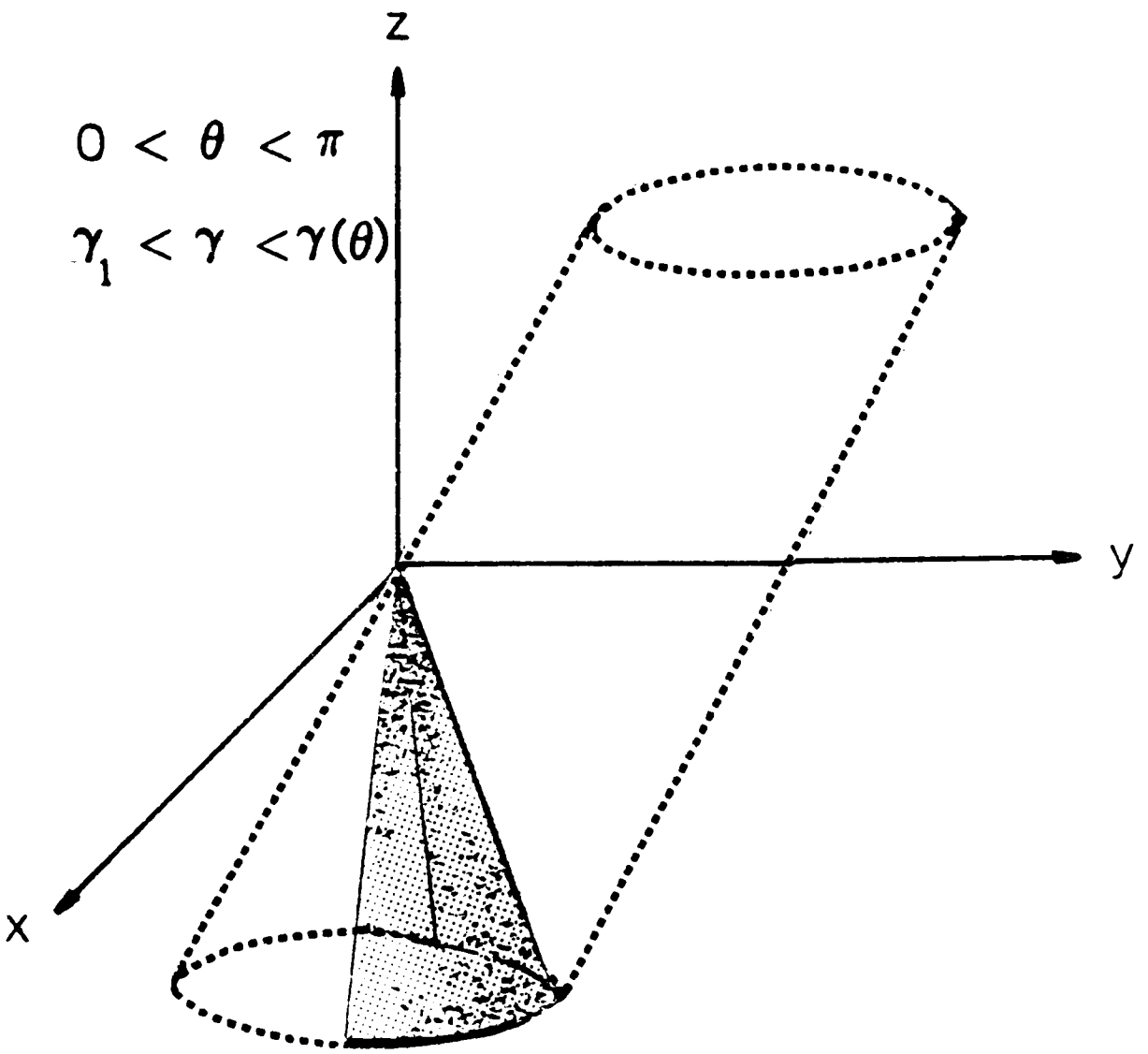
z
$0 < \theta < \pi$
$\gamma_1 < \gamma < \gamma(\theta)$
y
x

Figure 4.12: Limits of integration for region 6, applies only to case a.

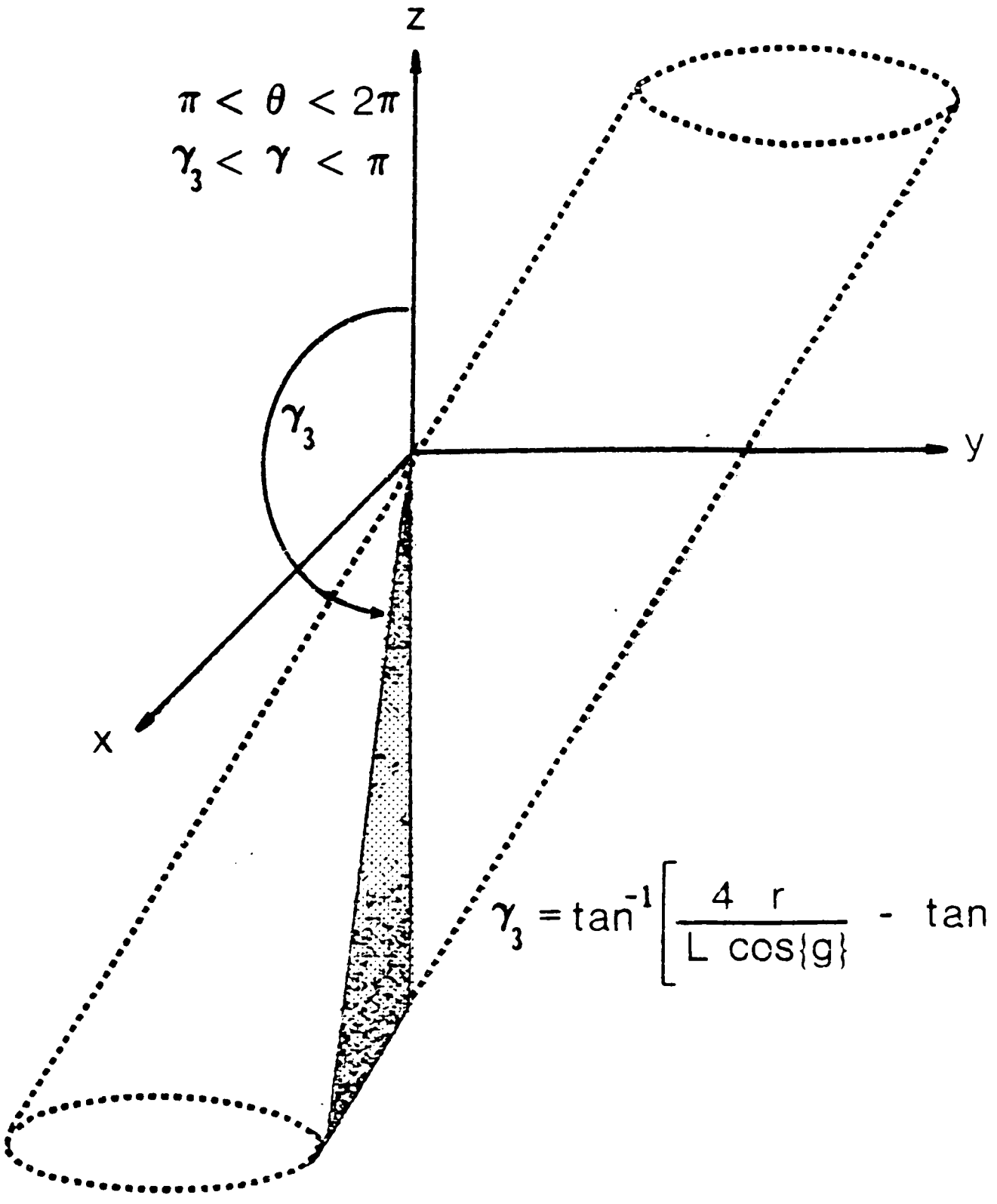

$$\gamma_3 = \tan^{-1}\left[\frac{4\ r}{L\ \cos\{g\}} - \tan g\right]$$

Region 7. This region is similar to region 2 in that intersections will occur for a narrow range of θ. We must consider intersections with both the cylinder and the plane which terminates the cylinder. The region is displayed in figure 4.13. This region will only apply when equation 4.16a is satisfied. The limits of the ellipse are defined in a manner similar to that used in other regions, and result in,

$$\theta_1 = \pi + \tan^{-1}\left[\frac{L\tan(g)}{2r} - \frac{1}{\cos(g)}\right]$$

$$\theta_2 = \frac{3\pi}{2} + \tan^{-1}\left[\frac{r}{\frac{L\tan(g)}{2} - \frac{r}{\cos(g)}}\right]$$

$$\gamma_1(\theta) = \tan^{-1}\left[\min\left(\frac{-B\pm\sqrt{B^2 - 4AC}}{2A}\right)\right]$$

$$\gamma_2(\theta) = \tan^{-1}\left[\max\left(\frac{-B\pm\sqrt{B^2 - 4AC}}{2A}\right)\right] \qquad (4.35)$$

where,

$$A = \frac{L^2\cos^2(\theta)}{4} + \frac{L^2\sin^2(\theta)\cos^2(g)}{4}$$

$$B = rL\sin(\theta)\cos(g) - \frac{L^2\sin(\theta)\sin(g)\cos(g)}{2}$$

$$C = \frac{L^2\sin^2(g)}{4} - rL\sin(g) \qquad (4.36)$$

The region must be divided into two subregions as in region 2. The

Figure 4.13: Limits of integration for region 7, applies only to case a.

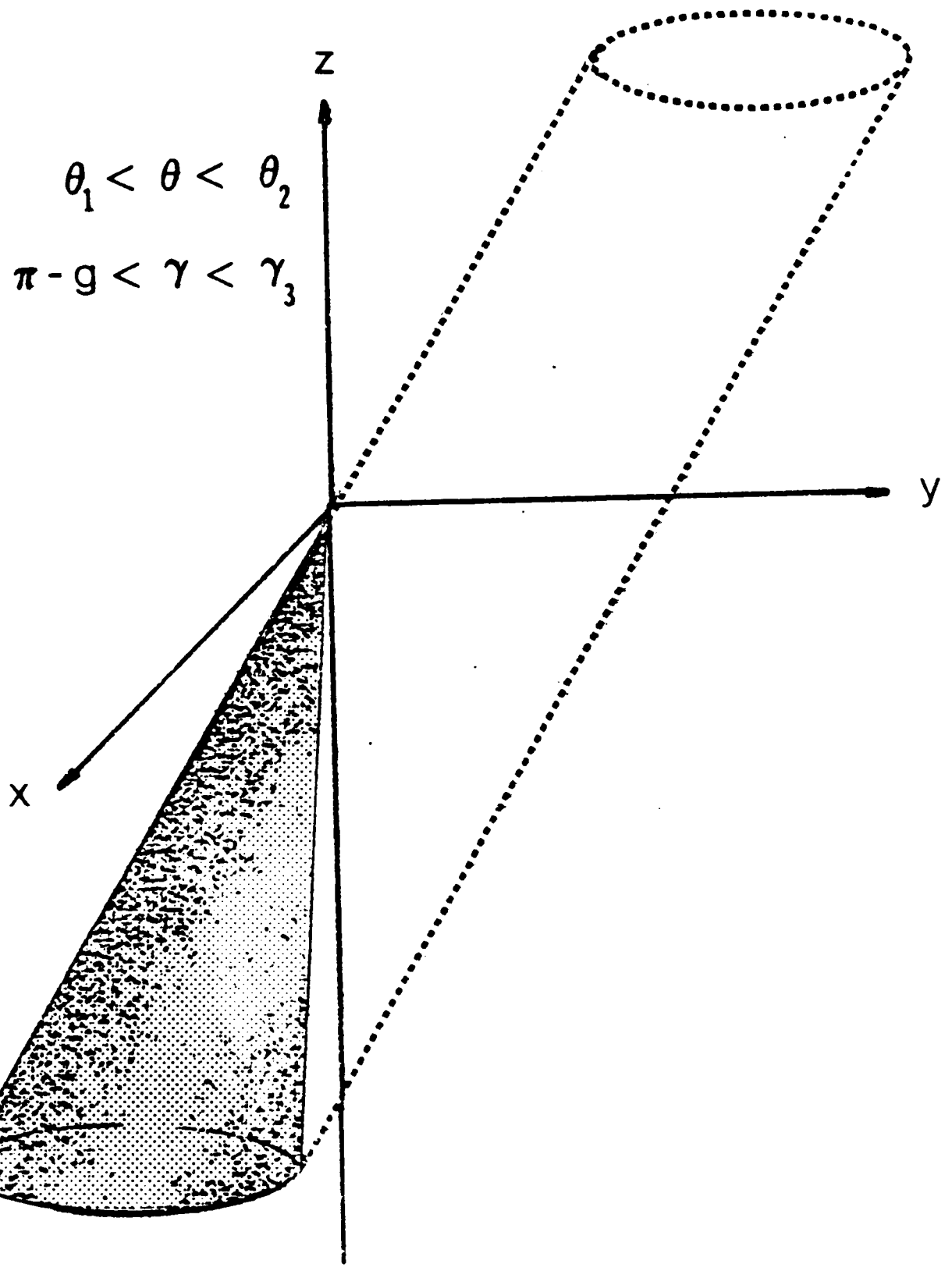
$\theta_1 < \theta < \theta_2$
$\pi - g < \gamma < \gamma_3$
z
y
x

average ρ for each subregion is then,

$$\rho_{7_1} = \frac{\int_{\theta_1}^{\theta_2} \int_{\pi-g}^{\gamma_1(\theta)} \rho(\theta,\gamma)d\gamma \; d\theta}{\int_{\theta_1}^{\theta_2} \int_{\pi-g}^{\gamma_1(\theta)} d\gamma \; d\theta}$$

$$\rho_{7_2} = \frac{\int_{\theta_1}^{\theta_2} \int_{\gamma_2(\theta)}^{\gamma_3} \rho(\theta,\gamma)d\gamma \; d\theta}{\int_{\theta_1}^{\theta_2} \int_{\gamma_2(\theta)}^{\gamma_3} d\gamma \; d\theta} \quad . \tag{4.37}$$

This value includes intersections with the cylinder in the area considered.

Region 8. Region 8 is the same area as region 7 but considers intersections with the plane not the cylinder. The limits are those defined in region 7. The average ρ is,

$$\rho_8 = \frac{\int_{\theta_1}^{\theta_2} \int_{\gamma_2(\theta)}^{\gamma_2(\theta)} \frac{-L}{2\cos(\gamma)} \; d\gamma \; d\theta}{\int_{\theta_1}^{\theta_2} \int_{\gamma_1(\theta)}^{\gamma_2(\theta)} d\gamma \; d\theta} \quad . \tag{4.38}$$

Region 9. This region applies when equation 4.16b is satisfied and is shown in figure 4.14. Only intersections with the cylinder are included in this region. The average ρ is,

$$\rho_9 = \frac{\int_{\pi}^{2\pi}\int_{\pi-3}^{\gamma_1(\theta)} \rho(\theta,\gamma)\, d\gamma\, d\theta}{\int_{\pi}^{2\pi}\int_{\pi-3}^{\gamma_1(\theta)} d\gamma\, d\theta} \tag{4.39}$$

where $\gamma_1(\theta)$ is defined in region 7.

Region 10. The area of this region is the same as region 9; however, in this region intersections with the plane and not the cylinder are considered. The average ρ is,

$$\rho_{10} = \frac{\int_{\pi}^{2\pi}\int_{\gamma_1(\theta)}^{\pi} \frac{-L}{2\cos(\gamma)}\, d\gamma\, d\theta}{\int_{\pi}^{2\pi}\int_{\gamma_1(\theta)}^{\pi} d\gamma\, d\theta}\,. \tag{4.40}$$

To determine the overall average value for ρ we must determine the weighted average for all of the regions which apply. When equation 4.16a is satisfied the average ρ will be the sum of the numerators of equations 4.18, 4.27a, 4.27b, 4.28, 4.34, 4.37a, 4.37b, and 4.38, divided by the sum of the denominators of the same equations. When equation

Figure 4.14: Limits of integration for region 9, applies only to case b.

$\pi < \theta < 2\pi$

$\pi - g < \gamma < \pi$

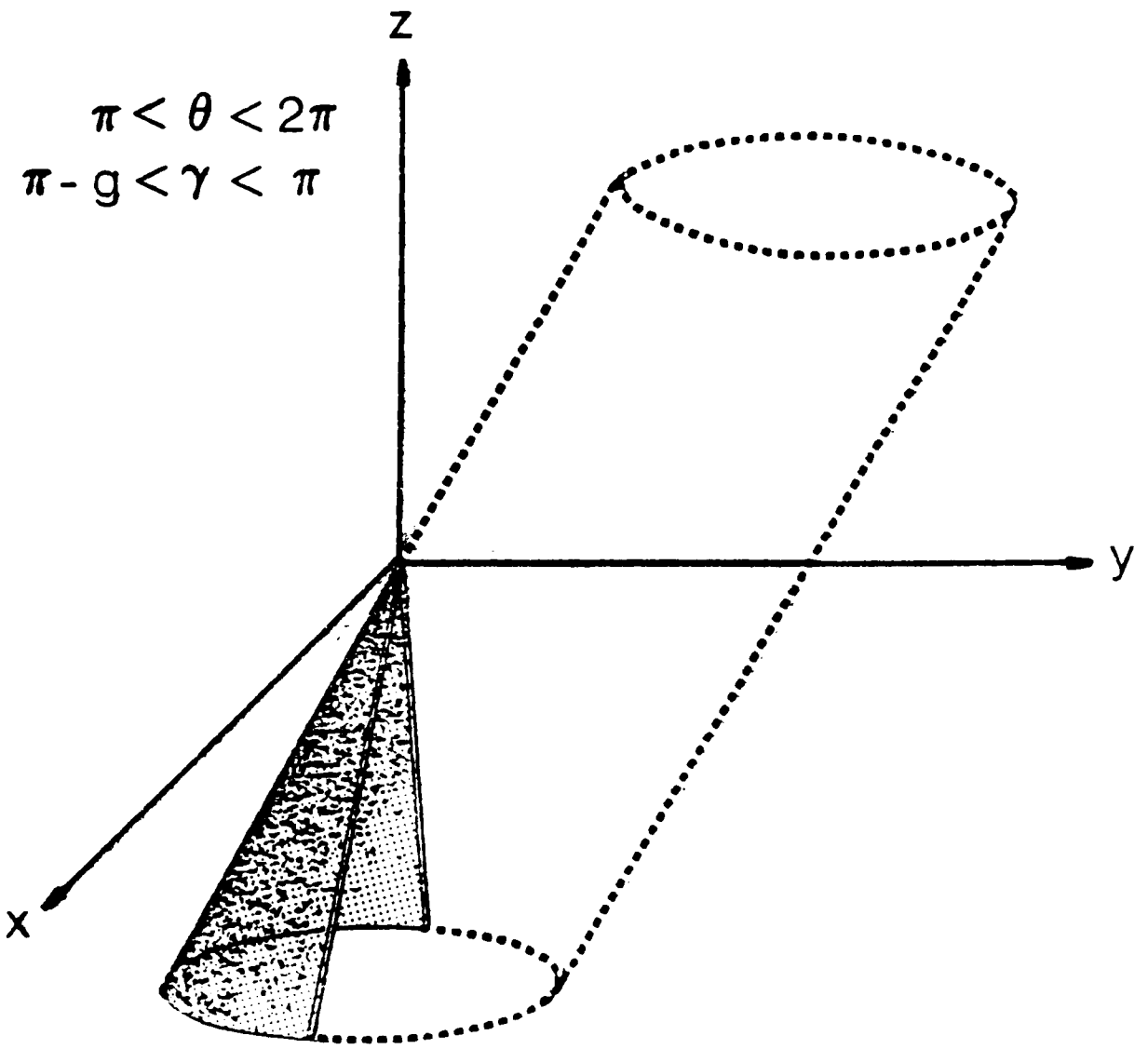

4.16b is satisfied the average ρ will be the sum of the numerators of equations 4.18, 4.27a, 4.27b, 4.28, 4.31, 4.32, 4.39, and 4.40, divided by the sum of the denominators of the same equations. Since the entire circumference of the cylinder may not be observed the volume to associate with this average value for ρ may be less than the volume of the cylinder. If we let W be the width on the wall of the cylinder which is observed, then the fraction of the circumference observed, F, is,

$$F = W/(2 \pi r). \tag{4.41}$$

The total volume of the segment of the cylinder, V_t, is

$$V_t = \pi r^2 \quad L \tag{4.42}$$

therefore the volume to associate with the average ρ, V, is

$$V = V_t \quad F$$

$$= r \; L \; W/2. \tag{4.43}$$

Integration Routine

Based on the system developed a FORTRAN program was written to numerically integrate the equations listed in the previous paragraph. A listing of the program is included in the appendix, along with a nomograph for determining the average predicted by the model. The integration was accomplished using Simpson's Rule, with several step sizes tested. It was determined that for a range of the number of intervals, corresponding to various step sizes, the results were not affected. A range from 5 to 30 intervals were tested for several regions. As a result all integrations were done using 30 intervals in each region.

This step size was chosen because the computer time required was not excessive and it was assumed that the smaller intervals would provide the most accurate integration.

Several tests can be performed to insure the accuracy of the equations developed to this point. The most important will be to insure that equation 4.11 yields the proper value of the length. If we set θ equal to $\pi/2$ and γ equal to $g+\pi$, the resulting length should be the diameter of the tube, 2r. Applying these values in equation 4.11 the resulting ρ is the appropriate value. Another test is to compare the average value obtained in one of the regions to the minimum and maximum values for ρ in that region.

In region 2 the minimum value for ρ is zero, since there is a possibility of a tangent intersection. The maximum value will occur when $\gamma = \gamma_2$ and $\theta = \pi/2$. In region 3 the minimum value will be the intersection which is parallel to the cylinder at $\theta = \pi/2$, and the maximum is the same as region 2. For region 5 the maximum occurs when $\gamma = \gamma_1$ and $\theta = \pi/2$, and the minimum occurs when $\gamma = \pi$. In this case the minimum is always L/2. For region 10 the minimum is again L/2 and the maximum occurs when $\gamma = \pi-g$, which is L/2cos(g). Table 4.2 displays the maximum, minimum, and integrated average for each of these regions at several combinations of values for r, L, and g.

Although this is not rigorous proof of the accuracy of the equations or integration routine it does imply they are correct. With only one exception (g=30 r=2.54 and L=20) the average value is between the

Table 4.2: Comparison of model output for average ρ and the minimum and maximum possible values for selected regions and cylinder parameters.

A: Region 2

g	r	L=10 max.	L=10 min.	L=10 aver.	L=20 max.	L=20 min.	L=20 aver.
15	2.54	8.28	0.0	5.20	12.77	0.0	8.77
15	5.08	12.87	0.0	6.78	16.56	0.0	10.41
30	2.54	10.08	0.0	5.97	15.35	0.0	11.00
30	5.08	15.54	0.0	7.61	20.16	0.0	11.97
45	2.54	13.17	0.0	7.54	19.88	0.0	12.11
45	5.08	20.00	0.0	9.51	25.34	0.0	15.08

B: Region 3

g	r	L=10 max.	L=10 min.	L=10 aver.	L=20 max.	L=20 min.	L=20 aver.
15	2.54	8.28	5.18	6.19	12.77	10.35	11.24
15	5.08	12.87	5.18	7.17	16.56	10.35	12.32
30	2.54	10.08	5.77	7.28	15.35	11.55	13.08
30	5.08	15.54	5.77	8.52	20.16	11.55	14.55
45	2.54	13.17	7.07	9.29	19.88	14.14	16.55
45	5.08	20.00	7.07	10.92	25.34	14.14	18.58

C: Region 5

g	r	L=10 max.	L=10 min.	L=10 aver.	L=20 max.	L=20 min.	L=20 aver.
15	2.54	6.35	5.0	5.31	10.33	10.0	10.11
15	5.08	10.45	5.0	6.00	12.71	10.0	10.63
30	2.54	5.82	5.0	5.23	10.00	10.0	10.00
30	5.08	10.16	5.0	5.98	11.64	10.0	10.45
45	2.54	5.46	5.0	5.14	10.39	10.0	N/A
45	5.08	10.62	5.0	6.00	10.91	10.0	10.29

Table 4.2: Continued.

D:		Region 10					
			L=10			L=20	
g	r	max.	min.	aver.	max.	min.	aver.
15	2.54	5.18	5.0	5.05	10.35	10.0	10.03
15	2.54	5.18	5.0	5.11	10.35	10.0	10.10
30	2.54	5.77	5.0	5.07	11.55	10.0	9.92
30	2.54	5.77	5.0	5.19	11.55	10.0	10.14
45	2.54	7.07	5.0	5.06	14.14	10.0	N/A
45	2.54	7.07	5.0	5.25	14.14	10.0	10.11

N/A indicates that this combination of L, r, and g does not apply to this region

maximum and the minimum. In the one instance where the value is too small it is within 1.0 mm of the minimum value which could be attributed to the round off error in the integration routine. For this region the average value only exceeds the minimum by about this amount for all of the other combinations.

Model Testing

From the soil sampling described in Chapter III the root length density was calculated for the entire soil profile in the two water treatment plots. Using the average number of counts observed on the wall of the nine mini-rhizotrons at the 15^{o} and 30^{o} angle for each treatment, a value for RLD was calculated based on the average ρ predicted by the model. Figure 4.15 is a plot of the RLD from cores versus RLD from the mini-rhizotrons, across all treatments and angles. The correlation coefficient between the two measures of RLD is 0.39 and is

Figure 4.15: Root length density measured by mini-rhizotrons versus that measured by soil cores, for all treatments and installation angles.

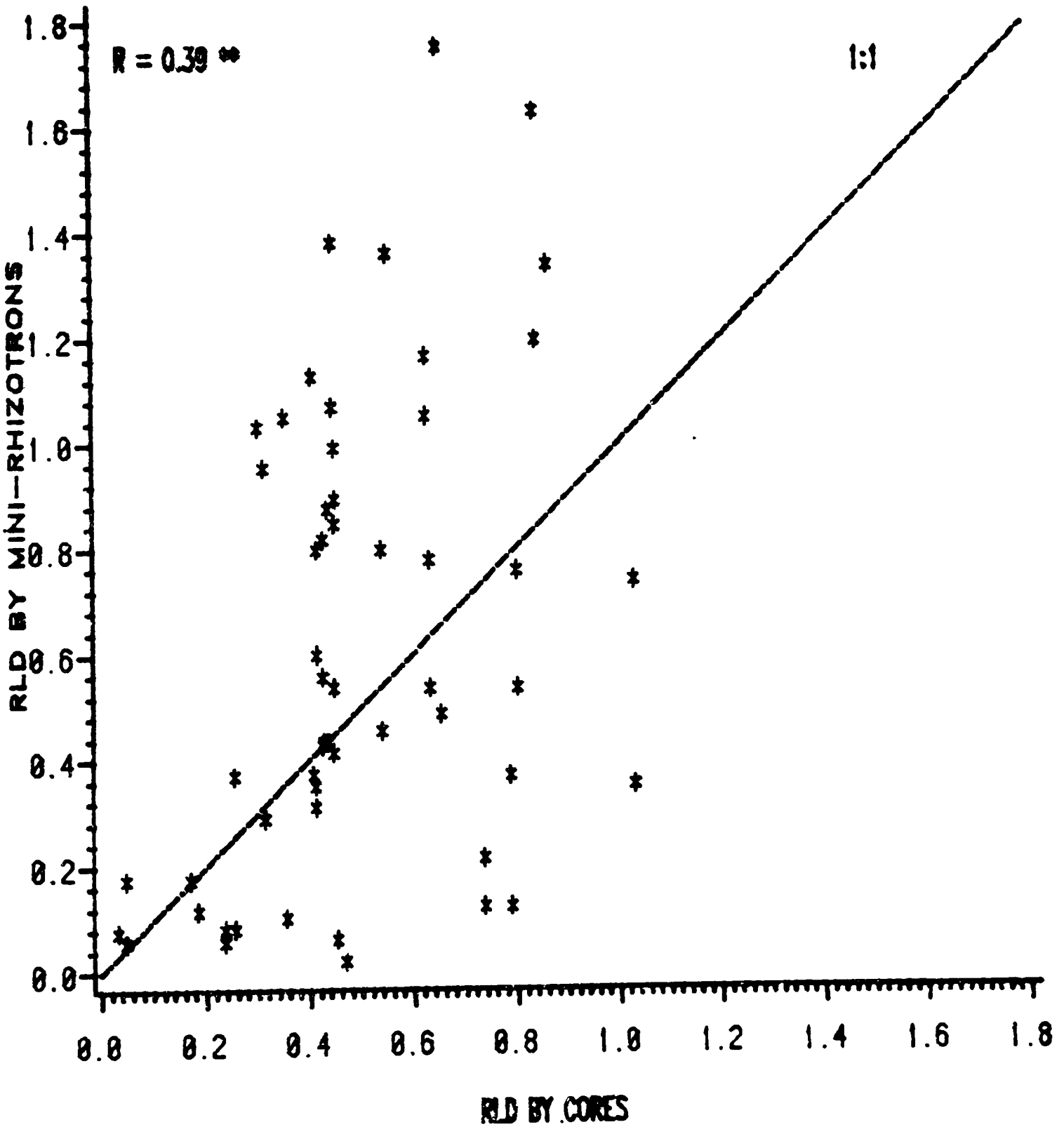
ALL TREATMENTS AND ANGLES
R = 0.39 **
1:1
RLD BY MINI-RHIZOTRONS
RLD BY CORES
0.0
0.2
0.4
0.6
0.8
1.0
1.2
1.4
1.6
1.8

significant at the 99% level. As can be seen there is a significant amount of scatter in the plot. This may be an indication of an interface problem in the installation of the mini-rhizotrons. The soil at the site of this project (Olton clay loam, fine, mixed, thermic Aridic Paleustoll) has a well defined medium and subangular blocky structure with cleavage planes predominating in two distinct orientations. This is apparent from the frequency plot of root growth angle in Chapter III. Roots tend to follow these planes of weakness, which are either horizontal or vertical in orientation. In the installation of the mini-rhizotrons these planes are disrupted at the interface, and the smearing of the soil during the installation of the tubes may create a high strength layer. Since, in general, roots do not penetrate the soil peds but follow these planes, any disruption of the plane will block root growth in that direction. This disruption would account for the reduced concentration of roots at the interface and would result in the underestimation of RLD. After an intersection has occurred with the mini-rhizotron there must be a path of lower resistance for the root to follow in order for the root to grow away from the interface. If the natural cleavage planes in the soil are blocked during the installation process the root will tend to remain at the interface and continue growth along the face of the tube until a zone of weakness is encountered. This may explain the overestimation of RLD in some zones along the mini-rhizotron.

This soil has only a slight shrink-swell potential but the predominate clay mineral is montmorillonite, which does shrink during

drying. If the blocking of the natural cleavage planes is the cause of the scatter in the data, the dryland treatment would be expected to have a higher correlation than the irrigated treatment, because the shrinkage of the soil would tend to reestablish the natural cleavage planes. Figures 4.16 and 4.17 are the plots of the two measures of RLD for the dryland and irrigated treatments, respectively. The correlation coefficients are 0.57 and 0.03 for the dryland and irrigated treatments, respectively. The correlation is significant at the 99% level for the dryland treatment but is not significant for irrigated, confirming, to some degree, the previous hypothesis. The regression line for the dryland treatment has a slope near 1.0 and an intercept not significantly different from zero. The highest correlation coefficient was found in the dryland treatment with an installation angle of 30^{o}. A plot of the two measures of RLD is displayed in figure 4.18, the correlation coefficient is 0.70 and is significant at the 99% level.

There is only a small range in the values of RLD in this project, 0.0 to 1.2 cm/cm^3, which is typical of cotton. With this narrow range any scatter in the relationship between the two techniques will be very apparent. The regression and correlation analysis indicate that there is a significant linear relationship between the number of roots intersecting the mini-rhizotron and the bulk soil RLD, which is what the model predicted through its development.

The conversion of root counts from the mini-rhizotrons to RLD was based on the coefficient developed from the model using the assumption of random root growth angles. The observations from the trench profile

Figure 4.16: Root length density measured by mini-rhizotrons versus that measured by soil cores, for the dryland treatment for all angles.

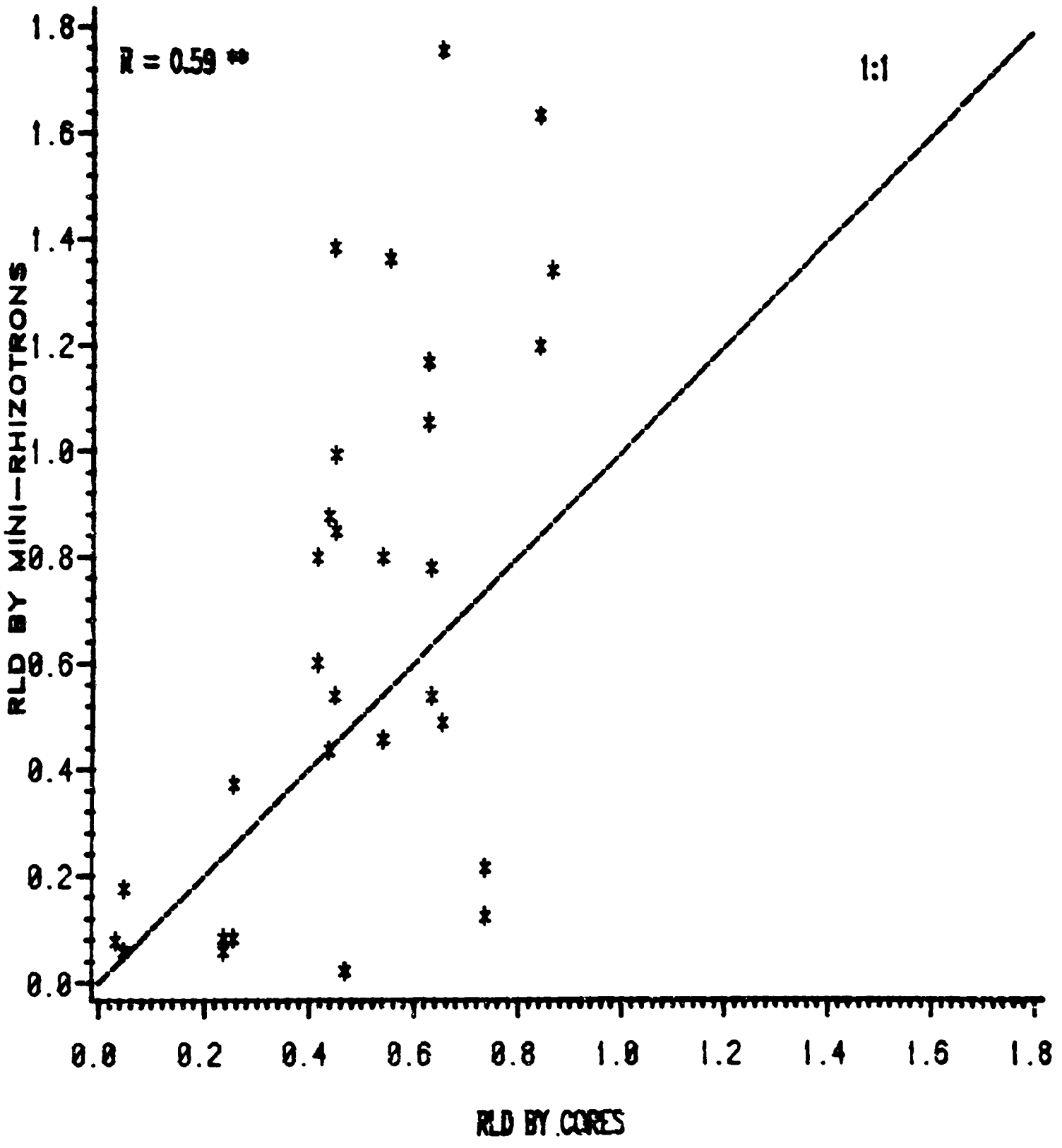
DRYLAND
R = 0.59 **
1:1
RLD BY MINI-RHIZOTRONS
RLD BY CORES
0.0
0.2
0.4
0.6
0.8
1.0
1.2
1.4
1.6
1.8

Figure 4.17: Root length density measured by mini-rhizotrons versus that measured by soil cores, for the irrigated treatment for all angles.

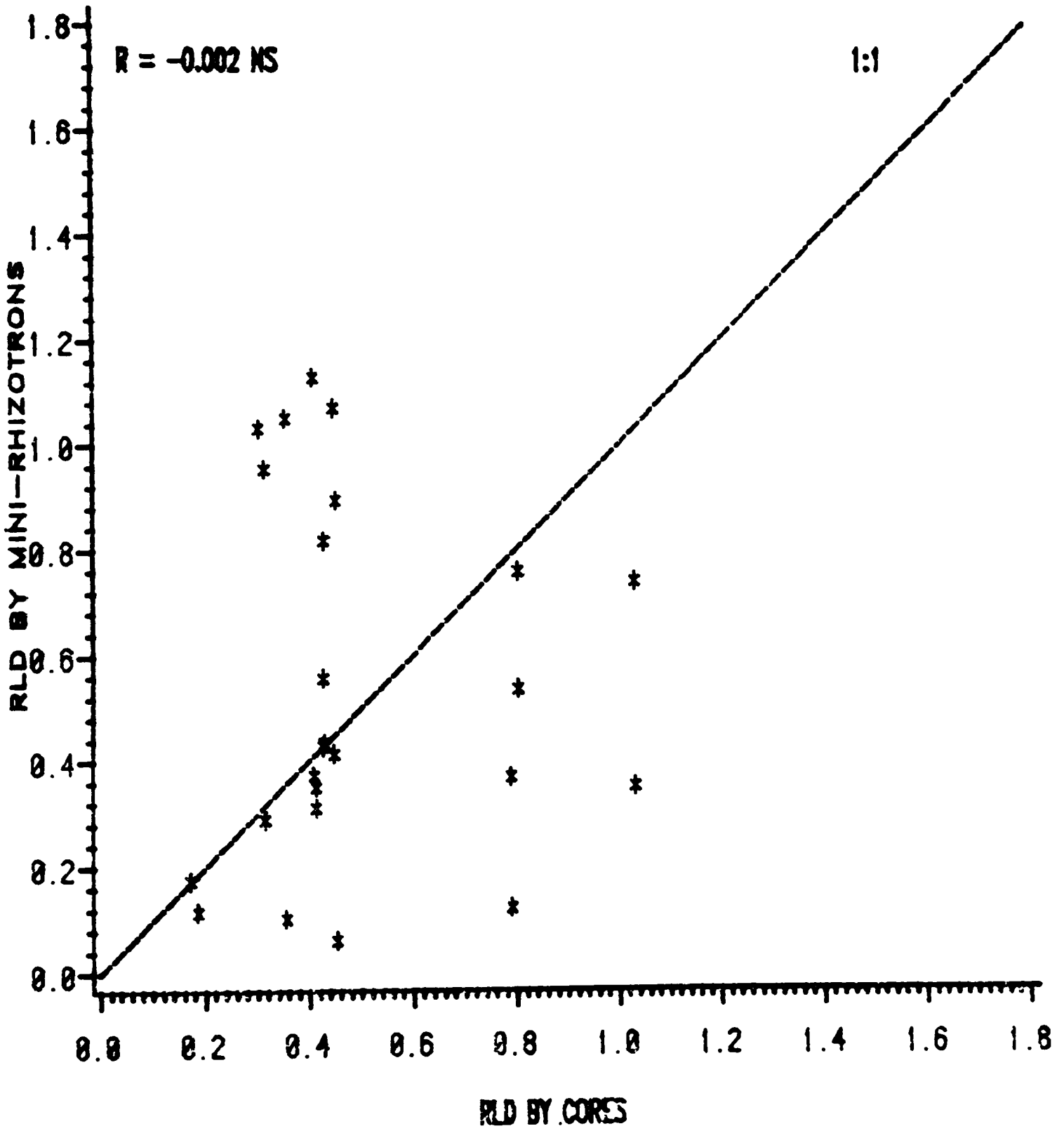
IRRIGATED
R = -0.002 NS
1:1
RLD BY MINI-RHIZOTRONS
RLD BY CORES
0.0
0.2
0.4
0.6
0.8
1.0
1.2
1.4
1.6
1.8

Figure 4.18: Root length density measured by mini-rhizotrons versus that measured by soil cores, for the dryland treatment and 30^{o} installation angle.

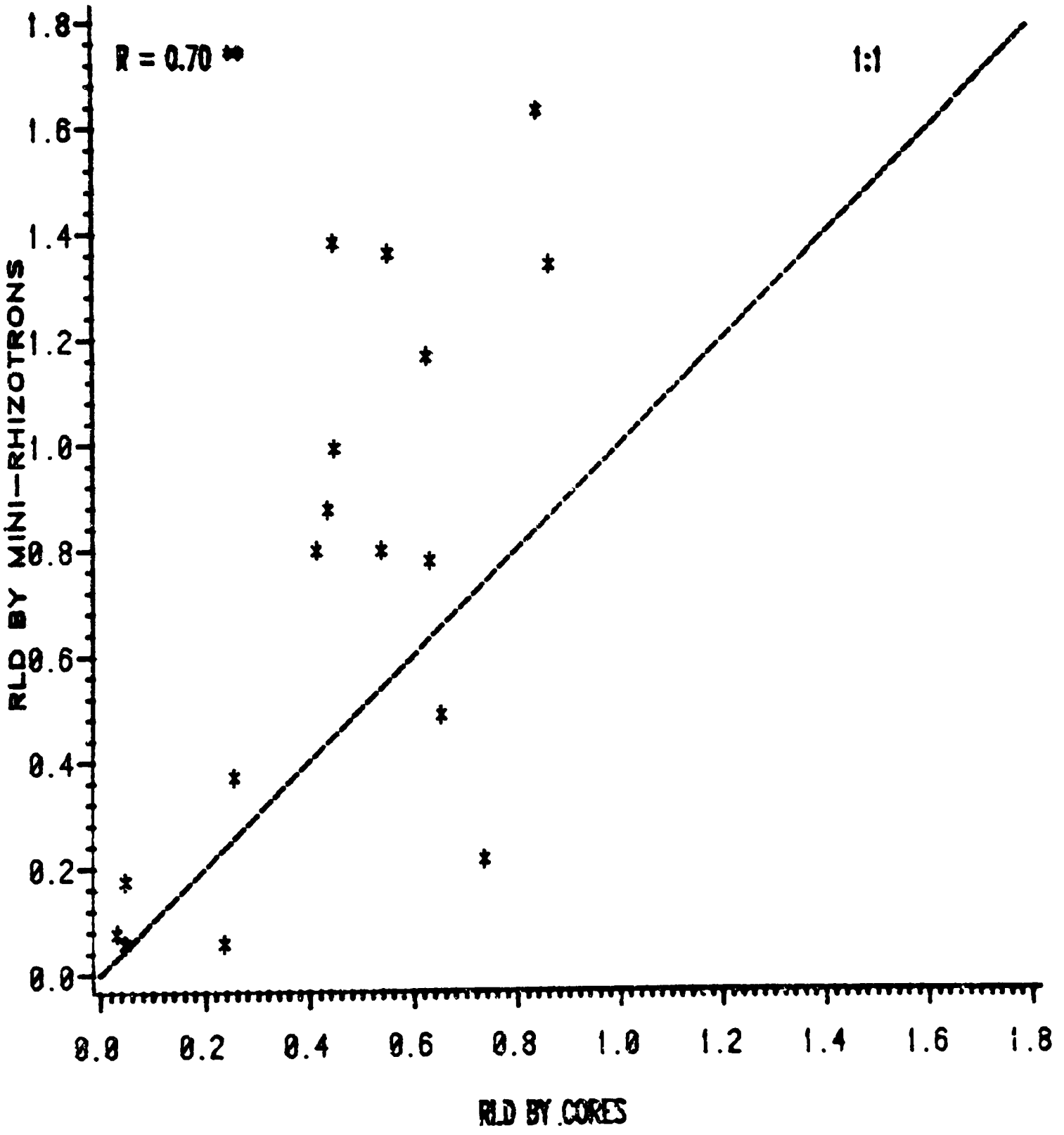
DRYLAND 30 DEGREES
R = 0.70 **
1:1
RLD BY MINI-RHIZOTRONS
RLD BY CORES
0.0
0.2
0.4
0.6
0.8
1.0
1.2
1.4
1.6
1.8

described in Chapter III indicated that root growth was not random, but followed two predominant angles. The distribution did not follow a known probability density function which could be used in the model. If a probability density function could be found and used in the model the relationship might be improved.

Each point on figures 4.15 - 4.18 represent the average of 10 soil cores and 9 mini-rhizotrons. Because of the large variance which normally occur in studies of root growth by any technique, this number of samples may be too small to establish a tight coupling between the two techniques. Chapter V shows the relationship between the detectable difference and the number of samples required for soil cores and mini-rhizotrons. In general the observations shown in figures 4.15 - 4.18 are within the confidence band around the one-to-one line, indicating that with the number of samples used we can accept the null hypothesis that the two techniques agree.

CHAPTER V

STATISTICAL PROPERTIES OF THE MINI-RHIZOTRON TECHNIQUE

In order to fully document the mini-rhizotron technique the statistical properties of observations should be quantified. Since observations of root systems have large variances, this becomes an important property of the technique. Sanders and Brown (1978) reported a coefficient of variability for the technique which was lower than the value for soil coring, while Upchurch and Ritchie (1983, and 1984) reported higher values. The capability of a technique to detect statistically significant differences between treatments with a specific number of observations is a function of the coefficient of variability. Considering the fact that the number of observations in the mini-rhizotron technique is controlled by the number of tubes which can be installed and observed it becomes important to determine an optimum number of tubes.

The results obtained from the experiments described in the previous chapter will be used to determine the variability of mini-rhizotron observations. This will be compared with the variability of other root observation techniques reported in the literature as well as the results of the soil coring described in Chapter IV. Using this information the minimum number of tubes required to detect specified differences at the desired confidence level can be calculated.

In all statistical analysis procedures some assumption is made concerning the statistical distribution of the observations. Generally the

population is assumed to be normally distributed. This may not be the case for root observations (Dyer and Brown, 1982). If this assumption is not satisfied for a particular procedure, the results of that procedure will be invalid, or at least the confidence levels will be erroneous. In the application of this technique it will be important to know the distribution of the observations so that appropriate statistical tests can be applied to the results, or an evaluation of the confidence level can be made.

Using the observations described in the previous chapters it was determined that the distribution of the observation was not normal. However there was not sufficient information to determine the exact distribution. The distribution appeared to be bimodal with a large fraction of small values, and then a somewhat normal distribution at the larger values. Because of the lack of information on the exact form of the distribution tests were made assuming normality. The major effect on the results of the testing will be to reduce the level of confidence which can be associated with the test.

From the observations described in the previous chapters the variance and coefficient of variability was calculated for cores and minirhizotron in the dryland and irrigated plots. These values are shown in table 5.1. From the information in table 5.1 the minimum number of samples required for specific differences to be statistically significant can be calculated using certain assumptions. Assuming normality of the observations and a confidence level of 95% the relationship between the number of samples required and the difference detected is shown in

Table 5.1: Variance and coefficient of variability for RLD determined by soil cores and mini-rhizotrons for the dryland and irrigated treatments.

	Dryland		Irrigated	
	var.	c.v.	var.	c.v.
cores	0.076	39	0.064	57
M - R	0.420	189	0.097	196

figure 5.1. As can be seen the number of samples required decreases exponentially as the difference increases. Because of the larger variance for the mini-rhizotron the number of samples required is larger. The variance for the dryland treatment is larger for both cores and mini-rhizotrons and therefore the number of samples required is larger. The variance for the mini-rhizotron is only slightly larger than cores in the irrigated treatment and requires only a few more samples than soil cores for most values of the detectable difference. This information provides an indication of the number of samples required but should be used with care because of the problems associated with the installation of the mini-rhizotrons in this project. The indication is that the variance reported may be too large because of the interface problems described in Chapter IV. If an improved installation procedure is used the number of samples required would be reduced assuming that the variance is affected by the installation procedure.

Table 5.2 gives the variance and coefficient of variability for a few projects reported in the literature. The variance was calculated from the reported coefficient of variability and mean, and is therefore

Figure 5.1: Relationship between the number of samples required and the detectable difference, at the 95% level, for the present project.

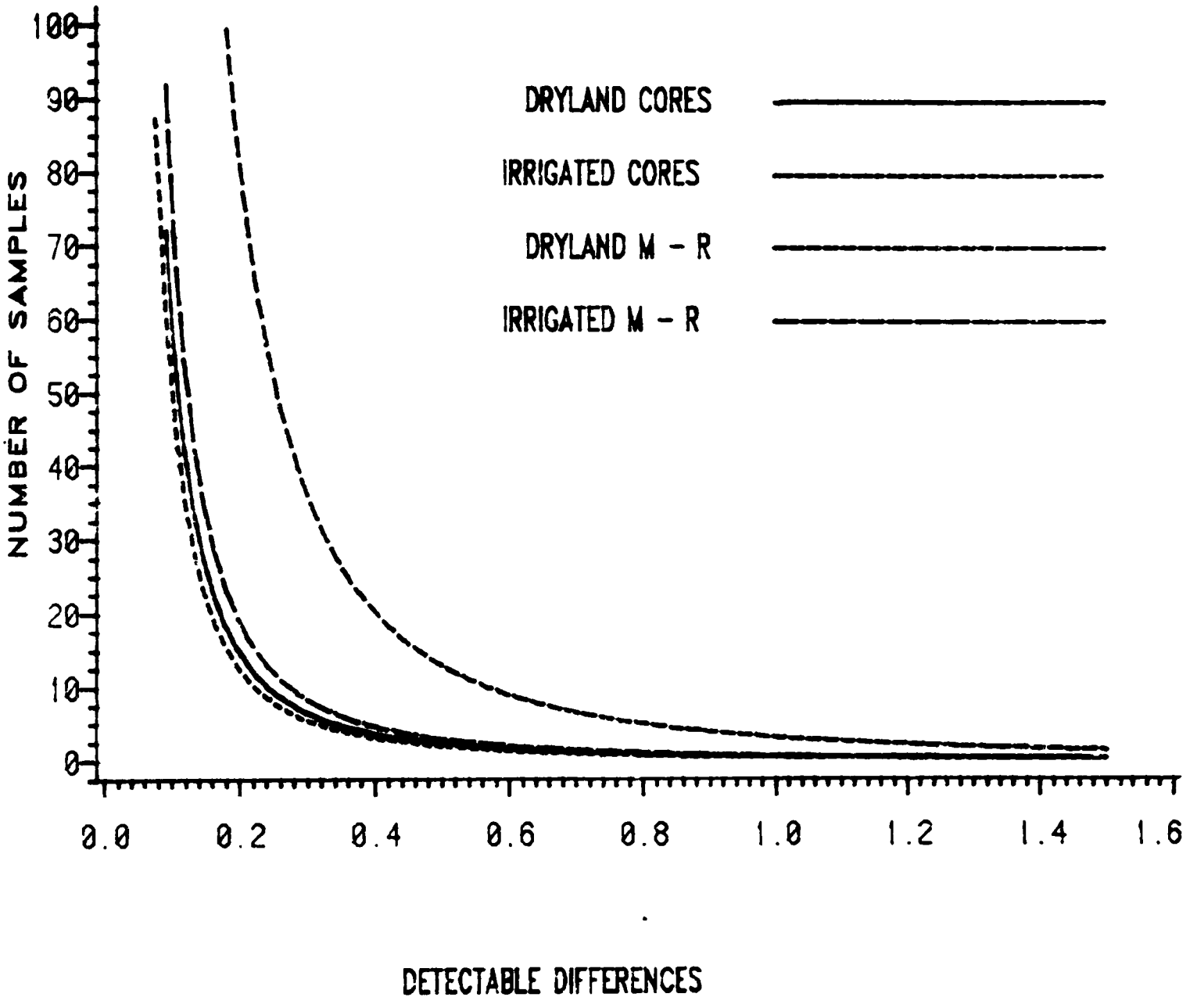
SAMPLES vs. DIFFERENCES
DRYLAND CORES
IRRIGATED CORES
DRYLAND M - R
IRRIGATED M - R
NUMBER OF SAMPLES
100
90
80
70
60
50
40
30
20
10
0
0.0
0.2
0.4
0.6
0.8
1.0
1.2
1.4
1.6
DETECTABLE DIFFERENCES

only an estimate of the correct value. Because the mean in this project was large the variance was large and the number of samples required to detect certain differences will be large.

Table 5.2: Variance and coefficient of variability for RLD reported in several projects.

		variance	C.V.
Sanders and Brown, 1978 (Soybeans)			
	cores	4.105	53
	M - R	0.258	14
Taylor and Klepper, 1975 (Cotton)			
	Rhizotron	0.203	30
Upchurch and Ritchie, 1983 (Sorghum)			
	Cores	0.212	27
	M - R	3.360	109

Figure 5.2 displays the relationship between the number of samples required and the detectable difference at the 95% confidence level. In the Sanders and Brown report the mini-rhizotron had an advantage over soil cores while in Upchurch and Ritchie cores required fewer samples than the mini-rhizotron. The use of the rhizotron by Taylor and Klepper was intermediate to the other reported values.

Because of the range in values of RLD it is not possible to predict the number of samples required for every project. Consideration should be given to the magnitude of the RLD values and to the difference between treatments that is important to the project. If very small dif-

Figure 5.2: Relationship between the number of samples required and the detectable difference, at the 95% level, from published reports.

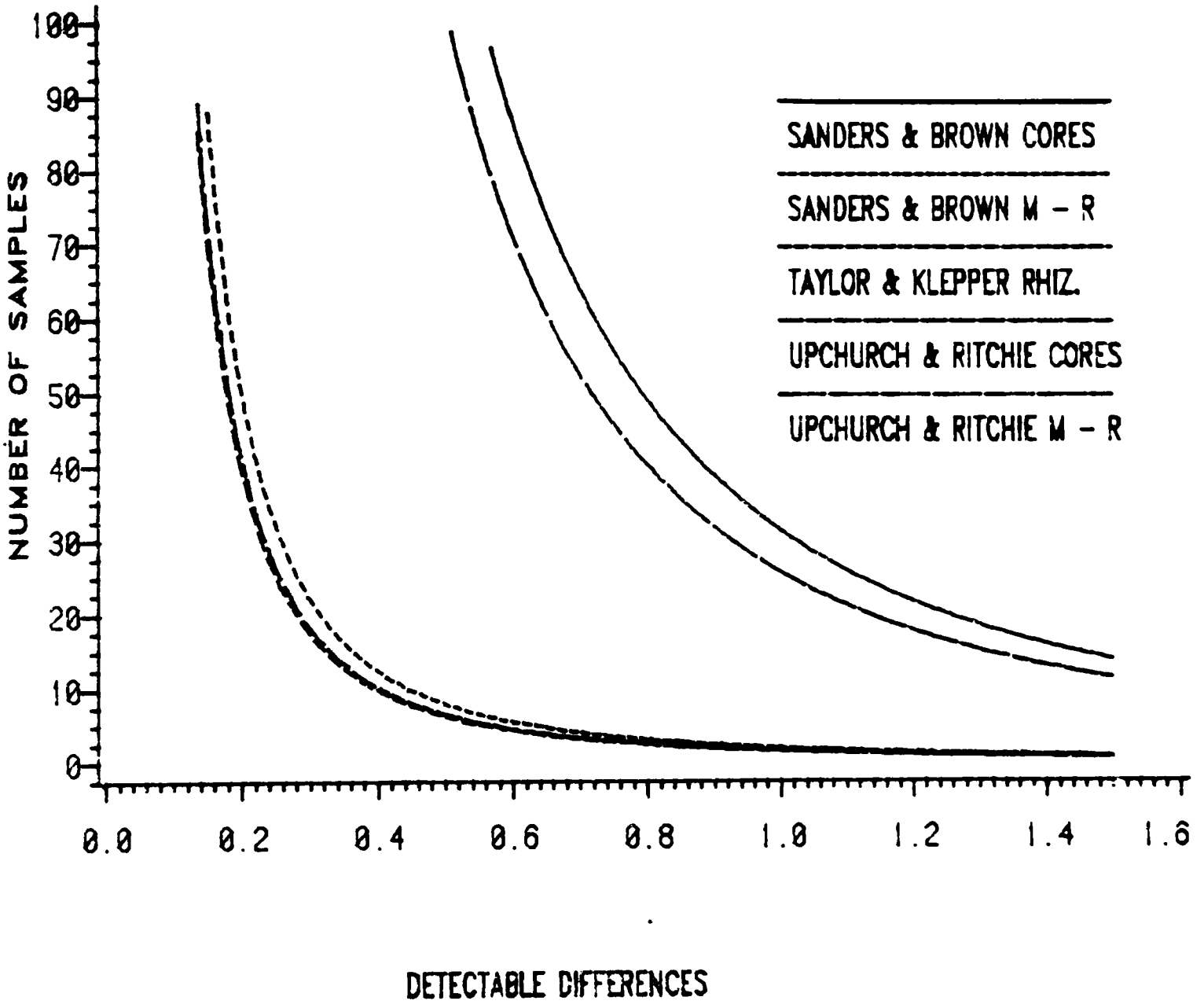
SAMPLES vs. DIFFERENCES
NUMBER OF SAMPLES
100
90
80
70
60
50
40
30
20
10
0
0.0
0.2
0.4
0.6
0.8
1.0
1.2
1.4
1.6
DETECTABLE DIFFERENCES
SANDERS & BROWN CORES
SANDERS & BROWN M - R
TAYLOR & KLEPPER RHIZ.
UPCHURCH & RITCHIE CORES
UPCHURCH & RITCHIE M - R

ferences in RLD are important then a large number of samples will be required, independent of the technique used for the observations. However if only large differences are important then the number of samples required will be reduced. These results serve to emphasize the importance of using a larger number of mini-rhizotrons for quantifying the rooting of a crop. The use of the mini-rhizotron system is based on probabilistic assumptions concerning the distribution of roots in the soil and their growth directions. The variances are large for any technique but are often largest for the mini-rhizotron. This large variance can only be overcome by making the sample size large enough detect the difference that is important to the project. The appropriate number of tubes will be affected by the results presented as well as by the limitations on the number of tubes which can be managed by the project.

CHAPTER VI

SUMMARY AND CONCLUSIONS

This project has resulted in the development of two models, which can be applied to the mini-rhizotron technique for root observation. The models are based on probabilistic assumptions concerning root growth directions in the soil. The models apply to the average number of roots that intersect the wall of several tubes buried in the soil, and not to individual observation tubes.

The ratio hypothesis has expanded the information which can be obtained from observations in mini-rhizotrons to include an indication of the overall orientation of the root system in situ. By determining the ratio of the number of roots which intersect the top of a mini-rhizotron to the number which intersect the bottom, the model predicts when the root system is more horizontal or more vertical than random in orientation.

Observations made on the wall of a trench confirmed the horizontal orientation of a cotton root system which had been predicted from application of the model to observations in mini-rhizotrons. The application of the model to the observations also predicted the existence of upward root growth, which was confirmed with the trench profile measurements. The model indicated a larger amount of upward root growth than was observed in the trench; however, an analysis of the trench technique indicated a possible underestimation of the magnitude of upward growth. When an adjustment was made to the observations from the trench to

correct for the underestimation, the modeled and observed ratios tended toward the same absolute value. The narrow range in the values of the ratio and probability density function for root growth angles resulted in a large degree of scatter in the relationship. A better agreement might be found if a larger range in the density function had occurred, which might be found in other plant species.

The model, relating the number of root intersections on the wall of a mini-rhizotron to the bulk soil RLD, predicted a linear relationship. The average length to associate with each intersection was determined assuming that root growth was affected only after an intersection, that roots could be represented by straight line segments, and that root growth direction followed some probability density function. The assumption that roots can be represented by straight lines can be removed if the tortuousity of the path of root growth is known. The average value of length to associate with each intersection was determined by integrating an equation, which described the length which would be internal to the cylinder if the cylinder were not in place, over all possible directions. The length can be weighted by the probability of the direction if the probability of root growth in that direction is known. The assumption of no interaction of the mini-rhizotron with root growth prior to an intersection is satisfied only to the degree that the installation procedure maintains the soil condition around the tube in its natural state.

The correlation coefficient between RLD determined applying the model to mini-rhizotron observations and from soil cores was low but

significant at the 99% level, when all treatments and angles were considered. The correlation was greatest, 0.70, in the dryland treatment and at the 30^{o} installation angle. The higher correlation in the dryland treatment may have been a result of the reestablishment of the natural soil structure at the interface as the soil dried. The average length to associate with each intersection was determined assuming random root growth angles. If the true probability density function were known the agreement between the techniques might be improved. The number of samples which were used in the testing may have been too small to obtain a tight coupling between the techniques. The large variance normally associated with root studies can result in significant scatter in the data.

The statistical properties of the mini-rhizotron system emphasize the need for a large sample size. The number of samples required to detect specific differences in RLD was large for both soil cores and mini-rhizotrons when the difference is small. The decision about the number of tubes to install will be affected by the reported variance, the magnitude of the expected RLD, the difference in RLD which is important to the project, and the resources of the project. The variance of the mini-rhizotron was larger than soil cores in this project, but in another project reported in the literature this result was reversed.

The usefulness of the mini-rhizotron technique has been expanded to include indications of the orientation of the root system through the ratio hypothesis. The conversion of root counts to RLD has been given a mathematical basis, with few assumptions. The primary disadvantage of

the system is the number of samples required. Because of the resources required in the installation process, long term use of permanently installed mini-rhizotrons is desirable. The cost of observations in mini-rhizotrons is less than the cost for soil coring after the initial installation (Upchurch and Ritchie, 1983). Research is needed on the procedure for installing the mini-rhizotrons to overcome the effect of the interface on the number of root intersections. The natural soil structure must be considered during the installation procedure to allow the assumption of no interaction of the mini-rhizotron with root growth prior to an intersection. The probability density function for root growth angles is required in both models. Little information is available about this function for various plant species. This information would be useful, not only in the context of these models but also in the basic understanding of the function of root systems.

LITERATURE CITED

Bates, G. H. 1937. A device for the observation of root growth in soil. Nature 139:966-967.

Bohm, W. 1974. Mini-Rhizotrons for root observations under field conditions. Z. Acker Pflanzenbau. 140:282-287.

Bohm, W., H. Maduakor, and H. M. Taylor. 1977. Comparison of five methods for characterizing soybean rooting density and development. Agron. J. 69:415-419.

Bohm, W. 1979. Methods of studying root systems. Ecological Studies, vol. 33. Springer-Verlag Berlin.

Brown, D. A. 1984. Characterization of soybean root distribution. Arkansas Farm Res. 33:3.

Dyer, D., and D. A. Brown. 1980. In-Situ root observation using fiber optic. video and fluorescence. Agron. Abstr. p. 80.

Dyer, D., and D. A. Brown. 1982. Computer modeling of crop root systems. Agron. Abstr. p. 174.

Gregory, P. J. 1979. A periscope method for observing root growth and distribution in field soil. J. Exp. Bot. 30:205-214.

Maertens, C. and Y. Clauzel. 1982. First observations on the use of endoscopy in in situ root studies of cultivated plants (Sorghum vulgare and Lolium multiflorum). Agronomie 2:677-680.

Newman, E. I. 1966. A method of estimating the total length of root in a sample. J. Appl. Ecol. 3:139-145.

Sanders, J. L., and D. A. Brown. 1978. A new fiber optic technique for measuring root growth of soybeans under field conditions. Agron. J. 70:1073-1076.

Taylor, H. M. and B. Klepper. 1975. Water uptake by cotton root systems: An examination of assumptions in the single root model. Soil Sci. 120(1):57-67.

Upchurch, D. R., and J. T. Ritchie. 1983. Root observations using a video recording system in mini-rhizotrons. Agron. J. 75:1009-1015.

Upchurch, D. R., and J. T. Ritchie. 1984. Battery-operated color video camera for root observations in mini-rhizotrons. Agron. J. 76:1015-1017.

Vos, J. and J. Groenwold. 1983. Estimation of root densities by observation tubes and endoscope. Plant and Soil 74:295-300.

Waddington, J. 1971. Observation of plant roots *in situ*. Can. J. Bot. 49:1850-1852.

APPENDIX A

FORTRAN INTEGRATION ROUTINE

This appendix contains a listing of the FORTRAN programs and subroutines used in the numerical integration of the equations developed in Chapter IV to determine the average length to associate with each root intersection. The programs were compiled and run on a Digital Equipment Corporation VAX/VMS 730 computer. The integration was done using Simpson's Rule for numerical integration. At certain points in the programs and subroutines the values of the two angles were adjusted by 0.01 degrees to prevent the occurrence of computer errors. At certain values of these angles the calculation of the length would be zero or infinite, which could result in division by zero or taking the square root of a negative number, if these corrections were not included. Each of the programs and subroutines include a title indicating when they apply.

```
PROGRAM NUMINT
C --------- PROGRAM TO NUMERICALLY INTEGRATE EQUATIONS ----------------
C
      REAL J, J1, J2, J3, L, K1, K2, K3, LEN
C
C ---  INTEGRAND FUNCTION ------------------------------------------
      RA(X,Y)= (COS(G)- (SIN(G)*COS(Y)/(SIN(Y)*SIN(X))))
      A10(X,Y)= .5*(COS(X-Y)-COS(X+Y))*((1/TAN(X))**2+RA(X,Y)**2)
      F(X,Y)= 2.*R*RA(X,Y)/A10(X,Y)
C ---  READ TUBE PARAMETERS ----------------------------------------
C        LEN =  INTERVAL LENGTH (CM)
C          G =  INSTALLATION ANGLE (RADIANS)
C          R =  TUBE RADIUS (CM)
      OPEN (UNIT=1,NAME='[DAN.DISS.INTEG]TUBE.PAR',TYPE='OLD')
      OPEN (UNIT=2,NAME='[DAN.DISS.INTEG]TUBE.OUT',TYPE='NEW')
      READ (1,100) LEN, R, G
 100  FORMAT (F5.3,5X,F5.3,5X,F20.17)
C
C ---  CALCULATE UPPER AND LOWER LIMITS FOR OUTSIDE INTEGRAL
      CALL UPP (B,G,LEN,R)
      CALL LOW (A,G,LEN,R)
C
C ---  READ THE NUMBER OF INTERVALS TO BE USED ----------------------
      READ (1,101) N, M
 101  FORMAT (I3,2X,I3)
C
C ---  BEGIN INTEGRATION PROCEDURE  ---------------------------------
      H=(B-A)/(2.*N)
      J1=0.
      J2=0.
      J3=0.
      DO 10 I = 1,(2*N+1)
       II=I-1
       X= A + II*H
       IF (X.EQ.0.) X= (3.14159265/18000.)
       IF (X.GT.(3.14159265-3.14159265/18000.)) THEN
       IF (X.GT.(3.14159265+3.14159265/18000.)) GOTO 99
       IF (I.EQ.1) X= 3.14159265+(3.14159265/18000.)
       IF (I.NE.1) X= 3.14159265-(3.14159265/18000.)
       ELSE
       END IF
 99    CONTINUE
       IF (X.GT.(2*3.14159265-3.14159265/18000.)) THEN
       X= (2*3.14159265-3.14159265/18000.)
       ELSE
       END IF
       CALL DD (X,DX,R,LEN,G)
       CALL CC (X,CX,R,LEN,G)
       HX= (DX - CX)/ (2.*M)
       F1= F(X,CX)
```

```
      F2= F(X,DX)
      IF (F1.LT.0.) F1=0.
      IF (F2.LT.0.) F2=0.
      K1= F1 + F2
      K2=0.
      K3=0.
       DO 11 JJ = 1, (2*M-1)
        Y= CX + JJ*HX
        Z= F(X,Y)
        IF (Z.LT.0.) Z=0.
        IF (JJ.EQ.2*(JJ/2)) THEN
         K2= K2 + Z
        ELSE
         K3= K3 + Z
        END IF
11      CONTINUE
       L = (K1 + 2.*K2 + 4.*K3) *HX/ 3.
       IF (II.EQ.0) GO TO 20
       IF (II.EQ.2*N) GO TO 20
       IF (II.EQ.2*(II/2)) THEN
        J2= J2 + L
       ELSE
        J3= J3 + L
       END IF
      GO TO 10
   20  J1= J1 + L
   10  CONTINUE
       J= (J1 + 2.*J2 + 4.*J3) *H/ 3.
       WRITE (2,200) J
   200 FORMAT (F10.3)
C       WRITE (5,*) J
       CLOSE (UNIT=1)
       CLOSE (UNIT=2)
       STOP
       END
```

```
      PROGRAM NUMPPL
C --------- PROGRAM TO NUMERICALLY INTEGRATE EQUATIONS ----------------
C
      REAL J, J1, J2, J3, L, K1, K2, K3, LEN
C
C ---  INTEGRAND FUNCTION ------------------------------------------
      F(X,Y)= LEN/(2.*COS(Y))
C ---  READ TUBE PARAMETERS ----------------------------------------
C        LEN =  INTERVAL LENGTH (CM)
C          G =  INSTALLATION ANGLE (RADIANS)
C          R =  TUBE RADIUS (CM)
      OPEN (UNIT=1,NAME='[DAN.DISS.INTEG]TUBE.PAR',TYPE='OLD')
      OPEN (UNIT=2,NAME='[DAN.DISS.INTEG]TUBE.OUT',TYPE='NEW')
      READ (1,100) LEN, R, G
 100  FORMAT (F5.3,5X,F5.3,5X,F20.17)
C
C ---  CALCULATE UPPER AND LOWER LIMITS FOR OUTSIDE INTEGRAL
      CALL UPP (B,G,LEN,R)
      CALL LOW (A,G,LEN,R)
C
C ---  READ THE NUMBER OF INTERVALS TO BE USED ---------------------
      READ (1,101) N, M
 101  FORMAT (I3,2X,I3)
C
C ---  BEGIN INTEGRATION PROCEDURE ---------------------------------
      H=(B-A)/(2.*N)
      J1=0.
      J2=0.
      J3=0.
      DO 10 I = 1,(2*N+1)
       II=I-1
       X= A + II*H
       IF (X.EQ.0.) X= (3.14159265/18000.)
       IF (X.GT.(3.14159265-3.14159265/18000.)) THEN
       IF (X.GT.(3.14159265+3.14159265/18000.)) GOTO 99
       IF (I.EQ.1) X= 3.14159265+(3.14159265/18000.)
       IF (I.NE.1) X= 3.14159265-(3.14159265/18000.)
       ELSE
       END IF
99     CONTINUE
       IF (X.GT.(2*3.14159265-3.14159265/18000.)) THEN
       X= (2*3.14159265-3.14159265/18000.)
       ELSE
       END IF
       CALL DD (X,DX,R,LEN,G)
       CALL CC (X,CX,R,LEN,G)
       HX= (DX - CX)/ (2.*M)
       F1= F(X,CX)
       F2= F(X,DX)
       IF (F1.LT.0.) F1=0.
```

```
      IF (F2.LT.0.) F2=0.
      K1= F1 + F2
      K2=0.
      K3=0.
       DO 11 JJ = 1, (2*M-1)
        Y= CX + JJ*HX
        Z= F(X,Y)
        IF (Z.LT.0.) Z=0.
        IF (JJ.EQ.2*(JJ/2)) THEN
         K2= K2 + Z
        ELSE
         K3= K3 + Z
        END IF
11      CONTINUE
       L = (K1 + 2.*K2 + 4.*K3) *HX/ 3.
       IF (II.EQ.0) GO TO 20
       IF (II.EQ.2*N) GO TO 20
       IF (II.EQ.2*(II/2)) THEN
        J2= J2 + L
       ELSE
        J3= J3 + L
       END IF
      GO TO 10
  20  J1= J1 + L
  10 CONTINUE
      J= (J1 + 2.*J2 + 4.*J3) *H/ 3.
      WRITE (2,200) J
  200 FORMAT (F10.3)
C      WRITE (5,*) J
      CLOSE (UNIT=1)
      CLOSE (UNIT=2)
      STOP
      END
```

```
PROGRAM NUMNPL
C --------- PROGRAM TO NUMERICALLY INTEGRATE EQUATIONS ----------------
C
      REAL J, J1, J2, J3, L, K1, K2, K3, LEN
C
C ---  INTEGRAND FUNCTION ------------------------------------------
      F(X,Y)= -LEN/(2.*COS(Y))
C ---  READ TUBE PARAMETERS ----------------------------------------
C        LEN =  INTERVAL LENGTH (CM)
C          G =  INSTALLATION ANGLE (RADIANS)
C          R =  TUBE RADIUS (CM)
      OPEN (UNIT=1,NAME='[DAN.DISS.INTEG]TUBE.PAR',TYPE='OLD')
      OPEN (UNIT=2,NAME='[DAN.DISS.INTEG]TUBE.OUT',TYPE='NEW')
      READ (1,100) LEN, R, G
 100  FORMAT (F5.3,5X,F5.3,5X,F20.17)
C
C ---  CALCULATE UPPER AND LOWER LIMITS FOR OUTSIDE INTEGRAL
      CALL UPP (B,G,LEN,R)
      CALL LOW (A,G,LEN,R)
C
C ---  READ THE NUMBER OF INTERVALS TO BE USED ---------------------
      READ (1,101) N, M
 101  FORMAT (I3,2X,I3)
C
C ---  BEGIN INTEGRATION PROCEDURE ---------------------------------
      H=(B-A)/(2.*N)
      J1=0.
      J2=0.
      J3=0.
      DO 10 I = 1,(2*N+1)
       II=I-1
       X= A + II*H
       IF (X.EQ.0.) X= (3.14159265/18000.)
       IF (X.GT.(3.14159265-3.14159265/18000.)) THEN
       IF (X.GT.(3.14159265+3.14159265/18000.)) GOTO 99
       IF (I.EQ.1) X= 3.14159265+(3.14159265/18000.)
       IF (I.NE.1) X= 3.14159265-(3.14159265/18000.)
       ELSE
       END IF
99     CONTINUE
       IF (X.GT.(2*3.14159265-3.14159265/18000.)) THEN
       X= (2*3.14159265-3.14159265/18000.)
       ELSE
       END IF
       CALL DD (X,DX,R,LEN,G)
       CALL CC (X,CX,R,LEN,G)
       HX= (DX - CX)/ (2.*M)
       F1= F(X,CX)
       F2= F(X,DX)
       IF (F1.LT.0.) F1=0.
```

```
      IF (F2.LT.0.) F2=0.
      K1= F1 + F2
      K2=0.
      K3=0.
       DO 11 JJ = 1, (2*M-1)
        Y= CX + JJ*HX
        Z= F(X,Y)
        IF (Z.LT.0.) Z=0.
        IF (JJ.EQ.2*(JJ/2)) THEN
         K2= K2 + Z
        ELSE
         K3= K3 + Z
        END IF
11      CONTINUE
       L = (K1 + 2.*K2 + 4.*K3) *HX/ 3.
       IF (II.EQ.0) GO TO 20
       IF (II.EQ.2*N) GO TO 20
       IF (II.EQ.2*(II/2)) THEN
        J2= J2 + L
       ELSE
        J3= J3 + L
       END IF
      GO TO 10
  20  J1= J1 + L
  10 CONTINUE
      J= (J1 + 2.*J2 + 4.*J3) *H/ 3.
      WRITE (2,200) J
  200 FORMAT (F10.3)
C      WRITE (5,*) J
      CLOSE (UNIT=1)
      CLOSE (UNIT=2)
      STOP
      END
```

```
      PROGRAM NUM1
C --------- PROGRAM TO NUMERICALLY INTEGRATE EQUATIONS ----------------
C
      REAL J, J1, J2, J3, L, K1, K2, K3, LEN
C
C ---  INTEGRAND FUNCTION ------------------------------------------
      F(X,Y)= 1.0
C ---  READ TUBE PARAMETERS ----------------------------------------
C        LEN =  INTERVAL LENGTH (CM)
C          G =  INSTALLATION ANGLE (RADIANS)
C          R =  TUBE RADIUS (CM)
      OPEN (UNIT=1,NAME='[DAN.DISS.INTEG]TUBE.PAR',TYPE='OLD')
      OPEN (UNIT=2,NAME='[DAN.DISS.INTEG]TUBE.OUT',TYPE='NEW')
      READ (1,100) LEN, R, G
 100  FORMAT (F5.3,5X,F5.3,5X,F20.17)
C
C ---  CALCULATE UPPER AND LOWER LIMITS FOR OUTSIDE INTEGRAL
      CALL UPP (B,G,LEN,R)
      CALL LOW (A,G,LEN,R)
C
C ---  READ THE NUMBER OF INTERVALS TO BE USED ---------------------
      READ (1,101) N, M
 101  FORMAT (I3,2X,I3)
C
C ---  BEGIN INTEGRATION PROCEDURE ---------------------------------
      H=(B-A)/(2.*N)
      J1=0.
      J2=0.
      J3=0.
      DO 10 I = 1,(2*N+1)
       II=I-1
       X= A + II*H
       IF (X.EQ.0.) X= (3.14159265/18000.)
       IF (X.GT.(3.14159265-3.14159265/18000.)) THEN
       IF (X.GT.(3.14159265+3.14159265/18000.)) GOTO 99
       IF (I.EQ.1) X= 3.14159265+(3.14159265/18000.)
       IF (I.NE.1) X= 3.14159265-(3.14159265/18000.)
       ELSE
       END IF
99     CONTINUE
       IF (X.GT.(2*3.14159265-3.14159265/18000.)) THEN
       X= (2*3.14159265-3.14159265/18000.)
       ELSE
       END IF
       CALL DD (X,DX,R,LEN,G)
       CALL CC (X,CX,R,LEN,G)
       HX= (DX - CX)/ (2.*M)
       K1= F(X,CX) + F(X,DX)
       K2=0.
       K3=0.
```

```
      DO 11 JJ = 1, (2*M-1)
       Y= CX + JJ*HX
       Z= F(X,Y)
       IF (JJ.EQ.2*(JJ/2)) THEN
        K2= K2 + Z
       ELSE
        K3= K3 + Z
       END IF
11     CONTINUE
      L = (K1 + 2.*K2 + 4.*K3) *HX/ 3.
      IF (II.EQ.0) GO TO 20
      IF (II.EQ.2*N) GO TO 20
      IF (II.EQ.2*(II/2)) THEN
       J2= J2 + L
      ELSE
       J3= J3 + L
      END IF
     GO TO 10
 20  J1= J1 + L
 10  CONTINUE
     J= (J1 + 2.*J2 + 4.*J3) *H/ 3.
     WRITE (2,200) J
 200 FORMAT (F10.3)
C     WRITE (5,*) J
     CLOSE (UNIT=1)
     CLOSE (UNIT=2)
     STOP
     END
```

```
C       LIMA1.FOR   REGION 1 CASE A)
C ---   LIMITS FOR INTEGRATION  ----------------------------------
C
      SUBROUTINE UPP (B,G,LEN,R)
      B= 3.141592654
      RETURN
      END
C
      SUBROUTINE LOW (A,G,LEN,R)
      A= 0.
      RETURN
      END
C
      SUBROUTINE DD (X,C,R,LEN,G)
      REAL LEN
      C= 3.141592654 - 3.141592654/18000.
      RETURN
      END
C
      SUBROUTINE CC (X,C,R,LEN,G)
      REAL LEN
      C= ATAN( TAN(G) +(4*R/(LEN*COS(G))))
      RETURN
      END
```

```
C       LIMB1.FOR   REGION 1 CASE B)
C ---  LIMITS FOR INTEGRATION  ----------------------------------
C
      SUBROUTINE UPP (B,G,LEN,R)
      B= 3.141592654
      RETURN
      END
C
      SUBROUTINE LOW (A,G,LEN,R)
      A= 0.
      RETURN
      END
C
      SUBROUTINE DD (X,C,R,LEN,G)
      REAL LEN
      C=ATAN( TAN(G) -(4.*R/(LEN*COS(G))))
      IF (C.LT.0.) C= 3.141592654 + C
      RETURN
      END
C
      SUBROUTINE CC (X,C,R,LEN,G)
      REAL LEN
      C= ATAN( TAN(G) +(4*R/(LEN*COS(G))))
      RETURN
      END
```

```
C          LIM21.FOR   REGION 2(1) CASE A+B)
C ---  LIMITS FOR INTEGRATION  ----------------------------------------
C
      SUBROUTINE UPP (B,G,LEN,R)
      REAL LEN
      B= (3.14159265/2.) + ATAN(R/((R/COS(G)) + (LEN*TAN(G)/2.)))
      RETURN
      END
C
      SUBROUTINE LOW (A,G,LEN,R)
      REAL LEN
      A= ATAN((1./COS(G)) + (LEN*TAN(G)/(2.*R)))
      RETURN
      END
C
      SUBROUTINE DD (X,C,R,LEN,G)
      REAL LEN
      A= (LEN*LEN/4.)* (COS(X)**2 + SIN(X)**2*COS(G)**2)
      B= -LEN*SIN(X)*COS(G)* (.5*SIN(G)*LEN + R)
      C= LEN*SIN(G)* (LEN*SIN(G)*.25 + R)
      Y2= (-B - SQRT(B*B - 4.*A*C))/(2.*A)
      C= ATAN( Y2)
      RETURN
      END
C
      SUBROUTINE CC (X,C,R,LEN,G)
      REAL LEN
      C= G
      RETURN
      END
```

```
C         LIM22.FOR   REGION 2(2)   CASE A+B)
C ---  LIMITS FOR INTEGRATION ----------------------------------------
C
      SUBROUTINE UPP (B,G,LEN,R)
      REAL LEN
      B= (3.14159265/2.) + ATAN(R/((R/COS(G)) + (LEN*TAN(G)/2.)))
      RETURN
      END
C
      SUBROUTINE LOW (A,G,LEN,R)
      REAL LEN
      A= ATAN((1./COS(G)) + (LEN*TAN(G)/(2.*R)))
      RETURN
      END
C
      SUBROUTINE DD (X,C,R,LEN,G)
      REAL LEN
      C= ATAN( TAN(G) +(4*R/(LEN*COS(G))))
      RETURN
      END
C
      SUBROUTINE CC (X,D,R,LEN,G)
      REAL LEN
      A= (LEN*LEN/4.)* (COS(X)**2 + SIN(X)**2*COS(G)**2)
      B= -LEN*SIN(X)*COS(G)* (.5*SIN(G)*LEN + R)
      C= LEN*SIN(G)* (LEN*SIN(G)*.25 + R)
      Y1= (-B + SQRT(B*B - 4.*A*C))/(2.*A)
      D= ATAN( Y1)
      RETURN
      END
```

```
C       LIM3.FOR   REGION 3    CASE A+B)
C  *****   TO BE USED WITH NUMPPL.FOR   ********
C ---  LIMITS FOR INTEGRATION ----------------------------------------
C
      SUBROUTINE UPP (B,G,LEN,R)
      REAL LEN
      B= (3.14159265/2.) + ATAN(R/((R/COS(G)) + (LEN*TAN(G)/2.)))
      RETURN
      END
C
      SUBROUTINE LOW (A,G,LEN,R)
      REAL LEN
      A= ATAN((1./COS(G)) + (LEN*TAN(G)/(2.*R)))
      RETURN
      END
C
      SUBROUTINE DD (X,D,R,LEN,G)
      REAL LEN
      A= (LEN*LEN/4.)* (COS(X)**2 + SIN(X)**2*COS(G)**2)
      B= -LEN*SIN(X)*COS(G)* (.5*SIN(G)*LEN + R)
      C= LEN*SIN(G)* (LEN*SIN(G)*.25 + R)
      Y1= (-B + SQRT(B*B - 4.*A*C))/(2.*A)
      Y2= (-B - SQRT(B*B - 4.*A*C))/(2.*A)
      D= ATAN( MAX(Y1,Y2))
      RETURN
      END
C
      SUBROUTINE CC (X,D,R,LEN,G)
      REAL LEN
      A= (LEN*LEN/4.)* (COS(X)**2 + SIN(X)**2*COS(G)**2)
      B= -LEN*SIN(X)*COS(G)* (.5*SIN(G)*LEN + R)
      C= LEN*SIN(G)* (LEN*SIN(G)*.25 + R)
      Y1= (-B + SQRT(B*B - 4.*A*C))/(2.*A)
      Y2= (-B - SQRT(B*B - 4.*A*C))/(2.*A)
      D= ATAN( MIN(Y1,Y2))
      RETURN
      END
```

```
C       LIM4.FOR   REGION 4  CASE  B)
C ---   LIMITS FOR INTEGRATION  ------------------------------------
C
      SUBROUTINE UPP (B,G,LEN,R)
      REAL LEN
      B= 3.14159265
      RETURN
      END
C
      SUBROUTINE LOW (A,G,LEN,R)
      REAL LEN
      A= 0.
      RETURN
      END
C
      SUBROUTINE DD (X,D,R,LEN,G)
      REAL LEN
      A= (LEN*LEN/4.)* (COS(X)**2 + SIN(X)**2*COS(G)**2)
      B= LEN*SIN(X)*COS(G)* (-.5*SIN(G)*LEN + R)
      C= LEN*SIN(G)* (LEN*SIN(G)*.25 - R)
      Y2= (-B - SQRT(B*B - 4.*A*C))/(2.*A)
      D= ATAN( Y2)
      IF (D.LT.0.) D= 3.141592654 + D
      D1=ATAN( TAN(G) -(4.*R/(LEN*COS(G))))
      IF (D1.LT.0.) D1= 3.141592654 + D1
      D= MAX(D,D1)
      RETURN
      END
C
      SUBROUTINE CC (X,D,R,LEN,G)
      REAL LEN
      A= (LEN*LEN/4.)* (COS(X)**2 + SIN(X)**2*COS(G)**2)
      B= LEN*SIN(X)*COS(G)* (-.5*SIN(G)*LEN + R)
      C= LEN*SIN(G)* (LEN*SIN(G)*.25 - R)
      Y2= (-B - SQRT(B*B - 4.*A*C))/(2.*A)
      D= ATAN( Y2)
      IF (D.LT.0.) D= 3.141592654 + D
      D1=ATAN( TAN(G) -(4.*R/(LEN*COS(G))))
      IF (D1.LT.0.) D1= 3.141592654 + D1
      D= MIN(D,D1)
      RETURN
      END
```

```
C       LIM5.FOR   REGION 5  CASE B)
C ---  LIMITS FOR INTEGRATION ----------------------------------------
C   *******   TO BE USED WITH NUMNPL.FOR  **********
C
      SUBROUTINE UPP (B,G,LEN,R)
      REAL LEN
      B= 3.14159265
      RETURN
      END
C
      SUBROUTINE LOW (A,G,LEN,R)
      REAL LEN
      A= 0.
      RETURN
      END
C
      SUBROUTINE CC (X,D,R,LEN,G)
      REAL LEN
      A= (LEN*LEN/4.)* (COS(X)**2 + SIN(X)**2*COS(G)**2)
      B= LEN*SIN(X)*COS(G)* (-.5*SIN(G)*LEN + R)
      C= LEN*SIN(G)* (LEN*SIN(G)*.25 - R)
      Y2= (-B - SQRT(B*B - 4.*A*C))/(2.*A)
      D= ATAN( Y2)
      IF (D.LT.0.) D= 3.141592654 + D
      RETURN
      END
C
      SUBROUTINE DD (X,D,R,LEN,G)
      REAL LEN
      D= 3.14159265
      RETURN
      END
```

```
C       LIM6.FOR    REGION 6   CASE  A)
C ---  LIMITS FOR INTEGRATION  ----------------------------------------
C *****      APPLIES ONLY WHEN 16A IS SATISFIED    *****
C
      SUBROUTINE UPP (B,G,LEN,R)
      REAL LEN
      B= 2.*3.14159265
      RETURN
      END
C
      SUBROUTINE LOW (A,G,LEN,R)
      REAL LEN
      A= 3.14159265
      RETURN
      END
C
      SUBROUTINE DD (X,D,R,LEN,G)
      REAL LEN
      D= 3.14159265 - 3.14159265/18000.
      RETURN
      END
C
      SUBROUTINE CC (X,D,R,LEN,G)
      REAL LEN
      D= ATAN( ((4.*R)/(LEN*COS(G))) - TAN(G))
      IF (D.LT.0.) D= D + 3.14159265
      RETURN
      END
```

```
C         LIM71.FOR   REGION 7(1)  CASE A)
C ---  LIMITS FOR INTEGRATION ----------------------------------------
C *****      APPLIES ONLY WHEN 16A IS SATISFIED    *****
C
      SUBROUTINE UPP (B,G,LEN,R)
      REAL LEN
      B= ATAN( R/((LEN*TAN(G)/2.) - R/COS(G)))
      B= 3.*3.14159265/2. + B
      RETURN
      END
C
      SUBROUTINE LOW (A,G,LEN,R)
      REAL LEN
      A= 3.14159265 + ATAN( (LEN*TAN(G)/(2.*R)) - 1/COS(G))
      RETURN
      END
C
      SUBROUTINE DD (X,D,R,LEN,G)
      REAL LEN
      A= (LEN*LEN/4)* (COS(X)**2 + SIN(X)**2*COS(G)**2)
      B= LEN*SIN(X)*COS(G)* (R - LEN*SIN(G)/2.)
      C= LEN*SIN(G)* (LEN*SIN(G)*.25 - R)
      Y1= (-B-SQRT(B*B-4.*A*C))/(2.*A)
      D= ATAN(Y1)
      IF (D.LT.0.) D= D + 3.14159265
      RETURN
      END
C
      SUBROUTINE CC (X,D,R,LEN,G)
      REAL LEN
      D= 3.14159265 - G
      RETURN
      END
```

```
C       LIM72.FOR   REGION 7(2)  CASE A)
C ---  LIMITS FOR INTEGRATION ----------------------------------------
C *****     APPLIES ONLY WHEN 16A IS SATISFIED    *****
C
      SUBROUTINE UPP (B,G,LEN,R)
      REAL LEN
      B= ATAN( R/((LEN*TAN(G)/2.) - R/COS(G)))
      B= 3.*3.14159265/2. + B
      RETURN
      END
C
      SUBROUTINE LOW (A,G,LEN,R)
      REAL LEN
      A= 3.14159265 + ATAN( (LEN*TAN(G)/(2.*R)) - 1/COS(G))
      RETURN
      END
C
      SUBROUTINE CC (X,D,R,LEN,G)
      REAL LEN
      A= (LEN*LEN/4)* (COS(X)**2 + SIN(X)**2*COS(G)**2)
      B= LEN*SIN(X)*COS(G)* (R - LEN*SIN(G)/2.)
      C= LEN*SIN(G)* (LEN*SIN(G)*.25 - R)
      Y1= (-B-SQRT(B*B-4.*A*C))/(2.*A)
      Y2= (-B+SQRT(B*B-4.*A*C))/(2.*A)
      D= ATAN( MAX(Y1,Y2))
      IF (D.LT.0.) D= D + 3.14159265
      RETURN
      END
C
      SUBROUTINE DD (X,D,R,LEN,G)
      REAL LEN
      D= ATAN( ((4.*R)/(LEN*COS(G))) - TAN(G))
      IF (D.LT.0.) D= D + 3.14159265
      RETURN
      END
```

```
C         LIM8.FOR   REGION 8  CASE A)
C ---  LIMITS FOR INTEGRATION ----------------------------------------
C *****     APPLIES ONLY WHEN 16A IS SATISFIED    *****
C
      SUBROUTINE UPP (B,G,LEN,R)
      REAL LEN
      B= ATAN( R/((LEN*TAN(G)/2.) - R/COS(G)))
      B= 3.*3.14159265/2. + B
      RETURN
      END
C
      SUBROUTINE LOW (A,G,LEN,R)
      REAL LEN
      A= 3.14159265 + ATAN( (LEN*TAN(G)/(2.*R)) - 1/COS(G))
      RETURN
      END
C
      SUBROUTINE DD (X,D,R,LEN,G)
      REAL LEN
      A= (LEN*LEN/4.)* (COS(X)**2 + SIN(X)**2*COS(G)**2)
      B= LEN*SIN(X)*COS(G)* (R - LEN*SIN(G)/2.)
      C= LEN*SIN(G)* (LEN*SIN(G)*.25 - R)
      Y1= (-B-SQRT(B*B-4.*A*C))/(2.*A)
      Y2= (-B+SQRT(B*B-4.*A*C))/(2.*A)
      D= ATAN( MAX(Y1,Y2))
      IF (D.LT.0.) D= D + 3.14159265
      RETURN
      END
C
      SUBROUTINE CC (X,D,R,LEN,G)
      REAL LEN
      A= (LEN*LEN/4.)* (COS(X)**2 + SIN(X)**2*COS(G)**2)
      B= LEN*SIN(X)*COS(G)* (R - LEN*SIN(G)/2.)
      C= LEN*SIN(G)* (LEN*SIN(G)*.25 - R)
      Y1= (-B-SQRT(B*B-4.*A*C))/(2.*A)
      Y2= (-B+SQRT(B*B-4.*A*C))/(2.*A)
      D= ATAN( MIN(Y1,Y2))
      IF (D.LT.0.) D= D + 3.14159265
      RETURN
      END
```

```
C       LIM9.FOR   REGION 9   CASE B)
C ---   LIMITS FOR INTEGRATION ----------------------------------------
C
      SUBROUTINE UPP (B,G,LEN,R)
      REAL LEN
      B= 3.14159265
      RETURN
      END
C
      SUBROUTINE LOW (A,G,LEN,R)
      REAL LEN
      A= 0.
      RETURN
      END
C
      SUBROUTINE DD (X,D,R,LEN,G)
      REAL LEN
      A= (LEN*LEN/4.)* (COS(X)**2 + SIN(X)**2*COS(G)**2)
      B= LEN*SIN(X)*COS(G)* (R - (LEN*SIN(G)/2.))
      C= LEN*SIN(G)* (LEN*SIN(G)*.25 - R)
      Y1= (-B-SQRT((B*B)-(4.*A*C)))/(2.*A)
      D= ATAN (Y1)
      IF (D.LT.0.) D= D + 3.14159265
      IF (D.LT.(3.14159265 - G)) D= 3.14159265 - G
      RETURN
      END
C
      SUBROUTINE CC (X,D,R,LEN,G)
      REAL LEN
      A= (LEN*LEN/4.)* (COS(X)**2 + SIN(X)**2*COS(G)**2)
      B= LEN*SIN(X)*COS(G)* (R - (LEN*SIN(G)/2.))
      C= LEN*SIN(G)* (LEN*SIN(G)*.25 - R)
      Y1= (-B-SQRT((B*B)-(4.*A*C)))/(2.*A)
      D= ATAN (Y1)
      IF (D.LT.0.) D= D + 3.14159265
      IF (D.GT.(3.14159265 - G)) D= 3.14159265 - G
      RETURN
      END
```

```
C       LIM10.FOR  REGION 10  CASE B)
C ---  LIMITS FOR INTEGRATION ----------------------------------------
C
      SUBROUTINE UPP (B,G,LEN,R)
      REAL LEN
      B= 2.*3.14159265
      RETURN
      END
C
      SUBROUTINE LOW (A,G,LEN,R)
      REAL LEN
      A= 3.14159265
      RETURN
      END
C
      SUBROUTINE CC (X,D,R,LEN,G)
      REAL LEN
      A= (LEN*LEN/4)* (COS(X)**2 + SIN(X)**2*COS(G)**2)
      B= LEN*SIN(X)*COS(G)* (R + LEN*SIN(G)/2.)
      C= LEN*SIN(G)* (LEN*SIN(G)*.25 - R)
      Y1= (-B-SQRT(B*B-4.*A*C))/(2.*A)
      Y2= (-B+SQRT(B*B-4.*A*C))/(2.*A)
      D= ATAN( MIN(Y1,Y2))
      IF (D.LT.0.) D= D + 3.14159265
      RETURN
      END
C
      SUBROUTINE DD (X,D,R,LEN,G)
      REAL LEN
      D= 3.14159265
      RETURN
      END
```

APPENDIX B

MODEL NOMOGRAPHS

Figures B.1, B.2, and B.3 are nomographs for determining the average length to associate with each intersection. Each figure represents a different value for L, the length of the interval of observation. The desired value is obtained by locating the appropriate figure for the interval length to be used, locate the installation angle on the abscissa, follow a line parallel to the ordinate until the line labelled with the appropriate tube diameter is reached, the value on the ordinate at this intersection point is the average length required.

These figures represent the correct value when root growth angles are randomly distributed, and the tortuousity is equal to 1.0. Although the relationship is not linear, linear interpolation between values will not introduce significant errors determining the average length.

Figure B.1: Nomograph for determining the average length to associate with each intersection, with an interval length of 10 cm. Random root growth and tortuousity of 1.0 is assumed.

MODEL NOMOGRAPH (L=10)

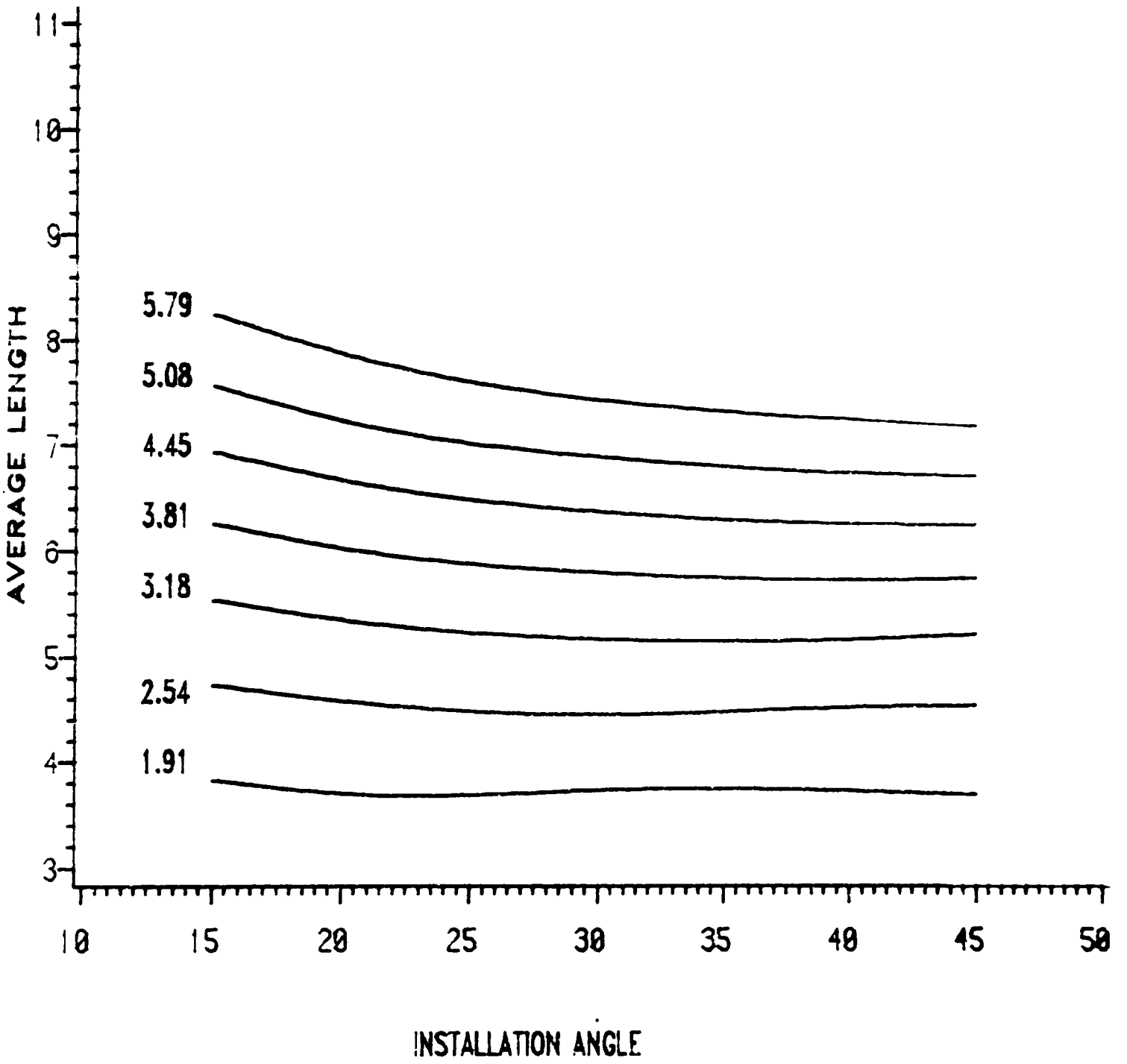

Figure B.2: Nomograph for determining the average length to associate with each intersection, with an interval length of 15 cm. Random root growth and tortuousity of 1.0 is assumed.

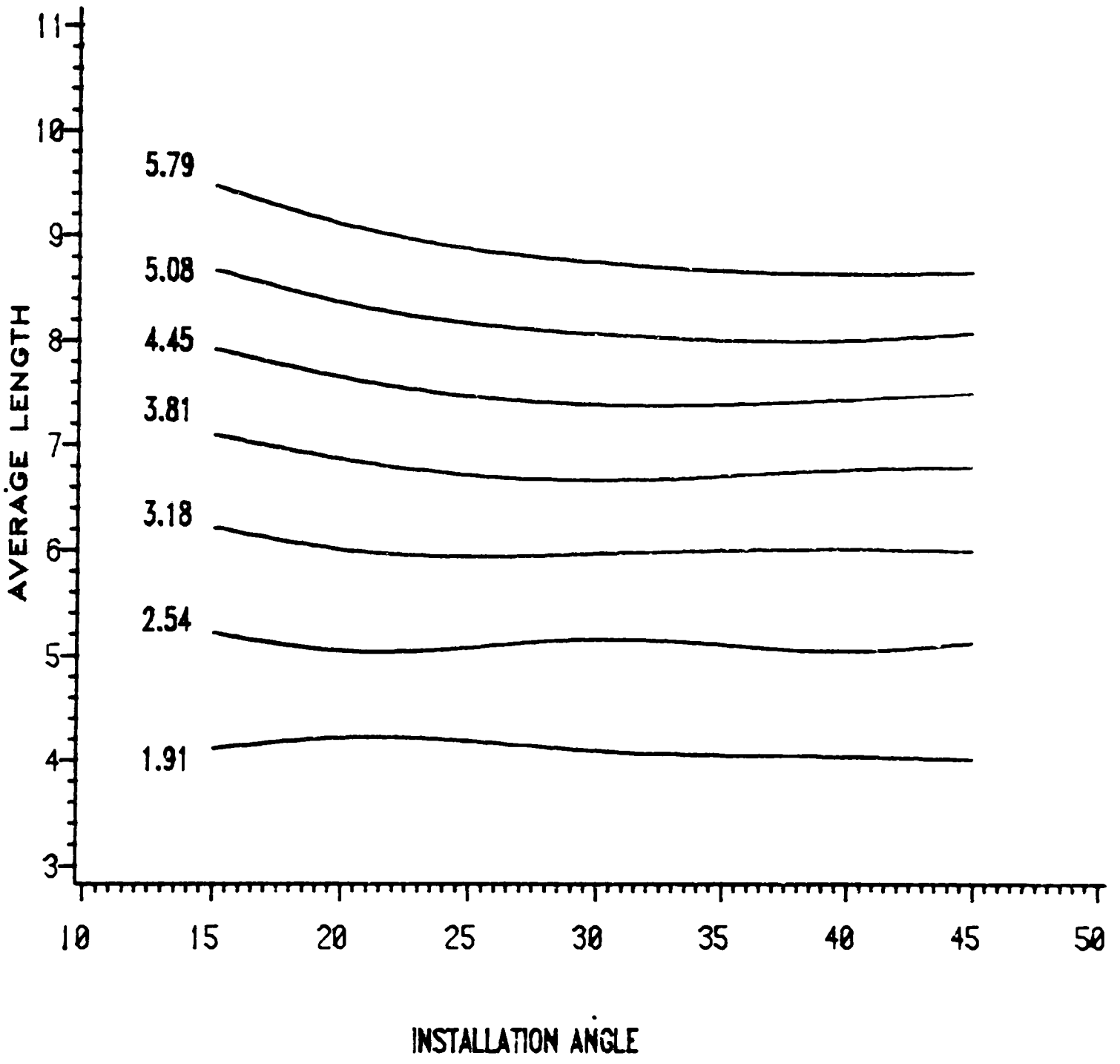
MODEL NOMOGRAPH (L=15)
AVERAGE LENGTH
11
10
9
8
7
6
5
4
3
5.79
5.08
4.45
3.81
3.18
2.54
1.91
10
15
20
25
30
35
40
45
50
INSTALLATION ANGLE

Figure B.3: Nomograph for determining the average length to associate with each intersection, with an interval length of 20 cm. Random root growth and tortuousity of 1.0 is assumed.

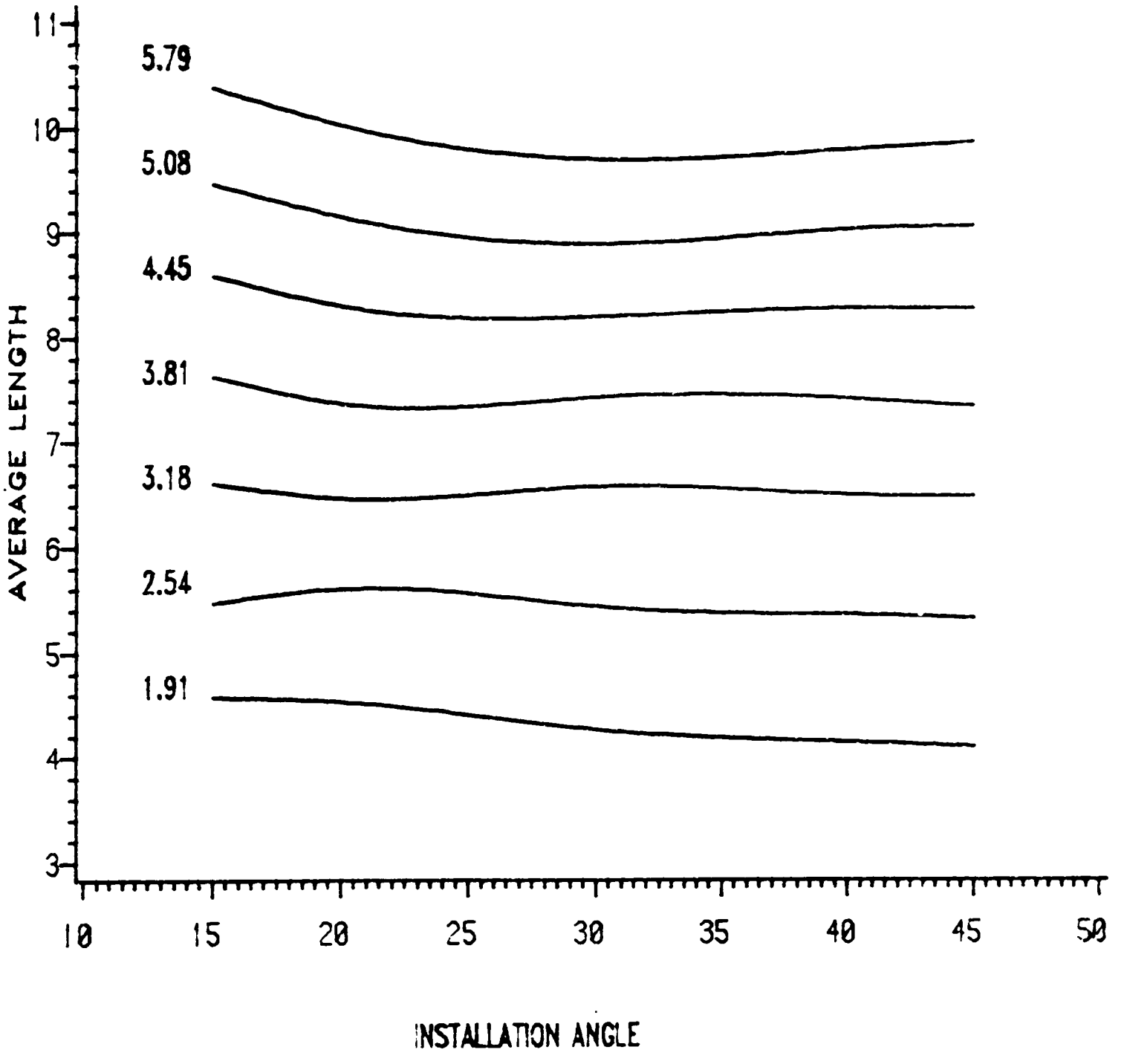
MODEL NOMOGRAPH (L=20)
AVERAGE LENGTH
11
10
9
8
7
6
5
4
3
5.79
5.08
4.45
3.81
3.18
2.54
1.91
10
15
20
25
30
35
40
45
50
INSTALLATION ANGLE